Preparation and characterization of silicone nanocomposites by UV-induced hydrosilation for outdoor polymeric insulators

POLITECNICO DI TORINO

PhD in Materials Science and Technology

Final Dissertation

XXVI Cycle

Preparation and characterization of silicone nanocomposites by UV-induced hydrosilation for outdoor polymeric insulators

Sophie Marchi

Tutor: Prof. Marco Sangermano

January 29th 2014

INDEX

INTRODUCTION

In the late 1950s, due to the rapid growth in demand for electrical power in North America, the necessity of a suspension-type line insulator with reduced weight and improved electrical and mechanical characteristics was considered a prerequisite to transmission at high voltage. For these reasons, insulators, that are the most important equipment in an electrical power system, needed to meet not only the new electrical stresses but also the increased mechanical loads that came with the new transmission and distribution lines.

Many efforts have been made to improve the performance of insulation especially in polluted conditions. With this purpose, polymeric insulators are becoming more and more accepted among power plants around the world in place of the conventional ceramic insulators for use as electrical insulators for high-voltage lines. The electrical characteristics of the insulation must be kept constant as much as possible. As a result, they need good electrical and mechanical performance to withstand a wide range of operating conditions, including environmental stresses. For this reason, the insulator should be resistant to atmospheric attacks, UV radiations, physical and chemical degradation. Two materials commonly used for insulating polymeric composites are silicon rubber and EPDM (ethylene propylene diene monomer). Silicone rubber nanocomposites usable as an outdoor insulating material have been also developed.

The doctoral thesis concerns the preparation and characterization of silicone polymers using the UV-hydrosilation reaction in order to obtain materials with high electrical insulating properties. This reaction is typically the addition of a silane bond across a double bond to form silicone polymers. This method progressively became the method of choice for the synthesis of organofunctional silanes and is still used today in silicone industry. This process allows to save energy and processing time. In this regards, the potential for UV curable system is increasing quite significantly.

Moreover, due to the room temperature curing and the very short time before gelation occurs, any nanoparticles dispersed can be frozen in and thus, agglomeration is highly reduced. Therefore, UV curable systems are very promising but so far they are mainly applied for coating applications. It was however reported that UV-induced hydrosilation reaction can be effective in curing some centimeters thick materials. For this reason, thick nanocomposite materials with advanced properties could be obtained by combining the well known advantages of the UV-curing reaction with the hydrosilation process.

In a first part, the mechanism of the UV-hydrosilation reaction was investigated taking into account the use of different catalysts and additives, as well as different silicone oligomers. Furthermore, it was examined the influence of the monomers molecular weight on the reactivity of the system and on the final properties of the material.

Once determined the most promising material composition, the curing conditions and the properties of the silicone matrices, the next step was the preparation and characterization of silicone composites materials by adding different inorganic nanoparticles within the polymeric matrices (both micro and nano sized). The incorporation of inorganic material can lead to higher mechanical properties, better electrical properties, thermal endurance, hardness and improved scratch resistance. However, the final performances of the composite material is governed by the complex interplay of the different components in the precursor formulation and finally by the dispersion of the inorganic parts in the matrix and the specific interface interactions between the particles and the polymeric matrix.

To minimize the phenomena of agglomeration and increase the interactions between the organic and inorganic phases, in-situ generation of the inorganic domains through a sol-gel process was investigated. Several parameters such as the time, the amount and the nature of the inorganic precursor were examined. Different particles were effectively produced (such as silica , titania or aluminium hydroxide). Finally, it was evaluated the possibility to activate the hydrosilation reaction by blue light irradiation. The properties of both unfilled and filled materials were evaluated and compared to the UV-induced hydrosilation.

1. HIGH VOLTAGE INSULATORS FOR OUTDOOR USE

Electrical insulators are used in every medium and high voltage transmission lines and play an extremely important role in safety. The main purpose of these devices is the effective separation of power lines and ground structures without allowing current through themselves. The modeling of the electric field distribution, which is not commonly achieved, results however essential for the design of these devices [1]. They can also be used as mechanical supports for power lines.

Insulators used for high voltage power transmission developed rapidly more than 150 years ago and can be made from glass, porcelain or polymer composites. Different types of insulators are employed on overhead lines (called line insulators) depending on their function. The classification of power line insulators are reported in Figure 1.1.

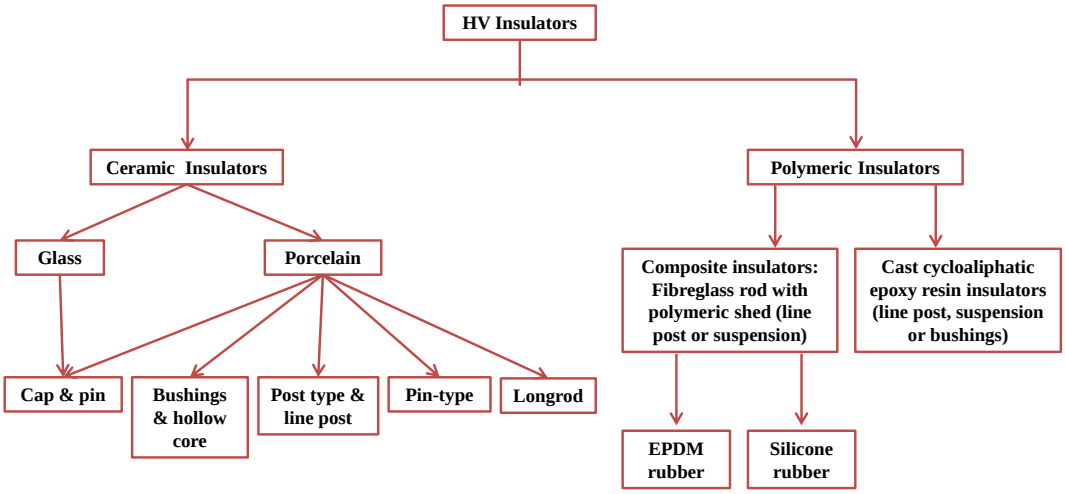

Figure 1.1: Classification of power line insulators

Porcelain pin-type insulators or cap and pin insulators are appropriated for power transmission while post-type and line post insulators are mainly used to support the high voltage conductor. Longrod insulators are similar to the previous ones but are lightweight, with reduced sizes and are used as suspension insulators.

Two materials commonly employed for composite polymeric insulators are silicone rubber and EDPM (ethylene propylene diene monomer). Epoxy resin can also be used to obtain post line insulators.

1.1. Overview of electrical insulators

Conductors for long transmission are required for electric power delivery from the generation site to the consumer. In order to minimize losses during the transmission and distribution, conductors mostly operate at high voltage. The major functions of insulators are to isolate the conductor from the sustentation, to act as a substructure of the conductor itself, to protect the costly apparatus involved in the power system [2] and to be the first to operate breakdown during over-voltages propagation. Therefore, several aspects need to be taken into consideration for applications in high voltage electrical engineering. The first one is the improvement in transmission and distribution conductor to reduce losses. The reduction of both equipments and components size is also important [3].

In order to ensure the functioning of the material, the electrical performances of the insulators need to be kept constants as much as possible. In consequence, they need good electrical and mechanical performances to withstand the wide range of operating conditions; including environmental stresses. That is the reason why insulators need to be resistant to weathering, chemical and physical degradation by water, UV radiations and chemical attacks.

Improved hydrophobicity on insulators suppresses leakage current and partial discharges under heavily contaminated conditions and prevents insulator flashover. Resistance to tracking, erosion, flammability as well as arc resistance are required due to the high electrical stresses that the insulators need to support. Good tear strength is interesting for the material demolding and also for the mechanical stresses [4]. Insulators also require low dielectric loss in order to be able to withstand heat maintaining their dielectric strength.

Thermal properties of insulator materials determine their ability to resist to the temperature rise during service. The high temperatures reached on the material

surface can come from bushfires as well as from solar radiations. Good structure retention under heat, low thermal expansion coefficient and non-flammability are therefore crucial for the insulator materials..

Insulators also need have minimum electrical, chemical and mechanical properties in order to guarantee the correct performances. The choice of the materials used depends on many factors such as the load or stress they have to come across in their application. In the following will be discuss the different materials used for high voltage insulators.

1.2. Materials used for high voltage insulators

Insulators for outdoor applications are made from three main types of materials: porcelain and glass insulators (considered as ceramic insulators) and polymer insulators called composites insulators. The main characteristics, properties and defects of these three kind of insulators are studied.

Despite their insulating role, insulators need also to fulfill well their mechanical responsibilities (such as construction support and load bearing) and to withstand other stresses during application. This means that good tensile strength but also good bending and high compression strengths are required, depending on their applications. The mechanical properties necessaries for a better design and mechanical stress withstand are a high elastic and high hardness modulus [5]-[7] .

The performances of the insulator in the transmission system are altered by various factors as they are exposed to numerous conditions prior and during their application. Each type of insulator has precautions that need to be followed to avoid defects. Due to the diverse properties obtained for each material used, defects will be of different types.

Defects on insulators can be caused by accident during processing, distribution or installing. Multi ageing stresses, such as UV radiations, pollution, humidity, are mostly the major cause of defects in the outdoor insulators [8]-[13]. Moreover, in long term service, they are also continuously subjected to mechanical stress

(vibration, tension and temperature gradient), thermal stresses and electrical stresses which are unavoidable in normal operation.

1.2.1. Ceramic insulators

The use of inorganic materials such as porcelain and glass for ceramic insulators in outdoor applications started more than 150 years ago.

1.2.1.1. Porcelain insulators

Porcelain insulators were first introduced in the 1850's and are still the most widely used outdoor insulating material for high voltages. The properties of porcelain insulators depend upon the particles sizes, crystals and pores that constitute the material. Insulators made from porcelain mainly contain clay, quartz or alumina and feldspar. Glazing can be employed to smooth the insulator surface, improve hydrophobicity and increase the mechanical strength.

Ceramic insulators present many advantages such as electrical properties, absence of deformation under stress (at room temperature) and higher resistance to environmental changes [14]. They are widely used in the microelectronic devices and in power transmission lines.

Although porcelain insulators are still used worldwide; design and manufacture need to be enhanced to meet the requirements of modern power transmission systems.Indeed, there are some limitations for the sheds design that can satisfy the surface electrical leakage distance needed for higher voltage transmission. Moreover, it results inconvenient to use ceramic insulators in systems above 100 kV due to their weight. In fact, they will become too long, massive and easily damageable [15].Indeed, porcelain materials are brittle and present very low tensile strength compared to toughened glass. During the firing cycle, thermal mismatch between external glaze and core material can cause internal micro-cracks that reduce mechanical and electrical performances. In some cases, silica or alumina can increase the glaze mismatch and strengthen the macroscopic surface.

The important electrical properties of porcelain insulators are low values of relative permittivity, loss tangent and high volume resistivity that depend on ion mobility. As temperature increases, the loss tangent increases substantially and relativity decreases leading to a limited use of ceramic insulators [5].

1.2.1.2. Glass insulators

The first glass insulator was proposed for telegraph lines while suspension insulators for transmission lines appeared at the beginning of the 20^{th} century [5].Glass was then progressively used for high voltages with the development of power transmission. It required heavier conductors and higher strength insulators which resulted a problem. In fact, glass is a brittle and easily fracturable material due to the mechanical stresses on its surface. Moreover, ordinary glass contains microscopic cracks that can propagate freely leading to a mechanically weak material.

A toughening technique, introduced in 1925, improved mechanical strength, fatigue characteristic, resistance impact and decreased the damage rate caused by mishandling [2],[5]. Furthermore, toughened glass presents a highly compressed skin to limit crack formation and store strain energy. This energy will be released by forming small fragments if hit.

The relative permittivities of toughened glass and glazed ceramic are similar due to the permittivity on the glazed ceramic being dominated by a glassy component. As toughening increased mechanical strength of glass, a thinner shell can be used compared to ceramic insulators. Glass also presents high dielectric strength but internal strains cannot be avoided during casting of the thick irregular shapes necessary for the insulators [16].

Three mainly defects are reported in glass insulators: seeds, stones and cords. Seeds are small gaseous bubbles in the glass that were not removed completely during manufacture. Stones are small crystals in the glass and cords are amorphous sections due to an inadequate or inappropriate mixtures. Designs of glass insulators are similar to those of the porcelain insulators.

Porcelain and glass insulators possess an elevate capacity to withstand heat from dry band arcing resulting in a high resistance before serious surface

degradation. However, because of their high surface energy, these materials are highly wettable when exposed to wet conditions like fog, dew, and rain. When contamination is also present, leakage current can take place more easily leading to flashover and power system outage. Flashover is still considered the most serious problem of insulators in service [17].

To help prevent disruptions of the power system due to insulator contamination, maintenance measures are employed. The most common practice is to maintain a regular insulator washing and cleaning schedule [18]. Regularly wash insulators are used to prevent flashover in heavily polluted areas [19]. However, this practice, although effective, is quite costly over the long term.

In the 1950's appeared the revolutionary concept of replacing the self-supporting block of porcelain or glass by a composite structure of support bearing rod and protecting housing, each made of polymeric materials. Large economic savings were expected from the change, but it required new thinking as regards the selection and design criteria for materials as well as for assembling technologies.

1.2.2. Composite (Polymer) insulators

The interest in very high voltage power transmissions encouraged industry to produce lightweight insulators with better electrical and mechanical properties as replacements of traditional porcelain and glass insulators [20]-[22]. Years of work allowed the selection of optimal material compositions and manufacturing technologies causing that non-ceramic insulators became fully accepted in the market as an alternative solution in designing high voltage power lines and substation components [23].

The development of composite (or polymer) insulators increased significantly in the 1960's [5],[13]. The major advantages are their easy handling, reduced breakage and damage (during construction), lower overall installation cost of overhead lines [24],[25] and convenient maintenance [26]-[29]. Composite

insulators also present superior properties in the presence of heavy pollution and wet conditions due to their high hydrophobicity leading to a self-cleaning device.

High electrical parameters such as low dielectric permittivity, high breakdown voltage, high surface and volume resistance are also desirable characteristics of ceramic insulators [27],[30]-[32]. They are currently applied in a wide range of applications including bushings, transmission insulators or cable terminations.

This type of insulators are separated into three components: (i) a core made of glass fiber (to reinforce resin rod system), (ii) external weathersheds made of polymer and (iii) metal fittings for attachment (see Figure 1.2).

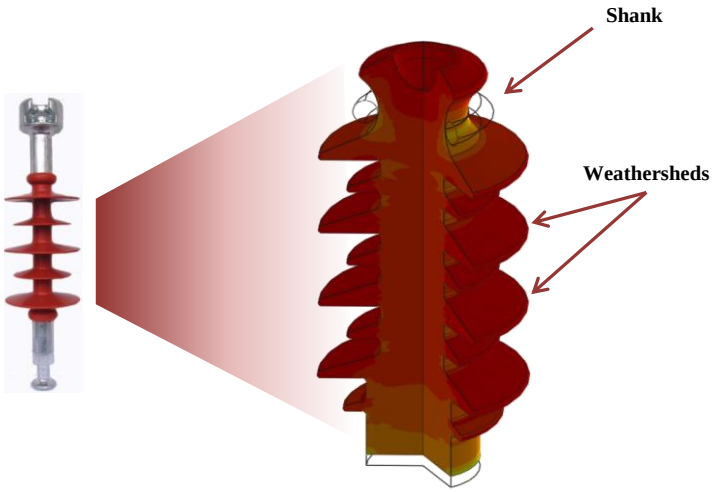

Figure 1.2: Shape of a composite insulator

The use of fiberglass as a core aims to improve the load bearing ability and also to act as an insulating part. Today, vinyl ester resin can also be introduced as a core. The weathersheds are made from various polymer materials and designs in many different shapes to provide maximum insulation.

Since the glass fiber cores are sensitive to water penetration and contaminant [33]-[34], polymers are used to protect the core from moisture ingress. Therefore, they need to withstand weathering without losing mechanical and electrical properties and to be able to work in a large range of temperatures from -40°C to 120°C. The weathersheds are also intended to protect the fiber glass rod from the electrical surface discharges by providing an extended creepage distance (that is the length of the leakage path along the surface from one end to the other) [35].

The first polymeric insulators were made from epoxy but it resulted not very useful in outdoor environments [23]. Non-ceramic insulators containing ethylene-propylene rubber (EPR) were then made by different companies in France and USA in the late seventies. Silicone rubbers (SIR) were presented later on in USA and Germany[36]. Ethylene-propylene-diene rubber (EPDM) were also used [19],[37],[38].

Ohio Brass introduced then an alloy consisting of EPDM and SIR to couple the properties of two materials [31].Ethylene-propylene-diene rubber is used in HV insulators due to its combination of superior electrical properties such as its flexibility over a wide temperature range and its resistance to moisture and weather. However, EPDM endures from UV radiation and loss of hydrophobicity. Properly, these alloys present excellent electrical and mechanical properties due to the presence of EPDM and are hydrophobic thanks to the silicone content. The main drawback is that these materials do not yet have the long-term service life of glass and porcelain [39],[40].

Polymeric insulators with weathersheds made from silicone rubber present a superior performance under wet and polluted conditions compared to other polymers (such as epoxy, ethylene vinyl acetate…) thanks to their relative high hydrophobicity.

The SIR are used in composite insulators as housing on a load-bearing structure of e.g. glass-fiber reinforced plastics. They are almost exclusively based on polydimethylsiloxane (PDMS). They have low density, hydrophobic surface properties, low surface and bulk conductivity, fracture toughness over a wide temperature range, that give them distinct advantages compared to ceramic materials. Low weight, vandalism resistance, contamination resistance and long-term endurance are important characteristics of polymeric composite insulators with SIR housings [36]. The hydrophobicity of the insulator surface avoids the formation of continuous water films in wet and heavily contaminated conditions. Instead, the water droplets formed simply run off the surface. This phenomenon contributes to the suppression of leakage current and partial discharges on insulator surfaces and therefore, SIR provides an improved electrical performance under wet and contaminated environments over porcelain and glass.

A SIR is initially very water repellent due to its hydrophobic character but electrical discharges or hard contamination can progressively cause oxidation of the polymer and the surface becomes more hydrophilic. After a consecutive sufficient period of break, hydrophobicity can be regained. Most researchers believe that migration of low molar mass PDMS from the bulk to the surface is the dominant mechanism for the hydrophobicity recovery [41]-[49].

Contamination, whereby the surface becomes covered with hydrophilic particles, is another reason for loss of hydrophobicity. It turns out that surface contaminated SIR also recover by migration of low molar mass PDMS [36]. It could be also explained by the presence of silicone oils. They can spontaneously emigrate to the surface from the bulk because the surface energy of air is lower than that of SIR. They serve as releasing agent in manufacturing process and play also an important role in the hydrophobicity of outdoor polymer insulators surface. This is due to the fact that they have very low surface energy (17-18 $dyne.cm^{-1}$) and allow the easy encapsulation of the pollutants on the surface. Addition of silicone oils can be required to enhance mixing as high quantity of inorganic fillers are necessary for the improvement of tracking resistance. The oils having low miscibility with silicone gum polymer serves as releasing agent.

Other important characteristics include thermal and oxidative stability, high degree of chemical inertness, resistance to weathering, and temperature-insensitive physical properties. These outstanding properties of the SIR are related to its unique molecular structure [50]-[53]. However, chemical resistance, corona endurance and tracking resistance of rubber are weaker than ceramic materials.

Where polymeric insulators are not applicable to replace ceramic insulators, a coating of SIR spread on porcelain insulators surface is an effective method of enhancing insulator performance. This concept has already been widely used as a maintenance tool by power utilities [54]-[60].

Despite their advantages of lightweight for transmission applications, composite insulators are susceptible to tracking and erosion, chalking and hardening of the shed, increase of contaminant deposition, discharges, electrical failure, bonding and brittle fracture. These failures have made some

manufacturers turn to production of composite insulators for distribution voltage level use only.

1.3. Defects on HV insulators occurring during service

Insulators are subjected to electrical, mechanical and environment stresses during service due to their wide role in power transmission. The conductor weight, sag, tension and wind can be responsible for the mechanical stresses while a high temperature ambient and a wide range of surface pollution are the main unavoidable factors of environmental stresses.

In particular, polymeric insulators are highly sensitive to the environment effects. UV sunlight causes a certain change in chemical bonds of the polymer because of cross-linking reactions. High temperatures increase the electrical conductivity that can cause discharges on the surface and subsequent surface degradation. This condition weakens the surface insulation significantly and may lead to breakdown. Moisture will obviously further decrease the surface insulation resistance as well as the presence of surface contamination due to pollution. Environmental effects on the polymer insulator provide therefore a substantial area for researchers to investigate [8],[33],[61]-[68].

For these reasons, the different stresses experienced by outdoors high voltage insulators can be hold out by only few materials. These stresses are summarized in Table 1.1 [69].

Table 1.1: Stresses on outdoor insulation

Classification	Stress
Environmental	UV, Moisture, Temperature, Chemical
Electrical	Dry Band Arcing, Partial discharge, Corona
Mechanical	Cyclic loads

When an excessive voltage is applied on the insulators surface, the material experiences electrical breakdown. This means that the electric field exceeds in any

point of the material the threshold breakdown field. The insulator quickly becomes a conductor thus leading to a large increase in current with an electric arc through or along the outside of the substance (depending on the nature of the electrical breakdown as it can take place by puncture arc or by flashover arc).

The leakage current is allowed to flow and causes dry bands in the high current density region. The voltage across the insulator is then exercised across the dry bands causing high electric stresses sufficient to ionize air and a discharge in the gas is then established.

It is mostly self-limiting but, if surface resistance is sufficiently low, discharges will be self-sustaining and overtime can propagate and bridge terminals causing flashovers [5]-[6]. Various contaminants such as dirt, pollution, salt and especially water present on the surface of the insulator can form a conductive path beyond it. The flashover voltage can be reduced by half when the insulator is wet. In consequence, surface flashover due to contamination can take place[5],[70].

The major part of high voltage insulators are drawn with a lower flashover voltage than puncture voltage in order to avoid damage and with a creepage length aiming to reduce leakage currents. Thus, the surface is designed with a series of side-by-side disc shapes that contains one or more sheds that act as protection to ensure wet conditions on the surface leakage path. Usually, creepage distances are on the order of 20-25 $mm.kV^{-1}$ but need to be enhanced in high polluted areas.

The interruption due to surface flashover results into great economic loss to the consumers as well as to the power company [71]. Various remedial measures have been suggested from time to time to rectify this problem. This includes cleaning, greasing and live washing or to put hydrophobic coating over the insulator surface. The latter was achieved on ceramic insulators but long term stability could not be reached [72]. Moreover, the hydrophobicity of housings can be lost temporarily by corona discharges, contamination and dry band arcing, leading to phenomena of tracking and erosion in the material. Tracking and erosion are irreversible degradation for composite insulators that reduce their electrical insulation properties and mechanical strength considerably [73]-[76]. Hence, in the last decade research targeted on the development of new insulating materials that combine the advantages of both ceramic and non-ceramic insulators. This

research was further stimulated by the appearance of nanotechnologies as nanomaterials present better properties with respect to their bulk analogues.

1.4. Electrical properties improvement by use of fillers

Even though polymeric insulators result lighter than ceramic insulators, they are sensitive to tracking and erosion, hardening of sheds, contamination from pollutants and electrical breakdown. In particular, silicone elastomers can be used as insulators only when the surface electrical stress is low enough to avoid dry band arcing. The resistance to the discharges effects is also necessary for the use in outdoor high voltage applications. In order to meet those requirements, it is impossible to use polymers without additives and fillers. The inclusion of fillers imparts tracking and/or erosion resistance as well as improves mechanical properties of the housing. Fillers are also used to reinforce physical properties or to impart certain processing characteristics. They can be reinforcing or extending fillers.

The reinforcing type improves hardness, tensile strength, modulus, tear strength and abrasion resistance of a compound. There are two kinds of reinforcing fillers: carbon black and fine-particle mineral pigment, such as silica [77]. Silica not only improves the physical and mechanical properties of a compound, but also prevents erosion that results from the electrical stress to which the compound is subjected during service. An extending filler is a loading or non-reinforcing material. It may be used to reduce cost or to impart other desirable properties to a compound. Alumina tri-hydrate (properly aluminum hydroxide named ATH) is a good example of extending filler used in high voltage polymeric materials to provide high electrical tracking and fire retardancy.

The common inorganic fillers used into improve the insulating properties of the materials are reported in Table 1.2. Coupling agents can also be employed to act as a bridge between the polymer and the fillers [78].

Numerous studies were carried out to also evaluate the effect of filler type, particle size and amount on the electrical insulating properties and in particular on the erosion resistance of the material [27],[69],[79]-[87].

Table 1.2: Common fillers incorporated into dielectrics to achieve engineering materials for electrical insulation

Filler	Property Modification	Engineering Insulation Improvement
$Al_2O_3.3H_2O$, SiO_2	Thermal Conductivity	Resistance to dry band arcing, Partial discharge & Corona
$BaTiO_3$, $BaTiO_3$ + Al	Relative permittivity	Electric field grading
SiC, Varistor (ZnO), Sb_2O_3 + SnO	Electrical Conductivity	Contamination performance Electric field grading

The thermal conductivity of the insulators can be improved in the presence of fillers that remove the damaging heat from the dry band arcing area. Typically, ATH is introduced in amount up to 50% into the formulation in order to impart flame-retardancy but is also able to enhance the tracking resistance and dielectric strength. This occurs by decomposition to aluminum oxide and water when heated to temperatures above 200°C. The liberation of water is an endothermic phenomena that leads to the surface cooling, which may extinguish an arc. Typical compounds also contain smaller proportions of silicone oil for process control. Other chemicals are also needed especially for the vulcanization (cross-linking) reactions [88].

Extensive research has been done concerning the addition of micro-sized fillers to solid dielectric materials forming composites for use as electrical insulation in high voltage applications [27],[86],[89],[90]. Usually, the amount of microfillers necessary to improve the dry band arcing resistance is on the range between 30 and 65% by weight and generally, ATH, alumina and silica are the most investigated.

In the recent years, a great deal of attention has been paid to the application of nanofillers in the field of electrical insulating materials [91]. Nonetheless, preliminary conclusions demonstrated that the use of nano-sized particles lead to comparable property enhancements with lower filler amount [92]-[93].

Relative permittivity can also be increased by insertion of fillers such as $BaTiO_3$.

These materials are used for different purposes including stress removal. Moreover, higher relative permittivity are usually reached by using a mixture between ceramic and metal fillers. Also in this case many studies have been done evaluating the effect of both concentration and type of filler [69], [87]-[100].

Therefore, composite insulators (mostly PDMS based) are most commonly used in high voltage applications but only when their inherent weaknesses (mechanical strength, tracking, erosion) are overcome by reinforcement with some fillers, usually silica or aluminum hydroxide ($Al(OH)_3$) [57],[101]-[103].

References

[1] F. Mach, P. Karban. Prz. Elektrotech. 88 issue 7B (**2012**) 217.

[2] R.S. Gorur, E.A. Cherney, J.T. Burnham. USA: R.S. Gorur, Inc., Phoenix, Arizona (**1999**).

[3] C. Sumereder, M. Muhr. 19th International Conf. on Electricity Distribution, Vienna (**2007**).

[4] IEC Technical report TR62039. First edition (**2007**)-03.

[5] J.S.T. Looms. IEE power engineering series. London: Peter Peregrinus 7 (**1988**) 276.

[6] R. Bartnikas. Engineering Dielectric (**1987**).

[7] E. Kuffel, W.S. Zaengl. Pergamon Press (**1984**).

[8] T. Pollock, C. Pelletier, R. Chapman, R. Sundararajan. Conf. Electr. Insul. and Dielectric Phenomena 2 (**1999**) 695.

[9] A.J. Philips, D.J. Childs, H.M. Schneider. IEEE Trans. Power Del. 14 (**1999**) 258.

[10] S. Kumagai, N. Yoshimura. IEEE Trans. Dielectr. Electr. Insul. 8 (**2001**) 203.

[11] G. Xu, P.B. McGrath, C.W. Burns. IEEE, Piscataway, NJ, USA 96CB35972 (**1996**).

[12] V.K. Agarval, H.M. Banford, B.S. Bernstein, E.L. Brancato, R.A. Fouracre, G.C. Montanari, J.L. Parpal, J.N. Seguin, D:M. Ryder, J. Tanaka. IEEE Elect. Insul. Mag. 11 (**1995**) 37.

[13] R.S. Gorur, G.G. Karady, A. Jagota, M. Shah, A.M. Yates. IEEE Trans. Power Del. 7 (**1992**) 525.

[14] R.C. Buchanan. M. Dekker Eds. New York **1991**.

[15] R.A. Islam, Y.C. Chan, M.F. Islam. Mat. Sci. Eng. B-Solid. 106 (**2004**) 132.

[16] H. Cotton. The English Universities Press, Ltd. (**1958**) LOC TK3001.C65.

[17] K.S. Sidhu. Water Energy Int. 64 issue 3 (**2007**) 20.

[18] J.S. Forrest. Proc. IEE 79 (**1936**) 401.

[19] E.A. Cherney, D.J. Stonkus. IEEE Trans. on PAS 100 (**1981**) 131.

[20] J. Mort, G. Pfister. Electronic Properties of Polymers, J. Wiley and Sons New York (**1982**).

[21] K.S. Cole, R.H. Cole. J. Chem. Phys. 9 (**1941**)341.

[22] J. Vanderschueren. J. Polym. Sci. 15 (**1977**)873.

[23] S.M. Gubanski. IEEE Trans. Dielectr. Electr. Insul. 17 (**2010**) 325.

[24] L.H. Meyer, S.H. Jayaram, E.A. Cherney. IEEE Trans. Dielectr. Electr. Insul. 11 (**2004**) 1070.

[25] L.H. Meyer, S.H. Jayaram, E.A. Cherney. IEEE Trans. Dielectr. Electr. Insul. 11 (**2004**)620.

[26] G. Riquel, J.M. Fourmigué, R. Parraud. CIGRE(**1996**) Paper No. 33-304.

[27] R. Hackam.IEEE Trans. Dielectr. Electr. Insul.6 (**1999**) 557.

[28] H.M. Schneider, J.F. Hall, G.G. Karady, J. Renowden. IEEE Trans. Power Del.4 (**1989**)2214.

[29] L. Yang, W. Jianguo, Z. Mi, F. Chunhua, Z. Wenjun. 2008 International Conf. on High Voltage Engineering and Application, Chongqing, China, November 9-13, (**2008**)134.

[30] T. Tokoro, R. Hackam. IEEE Trans. Dielectr. Electr. Insul. 8 (**2001**) 1088.

[31] R.S. Bernstorf, T. Zhao.IEEE Electr. Insul. Mag. 14 (**1998**) 26.

[32] S.M. Gubanski. Proceeding of 13th Int. Symp. on High Voltage Engineering (ISH), (**2003**), Delft, Netherlands

[33] S.H. Carpenter, M. Kumosa. J. Mat. Sci. 35 (**2000**) 4465.

[34] J. Montesinos, R.S. Gorur, B. Mobascher, D. Kingsbury. IEEE Trans. Dielectr. Electr. Insul. 9 (**2002**) 236.

[35] M. Shah, J. Mackevich. IEEE Electr. Insul. Mag. 13 (**1997**) 5.

[36] J.F. Hall. IEEE Trans. Power Del 8 (**1993**) 376.

[37] B. Fuentes, T. Orbeck. IEEE Mexico October 29, (**1982**).

[38] E.A. Cherney. Position paper for the Canadian Electrical Association (ST-275) January **1987**.

[39] K. Bhowmick Anil, J. Konar, S. Kole, S. Narayanan. J. Appl. Polym. Sci. 57 (**1995**) 631.

[40] M. Ehsani,H. Borsi, E. Gockenbach, J. Morshedian, G.R. Bakhshandeh**.** Eur. Polym. J. 40 (**2004**)2495.

[41] A. De La O, R.S. Gorur, J. Chang.IEEE Trans.Power Del. 9 (**1994**) 2000.

[42] D.H. Han, H.Y. Park, D.P. Kang, H.G. Cho.IEEE Trans. Dielectr. Electr. Insul. 9 (**2002**) 323.

[43] Y. Hirano, T. Inohara, M. Toyoda, H. Murase, M. Kosakada.IEEE Trans. Dielectr. Electr. Insul. 8 (**2001**) 97.

[44] D.H. Han, H.Y. Park, D.P. Kang, K.E. Min. Proceedings of 6th International Conf. on Properties and Applications of Dielectric Materials (**2000**) 354.

[45] H. Deng, R. Hackam. IEEE Trans. Dielectr. Electr. Insul.5 (**1998**) 84.

[46] J.W. Chang, R.S. Gorur. IEEE Trans. Dielectr.Electr. Insul. 1 (**1994**) 1039.

[47] H. Homma, T. Kuroyagi, K. Izumi. IEEE Trans. Dielectr. Electr. Insul. 6 (**1999**) 370.

[48] X. Wang, N. Yoshimura.IEEE Trans.Dielectr. Electr. Insul. 6 (**1999**) 781.

[49] R.S. Gorur, J.W. Chang, O.G. Amburgey. IEEE Trans.Power Del. 5 (**1990**) 1923.

[50] D.H. Han, H.Y. Park, D.P. Kang, H.G. Cho, K.E. Min, K. Takasu, T. Knroyagi. IEEE Trans. Dielectr. Electr. Insul. 9 (**2002**) 323.

[51] R. Hackam. Proceedings of ISEIM (**1998**) 1.

[52] H.M. Schneider, W.W. Gnidi, J.T. Burnham, R.S. Gom, J.F. Hall. IEEE Trans. Power Del. 8 (**1993**) 325.

[53] B. Hardman, A. Torkelson. Encyclopedia of Polymer Science & Engineering, 2nd Ed., John Wiley & Sons Inc. 15(**1989**).

[54] J.H. Davis, D.E.W. Rees. Proc. IEE 112 (**1965**) 1607.

[55] R.G. Niemi, T. Orbeck. IEEE PES Summer Meeting (**1972**) paper C72 557-7.

[56] T. Orbeck, J. Braun, J. Seifferly. ESMO-83, Atlanta, Georgia, June 6-9, (**1983**).

[57] S.H. Kim, E.A. Cherney, R. Hackam. IEEE Trans. Power Del.5(**1990**) 1491.

[58] E.A. Cherney, R. Hackam S.H. Kim. IEEE Trans. Power Del.6 (**1991**) 1177.

[59] S.H. Kim, E.A. Cherney, R. Hackam.IEEE Trans. Power Del. 6 (**1991**) 1549.

[60] S.H. Kim, E.A. Cherney, R. Hackam. IEEE Trans. on Elec. Insul. 27 (**1982**) 1065.

[61] M.A.R.M. Fernando, S.M. Gubanski. IEEE Trans. Power Del. 15 (**2000**) 355.

[62] D. Birtwhistle, P. Blackmore, A. Krivda. IEEE Trans. Dielectr. Electr. Insul. 6 (**1999**) 612.

[63] G.H. Vaillancourt, S. Carignan, C. Jean. IEEE Trans. Power Del. 13 (**1998**) 661.

[64] A. De La O, R.S. Gorur, J.T. Burnham. IEEE Trans. Dielectr. Electr. Insul. 3 (**1996**) 827.

[65] T.G. Engel, M. Kristiansen, E. O'Hair. IEEE Trans. Magn. 27 (**1991**) 533.

[66] J.W. Chang, R.S. Gorur. IEEE 4th International Conf. on Properties and Applications of Dielectric Materials. (**1994**) NJ, USA,94CH3311-8.

[67] G.G. Karady, M. Shah, R.L. Brown. IEEE Trans. Power Del. 10 (**1995**) 1965.

[68] M.A.R.M Fernando, S.M. Gubanski. Trans. Dielectr. Electr. Insul. 6 (**1999**) 660.

[69] E.A. Cherney. Annual Report Conf. on Electrical Insulation and Dielectric Phenomena (**2005**) 1.

[70] P. J. Lambeth. Proc IEE, IEE Reviews 118 (**1971**) 1107.

[71] R. Sundararajan, R.S. Gorur. IEEE Trans. Dielectrc. Electr. Insul 3 (**1996**) 113.

[72] E.A. Cherney, R.S. Gorur. IEEE Trans. Dielectr. Electr. Insul. 6 (**1999**) 605.

[73] S. Kumagai, X. Wang, N. Yoshimura.IEEE Trans. Dielectr. Electric. Insul. 5 (**1998**) 281.

[74] S. Kumagai, N. Yoshimura. IEEE Trans. Dielectr. Electric. Insul. 6 (**1999**) 211.

[75] R.S. Gom, J. Montesinos, L. Varadadeslkan, S. Simmons, M. Shah. IEEE Trans. Dielectr. Electric. Insul. 4 (**1997**) 767.

[76] K. Eldridge, S. Boggs. IEEE Trans. Power Del. 14 (**1999**) 188.

[77] H. Long. "Basic compounding and processing of rubber. Rubber division, American chemical society(**1985**).

[78] J. Kroschwitz. Concise encyclopedia of polymer science and engineering. John Wiley & Sons (**1990**) 209.

[79] R.S. Gorur, E.A. Cherney, R. Hackam. IEEE Trans. Power Del. 3 (**1988**) 1892.

[80] S.H. Kim, E.A. Cherney, R. Hackam. IEEE Conf. on Electrical Insulation and Dielectric Phenomena (**1992**) 713.

[81] H. Deng, R. Hackam, E.A. Cherney. IEEE Trans. Power Del. 10 (**1995**) 1012.

[82] R. Omranipour, L. Meyer, S.H. Jayaram, E.A. Cherney. IEEE Conf. on Electrical Insulation and Dielectric Phenomena (**2001**) 632.

[83] S. Kumagai, N. Yoshimura. IEEE Trans. Dielectr. Electr. Insul. 8 (**2001**) 673.

[84] L. Meyer, V. Grishko, S. Jayaram, E.A. Cherney, W.W. Duley. IEEE Conf. on Electrical Insulation and Dielectric Phenomena (**2002**) 848.

[85] L. Meyer, S.H. Jayaram, E.A. Cherney.Trans. Dielectr. Electr. Insul. 11 (**2004**) 620.

[86] L.H. Meyer, E.A. Cherney, S.H. Jayaram. IEEE Elect. Insul. Mag. 20 (**2004**) 13.

[87] L.H. Meyer, S.H. Jayaram, E.A. Cherney.IEEE Trans Dielect. Electr. Insul. 11 (**2004**) 424.

[88] H. Hillborgl, U.W. Gedde. IEEE Trans Dielect. Electr. Insul. 6 (**1999**) 703.

[89] W. Lynch. Handbook of Silicone Rubber Fabrication, Van Nostrand Reinhold, (**1978**).

[90] H. Janssen, A. Herden, H.C. Karner. Intern. Symposium High Voltage Eng. Montreal (**1997**) 145.

[91] T. Tanaka. IEEE Trans Dielect. Electr. Insul. 12 (**2005**) 914.

[92] S. Rätzke, J. Kindersberger. XIVth Intern. Sympos. High Voltage Eng., Tsinghua University, Beijing, China (**2005**) C-09 1.

[93] L. Lei, W. Xishan, C. Dengke. Intern. Conf. Solid Dielectrics, Toulouse, France, (**2004**) 804.

[94] B. Nayak, P. Talwar A. Mansingh. IEEE 7th International Symposium on Applications of Ferroelectrics (**1991**) 334.

[95] M. Takeuchi. Proc. of the 3rd International Conf. on Properties and Applications of Dielectric Materials (**1991**) 1064.

[96] J. Pinghai, X. Chuanxiang,L. Fuyi, W. Shoutai. Electrical Electronics Insulation Conf. and Electrical Manufacturing & Coil Winding Conf. Proceedings (**1995**) 577.

[97] N.E. Frost, P.B. McGrath.Conf. on Electrical Insulation and Dielectric Phenomena (**1995**) 564.

[98] D.H Kuo, C.C. Chang, T.Y. Su, W.K. Wand, B.Y. Lin. J. Eur. Ceram. Soc. (**2001**) 1171.

[99] J.K. Nelson, J.C. Fothergill.Nanotechnology (**2004**) 586.

[100] Y. Shen, E.A. Cherney, S.H. Jayaram. IEEE International Symposium on Electr. Insul. (**2004**) 320.

[101] J. Hu, D.Y. Son. Silicones and Silicone-Modified Materials. S.J. Clarson, J.J. Fitzgerald, M.J. Owen, S.D. Smith Washington DC (**2000**).

[102] Y. Koshino, I. Nakajima, I. Umeda.Proceedings of EIM-30 Symposium, Toyohashi 465 (**1998**).

[103] E. Wendt, H. Jahn. Proceedings of Insul. News and Market Rep. Conf. Barcelona (**2000**).

2. SILICONE MATERIALS

Silicone materials have been produced commercially since the beginning of the 1940s. Nowadays they are used in many applications such as construction building, electrical, transportation, aerospace and cosmetics industries [1]. This is mainly due to the fact that silicone materials present both organic and inorganic materials properties which lead to a lot of advantages that cannot be found into organic rubbers.

2.1. General aspects and applications of silicones

Silicone polymers present a "polysiloxane" backbone made of sequences of$-[SiR_2-O]_n-$where R indicates alkyl groups such as methyl, vinyl, phenyl o per-fluoropropyl. These substituents can be easily varied and modulated in order to obtain silicone rubbers with different properties. The coexistence of inorganic $Si-O$ bonds, typical of minerals such as quartz or silica, and organic groups gives silicone a combination of interesting properties.

It is important to underline that the siloxane bonds$-Si-O-Si$ that form the backbone of the silicone chains are highly stable: with 433 kJ.mol^{-1}, their binding energy is higher than that of carbon-carbon bonds (355 kJ.mol^{-1}) that constitute rubbers from petrochemical. The lower silicon electronegativity (1.8) vs. carbon (2.5) leads to a very polarized Si-O bond, highly ionic (among 43%) giving rise to strong intermolecular interactions [2]-[4]. It is for this reason that, compared to common organic rubbers, silicones present a higher heat resistance and higher chemical stability. In addition, the siliceous structure gives them a particular affinity with the mineral fillers of this type.

Another important point is that silicone groups adopt an helical structure [5] (Figure 2.1) leading to low intermolecular forces between chains and therefore high elasticity, compressibility and flexibility even at very low temperatures.

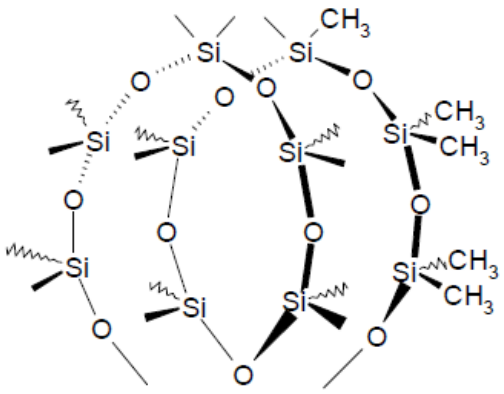

Figure 2.1: Helical structure of PDMS

Moreover, the organic groups, being oriented onto the external parts, can easily rotate around the backbone due to the high and flexible bond angle around the oxygen [6]. This high flexibility and the low intermolecular forces are reflected in the low glass transition temperatures (Tg~ -120°C) of the most common PDMS used. Due to the structural conformation of the silicone chains, the organic part can affect the properties of the material such as resistance or affinity with liquids and other mediums. They also define and govern the crosslinking of the material since the reaction occurs on them.

The dual nature of the material also has interesting implications for fillers incorporation and interactions with them. Silicones are usually loaded with various types of silica in order to impart the polymer sufficient toughness and others properties [5]-[8]. Indeed, silica particles actively participate in the filling of the intermolecular spaces between the chains supporting the intramolecular bonds. The affinity between silica and siloxane chains gives rise to a strong interaction between them and an excellent homogeneity of the mixture without segregation of the charges. For example, depending on the hardness desired, the amount of silica loaded is more or less high. Thanks to the small size of the fillers, the resulting material can retain a good transparency. Others fillers can be also used according to the final properties required such as thermal or electrical insulating enhancement [9]-[15].

The peculiar structure of silicones favors the properties diversity by varying the siloxane unit valence: oily, polymeric, resinous or crosslinked products can be obtained. Meantime, the presence of organic groups enhances the possibility to reach different range of modifications [16]. All these factors lead to a remarkable variety of silicone materials. Thousands of modern products rely in some way on silicones for performance and reliability [17]-[19] such as antifoam agents, silicone rubbers greases, paper coatings, release agents, sealants, hydrophobizing agents and silicone rubbers. Their unreactivity usually makes silicones non-toxic materials allowing them to be also used in food industry [23]. For instance, they give fundamental qualities to personal care products but they are also found in industrial or aerospace applications where they can increment the lifetime of the components. Silicone coatings can improve the conservation of historical monuments as well as windows or bathroom seals. Silicones are the ground materials for coolants in transformers, protective encapsulant for semiconductors but act also as foam-control in detergents [19]-[23]. The electronics and telecommunications industries also require silicones for the manufacturing of optical fibers, silicon wafers or solar cells. The different categories in which silicone materials can be applied are reported in Figure 2.2.

The silicone rubbers (generally used for insulators) are divided in two forms depending on their curing temperature. Usually, high-temperature vulcanizing (HTV) silicones are used for the production of the weathersheds while room temperature vulcanizing (RTV) silicones are employed as coating on ceramic surfaces to promote their pollution resistance.

HTV silicones are cured at high pressure and temperature and can be catalyzed by peroxide-induced free radicals or by hydrosilation reaction. This class of silicones is divided into Millable and Liquid Types according to the degree of viscosity. Liquid Silicone Rubber are usually employed for automated injection molding thanks to its excellent liquidity. On the contrary, RTV are cured at lower temperature by condensation reactions [24]. The difference in properties between HTV and RTV materials is due to the presence of linear low molecular weight species in HTV which diffuses better [25],[26]. Moreover, RTV silicone coatings

applied to ceramic outdoor insulators resulted more efficient, with long-term capacity to ensure anti-contamination properties [27].

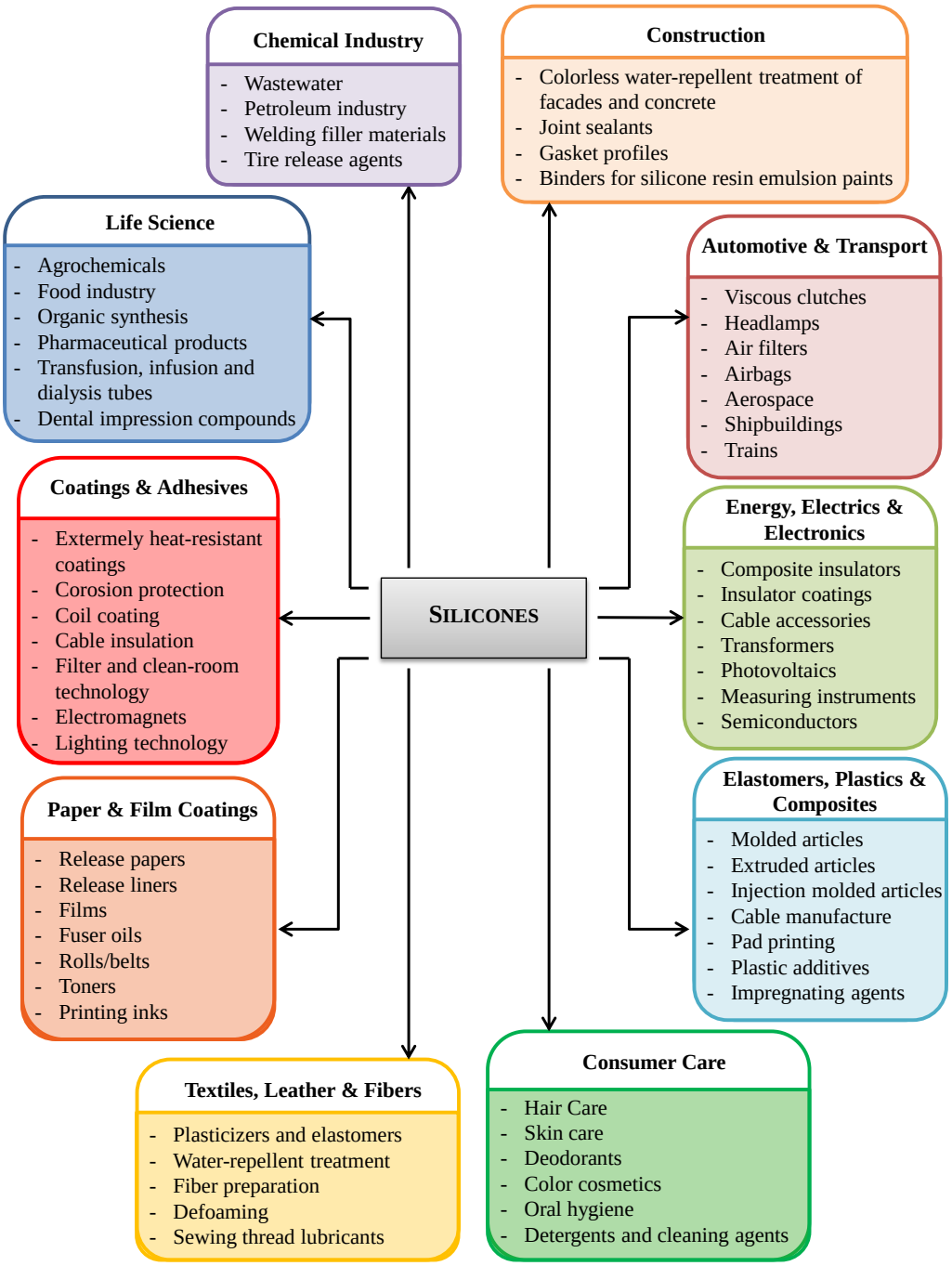

Figure 2.2: The extensive applications of silicones

2.2. Properties of silicone rubbers

Silicone rubbers initially found limited use to very specific fields in part because of the milder technical and design needs but also of their performances still far from those of today. However, with a slow but exponential growth, they became able to cover application areas unimaginable 50 years ago [28],[29].

The first property that originally attracted industry attention on them was their thermal stability and oxidation at high temperatures [4],[30]. Their heat resistance is far superior with respect to the organic rubbers. They can be used for an indefinite time at temperatures lower than 150 °C without registering any significant alterations of properties and for thousands of hours at 200 °C. Moreover, for short periods of time, temperatures up to 300°C can be tolerated. Therefore, silicone rubbers are employed to product components and parts for high-temperatures applications [31],[32].

Similarly, silicone rubbers present the highest cold resistance among the organic rubbers. They maintain their elasticity for temperatures up to -70°C and in some cases, they can tolerate extremely low temperatures (under -100°C). Usually, natural and ordinary rubbers exhibit considerable changes in deformation when exposed to drastic temperatures and are therefore not suitable for re-use. In contrast, silicones are relatively indifferent to temperature changes. Silicone oils present a viscosity variation with changing temperature lower than that of organic fluids [33]. The polymers retain an unusually high percentage of their resistance even for temperatures in the range of 200-250°C. Silicone paints not only resist to decomposition, but also to discoloration at high temperatures.

Silicone rubbers, more or less loaded with different minerals, present excellent insulators properties both in current and in alternating current. Moreover, they are not much affected by wet conditions and no rubbers are yet found to compete with the electrical properties of silicone rubbers for temperatures over 200°C. With a volume resistance between 10^{14} Ω.cm and 10^{16} Ω.cm and a strong resistance against corona discharge, they can be used for covering electrical cables and high-voltage systems [34].That is the reason why, in many countries, they have already replaced the epoxy resins in the production of insulation for high voltage. Specific

rubbers are also able to respond to very strict regulations of the sector in which, in addition to the electrical characteristics, flame resistance, thermal resistance, opacity and toxicity of fumes are also required.

Conductive silicone rubbers can also be manufactured by adding conductive fillers such as carbon black, silver and copper. In this way, the volume resistance can be reduced from 10^3 Ω.cm to few Ω.cm. They are mainly used for keyboard interfaces, antistatic material and shield materials for high voltage cables.

The silicone rubber by its nature does not burn easily, but once ignited continues to burn consistently. Moreover, in general, all silicones present the advantage of releasing few gases during combustion. However, it can be made a self-extinguisher material with addition of small amounts of flame retardants. Most common fillers used are metal oxides and hydroxides leading to silicone compounds in accordance with the regulations UL94 V-0 [35] or NF F 16-101 [36] without adding halogenated products as flame retardants, which could release toxic gases during combustion. Silicones are widely used in flame retardant applications thanks to their property against fire, especially for cables and wires. This is also due to the considerable resistance of the PDMS at high temperatures [37] since it starts to degrade at about 300 °C.

Contrary to organic polymers, when silicones are heated at high temperatures in the presence of oxygen, they release a residual silicon that acts as a barrier to the mass transport and retards the volatilization of decomposition products. Therefore, it reduces the amount of volatile compounds that burn in the gas phase and consequently the amount of heat that would return to the surface of the polymer. The residual silicon also serves to isolate the surface of the underlying polymer from the heat flow external, improving the thermal resistance [38].

Silicone rubbers, with respect to organic rubbers, usually present no extraordinary performance in terms of radiation resistance. However, this property can be enhanced by the presence of phenyl group in the material so that they can be used for cables in power plants and connectors. They also bear well environmental factors such as wind, rain, UV radiation and are therefore suitable for the production of articles with a strong aesthetic impact as they maintain their functional and esthetic characteristics for long periods. Moreover, they present

particularly high ozone resistance produced by electric corona-discharge that usually deteriorates quickly most of the organic rubbers [34].

Although having a good resistance to oils at room temperature, silicones are not as performant as nitrile butadiene rubbers (NBR) or chloroprene rubbers (CR). On the contrary, at high temperatures they manifest higher resistance [39]. In fact, organic rubbers start to lose their properties at temperatures above 100°C while silicones remain constants.

Due to their apolar organic nature, silicones also present excellent resistance to all polar solvents but also to both diluted bases and acids. Moreover, they present a strong tendency to swell, especially in non polar organic compounds such as benzene or toluene, but do not undergo decomposition or dissolution into them. This phenomenon is totally reversible by solvent removal and the original conditions are recovered [33]-[34]. This behavior is exploited for the molding materials that must withstand high temperatures and remain flexible at very low temperatures. However, they cannot be used in contact with strong acids and bases because they would be subject to a strong chemical deterioration.

Another important property of silicone rubbers is their water resistance. They can be soaked in water at temperatures ranging from 0°C to 100°C for long periods without deterioration of the mechanical strength or electric properties under atmospheric pressure. Moreover, the absorption of moisture in these conditions is less than 1% so that silicone rubbers are suitable for example in water sealing systems. Quite different is the behavior in high pressure steam over 150°C because of the low crosslinking density of the material that makes it more permeable to the molecules in the gaseous state [34].

With regard to the decay of the physical and mechanical properties, silicones can withstand steam for short exposures, but not at high pressures and temperatures since in such conditions Si-O bonds begin to break: the more the steam pressure increases, the faster the elastomer deteriorates due to hydrolysis. The resistance can be enhanced depending on the silicone rubber composition, curing agent and conditions of post curing.

Furthermore, silicone rubbers are physiologically inert and are employed for baby nipple and stoppers in medical applications [40].

Generally, not all silicones present all these properties simultaneously. The water repellency varies greatly from one product to another silicone. The same can be said of compatibility with organic materials. Some silicones do not have a particular stability to heat. However, most of the current uses of silicones dependent on one or more of the properties listed above [41].

References

[1] M. Biron. Techniques de l'Ingénieur October (**2007**) N2882.

[2] M.J. Owen. Chimie Nouvelle 85 (**2004**) 27.

[3] B. Hardman. Encycl. Polym. Sci. Eng. 15 (**1989**) 204.

[4] F.O. Stark, J.R. Falender, A.P. Wright. Compr. Organomet. Chem. 2 (**1982**) 305.

[5] E. Benedetti, C. Pedone, G.Allegra. Macromolecules 3 (**1970**) 16.

[6] M.J. Owen. Adv.Silicones and Silicone-Modified Materials 1051 (**2010**) 13.

[7] S. Thomas, R. Stephen. (Eds: J. Wiley and Sons) (**2010**).

[8] F.Y. Hshieh. Fire Mater. 22 (**1998**) 69.

[9] M. Sangermano, F. Deorsola, D. Fabiani, G. Montanari, G. Rizza. J. Appl. Polym. Sci 114 (**2009**) 2541.

[10] T. Tanaka, G.C. Montanari, R. Mulhaupt. IEEE Trans Dielect. Electr. Insul 11 (**2004**) 763.

[11] C. Zilg, D. Kaempfer, R. Mulhaupt, G.C. Montanari. IEEE Conf. Electr. Insul. Dielectr.Phenomena (**2003**) 546.

[12] G.C. Montanari, D. Fabiani, F. Palmieri, D. Kaempfer, R. Thomann, R, Mulhaupt. IEEE Trans Dielect. Electr. Insul.11 (**2004**) 754.

[13] Y. Yin, J. Chen, D. Xiao, D. Tu, R. Yin, H. Qian. IEEE 7th Int. Conf. Prop. Appl. Dielect. Mat. Nagoya (**2003**) 913.

[14] J.K. Nelson, Y. Hu. J. Phys. D: Appl. Phys.38(**2005**) 213.

[15] J.K Nelson, J.C. Fothergill. Nanotechnology 15 (**2004**) 586.

[16] R. Richter, G. Roewer, U. Böhme, K. Busch, F. Babonneau, H:P: Martin, E. Müller. Appl. Organomet. Chem. 11 (**1997**) 71.

[17] B.R. Wood, P. Hodge, J.A. Semlyen. Polymer 34 (**1993**) 3052.

[18] K.K. Kyodo Giken Kagaku. Patent J04248887 (**1992**).

[19] M.E. Dillon, D.K. Lange. Polym. Mater. Sci. Eng. 65 (**1991**) 84.

[20] M.J. Michael, T.M. Swager. Polym. Prepr. 331 (**1990**) 1196.

[21] G. Schottner. Chem. Mater. 13 (**2001**) 3422.

[22] G. Eberle, H. Schmidt, W. Eisenmenger. IEEE Trans. Dielectr. Electr. Insul. 3 (**1996**) 624.

[23] K. Zong, J.R. Reynolds. J. Org. Chem. 66 (**2001**) 6873.

[24] M. Amin, M. Akbar, S. Amin. Sci. China. Ser. E-Tech. Sci. 50 (**2007**) 697.

[25] J.P. Renders, I.R. Jandrell, S.M. Renders IEEE Trans. Dielectr. Electr. Insul. 6 (**1999**) 620.

[26] G. Momen, M. Farzaneh. Recent. Adv. Mater. Sci. 27 (**2011**) 1.

[27] E.A. Cherney. IEEE Electr. Insul. Mag. 11(**1995**) 8.

[28] T.D. Tilley. (Eds: S. Patai, Z. Rappoport). Chichester: John Wiley and Sons (**1989**).

[29] B. Marciniec, H. Maciljewski. (Eds: J. Matisons) Advances in Silicone Science 1(**2009**).

[30] W. Noll, Chemistry and technology of silicones, Academic Press (**1968**).

[31] D. Thomas. Polym 13 (**1972**) 479.

[32] A.W. Henry. Rubber Chem. Technol. 56 (**1982**) 83.

[33] W. Lynch. Handbook of Silicone Rubber Fabrication. (Eds: Van Nostrand Reinhold Company) June (**1979**).

[34] HRS Co. Ltd. Silicone Rubber Products. October (**2008**).

[35] UL 94. Standard for Safety of Flammability of Plastic Materials for Parts in Devices and Appliances testing. Underwriters Laboratories. USA.

[36] J. Troitzsch. Plastics Flammability Handbook. (Eds: Hanser Gardner Pubns) (**2004**).

[37] G. Camino, S.M. Lomakin, M. Lazzari. Polymer 42 (**2001**) 2395.

[38] F.Y Hshieh. Fire Mater. 22 (**1998**) 69.

[39] Sheet Rubber Handbook-Gasket & Packing Materials. Rubber Manufacturers Association (RMA)IP-40.

[40] ECETOC Joint assessment of commodity chemical no 26 (**1994**).

[41] R.N. Meals, F.M. Lewis. (Eds: Aldo Martello Editore) (**1959**).

3. HYDROSILATION REACTION

Silicone polymers can be cured following different methods, depending if a room-temperature vulcanization (RTV) or a high-temperature vulcanization (HTV) reaction is employed. The HTV silicones can be achieved mainly with 2 different methods.

The vulcanization reaction by using peroxides [1]-[2] occurs via a radical chain polymerization reaction which is started and promoted by homolitic cleavage of organic peroxides. The generated radicals can attach the vinyl C=C double bond with subsequent formation of chemical crosslinks between the polymeric chains (Figure 3.1).

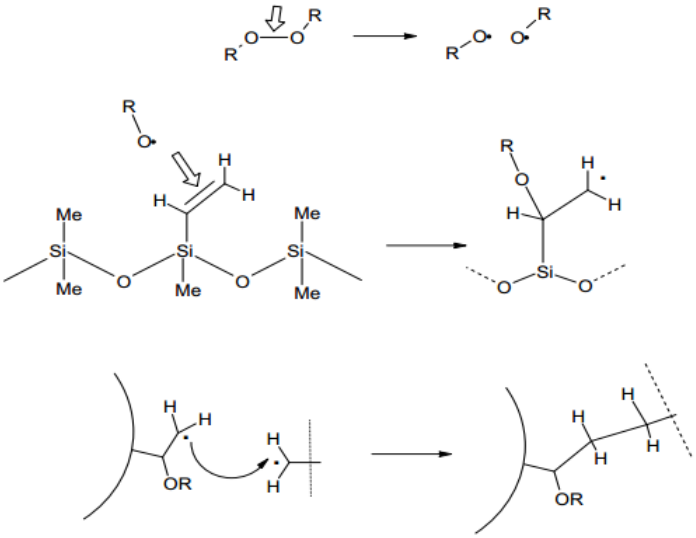

Figure 3.1: Vulcanization reaction by using peroxides

The vulcanization by using platinum catalyst is similar to a polymerization reaction. It is known as hydrosilation reaction and occurs between vinyl groups and silane groups present on different silicone chains [3]. This reaction is catalyzed by platinum compounds. (Figure 3.2).

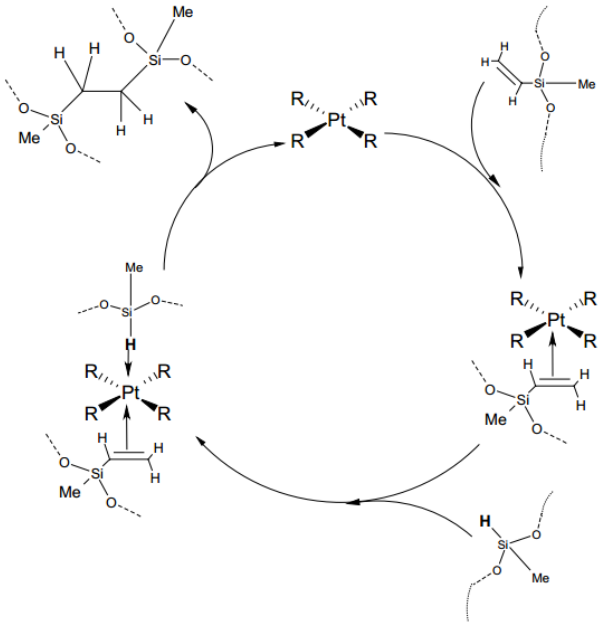

Figure 3.2: Vulcanization reaction by platinum catalysis

3.1. General aspects of hydrosilation reaction

As already mentioned, the hydrosilation is the addition of a Si-H bond across a double bond according to the scheme reported in Figure 3.3.

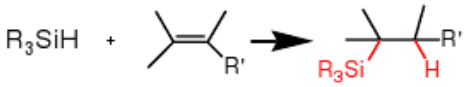

Figure 3.3: Hydrosilation reaction

This process progressively became the method of choice for synthesizing organofunctional silicon compounds and is still used in silicone industry to form crosslinked silicone polymers (Figure 3.4).

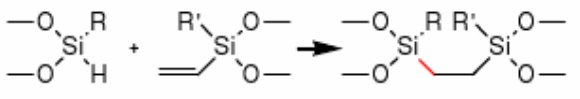

Figure 3.4: Silicone polymers crosslinking

This is a complex reaction and therefore it is difficult to make a really effective use of it. Numerous products were obtained by the reaction of silane with olefins as reported in Table 3.1 [4].

Table 3.1: Products obtained by the reaction of silanes with olefins

Silane	*Olefin*	*Product*
1. A monomer ($HSiCl_3$)	A monomer (C_2H_4)	An alkylsilane ($C_2H_5SiCl_3$)
2. A monomer ($HSiCl_3$)	An olefinic silane ($CH_2CHSiCl_3$)	A silethylene ($Cl_3SiCH_2CH_2SiCl_3$)
3. A monomer ($HSiCl_3$)	An organic polymer ($CH_2{=}CHRCH{=}CH_2$)	A silylated polymer $(Cl_3SiCH_2CH_2)_2R$
4. A monomer ($HSiCl_3$)	A siloxane polymer 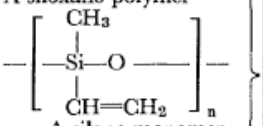 A silane monomer $CH_2{=}CHSiCl_3$	A silylated siloxane 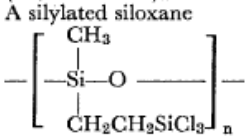
5. A polymer 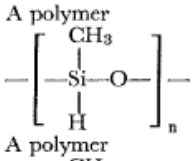		
6. A polymer 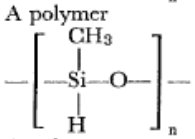	A monomer (C_2H_4)	An alkylsiloxane 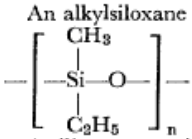
7. A polymer 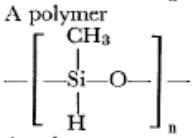	An organic polymer	A silicone-organic copolymer
8. A polymer 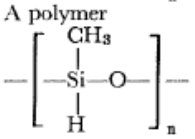	A siloxane polymer	A cross-linked or cured siloxane polymer

The hydrosilation reaction does not take place spontaneously at room temperature. The mixture has to be heated and catalyst are often needed. The temperature, catalyst and the groups on the olefine and silane affect the rate of the reaction.

Platinum catalysts, at concentrations as low as 10^{-6} molar can increase the reaction rate from 10^4 to 10^6 times as compared to those of uncatalyzed thermal reactions. Catalytic hydrosilation of olefines with soluble compounds of platinum was first described by Speier et. al. and the actual commercial catalyst ($H_2PtCl_6 \cdot 6H_2O$/*i*PrOH) bears his name [5],[6].

A transition metal complex, especially an electron-rich complex of a late transition metal (Co(I), Rh(I), Ni(0), Pd(0), or Pt(0)) activates both hydrosilanes, ($HSiR_3$) and a variety of substrates (typically alkenes) [7],[8]. A catalytic cycle which contains two steps is represented in Figure 3.5.

The conventional hydrosilation of alkenes achieved with the Speier catalyst is generally presumed to occur by the Chalk-Harrod mechanism (Figure 3.5, cycle A) [9]-[13]. Oxidative addition of a hydrosilane gives a hydride-silyl complex (**I**) which is coordinated with the substrate alkene (extremely rarely isolated at this stage).The complex (**I**) is subjected to migratory insertion of the alkene into the M-H bond (*hydrometallation*) to give the alkyl-silyl species (**II**). Reductive elimination of the alkyl and silyl ligands from the complex (**II)** forms the hydrosilation product.

Although the Chalk-Harrod mechanism describes an alkene isomerization, a second mechanism has been suggested which includes preferentially an alkene insertion into the M-Si bond (*silylmetallation*) by using Rh(I) or Co(III) catalyst precursor to form the β-silylalkyl-hydride intermediate (**III**) followed by reductive elimination to complete the hydrosilation [14]-[16] (Figure 3.5, cycle B).

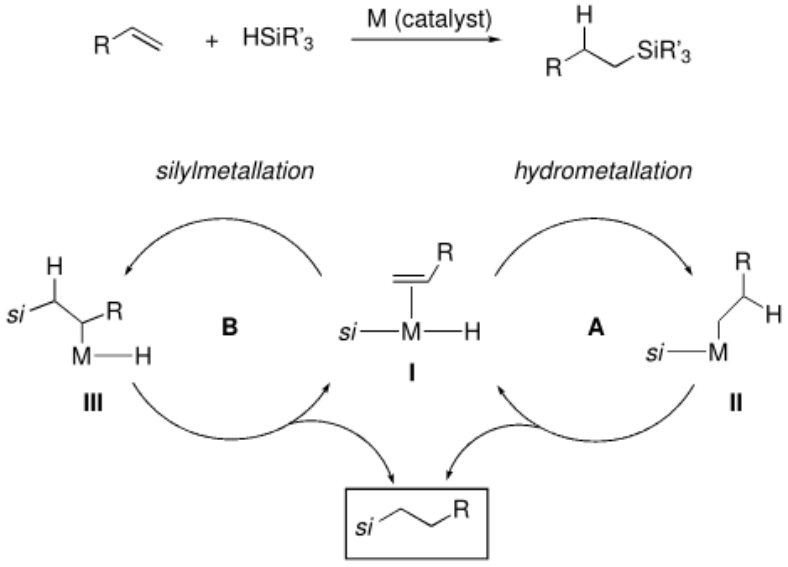

Figure 3.5: Mechanism of silylmetallation and hydrometallation

It is important to underline that hydrosilanes present a broad reactivity spectrum in the oxidative addition depending on the substituents on the silicon atom and the nature of the metal catalyst. Thus, Pt complexes tolerate any hydrosilane, such as $HSi(OR)_3$,$HSiCl_nMe_{3-n}$ or H_nSiR_{4-n} (n=1~3; R=alkyl or Ph) in the hydrosilation while, Pd complexes are applicable mostly to $HSiClnR_{3-n}$ (n=2, 3) and Rh complexes to preferably $HSiR_3$ [17].

Uncatalyzed thermal reactions are feasible and practical with simple olefins. At 250-350°C for alkyl or chlorosilane, or at 120°C for silane itself the reaction takes several hours, and yields obtained are ranging from 50 to 95%. If a few mole per cent of acetyl or benzoyl peroxide is added to the reaction mixture, reaction occurs at about 100°C.

Other free-radical initiators such as peresters, azobisisobutyronitrile, ultraviolet light produce similar effects. Free-radical initiators are appropriates for adding trichlorosilane to simple olefins when milder reaction conditions are necessaries with respect to thermal reactions. The mechanism of addition initiated by peroxides or irradiation seems to fit the free-radical mechanism, as proposed by Sommer et. al [18]-[19].

3.2. Photoactivated hydrosilation addition

Platinum complexes and many others are useful as catalysts for accelerating the thermally-activated addition reaction between compounds containing silicon-bonding hydrogen and compounds containing aliphatic unsaturation. However, processes for promoting UV or visible radiation activated addition reaction between these compounds are much less common.

3.2.1. Mechanism of reaction

Bis(acetylacetonate)platinum(II) (Figure 3.6 complex **1**) or $Pt(acac)_2$, was recently reported to serve as a photoactivated catalyst for hydrosilation addition of

silanes to alkenes [20]. This catalyst is activated by near-UV irradiation which is thought to produce a homogeneous catalyst by loss of one bidentate ligand in the presence of silicon hydride or olefin. The resulting complex **2** is the primary active catalyst, and once formed, **2** remains active such that the reaction proceeds without light. A less active heterogeneous catalyst, consisting of Pt(0)colloids [21], is also produced more slowly from **2**during and after irradiation.

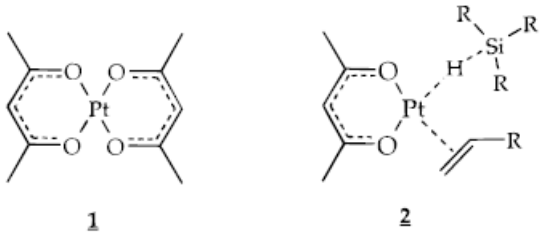

Figure 3.6: Photoactive Pt catalyst and its relative activated complex

Other examples of catalysts for the hydrosilation reaction which are activated by radiations were also reported: η(2-cyclopentadienyl) trialkylplatinum forms colloidal platinum hydrosilation catalyst when irradiated in solutions containing silanes [22].

Correlation between results of hydrosilation formation and spectral changes, which accompanies irradiation of $Pt(acac)_2$ in the presence of Et_3SiH or Et_3Si(vinyl), indicate that the irradiation time required to generate the active hydrosilation catalyst corresponds to the time required for essential complete disappearance of the long-wavelengths UV absorption band of the $Pt(acac)_2$ and for the formation and destruction of primary photoproduct detected both by UV and ^{1}H-NMR spectroscopy [23]. However, the complete photodecomposition of $Pt(acac)_2$,to liberate both ligands and form colloidal platinum, does not occur during this brief irradiation period. These observations make postulate that short periods of irradiation result in the formation of homogeneous hydrosilation catalyst which is slowly converted to a less active heterogeneous catalyst similar to that formed upon $Pt(acac)_2$thermal decomposition (reported in Figure 3.7).

This mechanism, proposed by Lewis et al.[20], is extended to the current polymerization system. In this mechanism, the absorption of two photons is

required to cleave a ligand from **1** and produce the secondary photoproduct **2** which is believed to be a homogeneous catalyst. Further absorption of light by **2** leads to destruction of the homogeneous catalyst and formation of a heterogeneous hydrosilation catalyst consisting of Pt(0). Platinum colloids growth during addition reactions was reported as a result of the latter process.

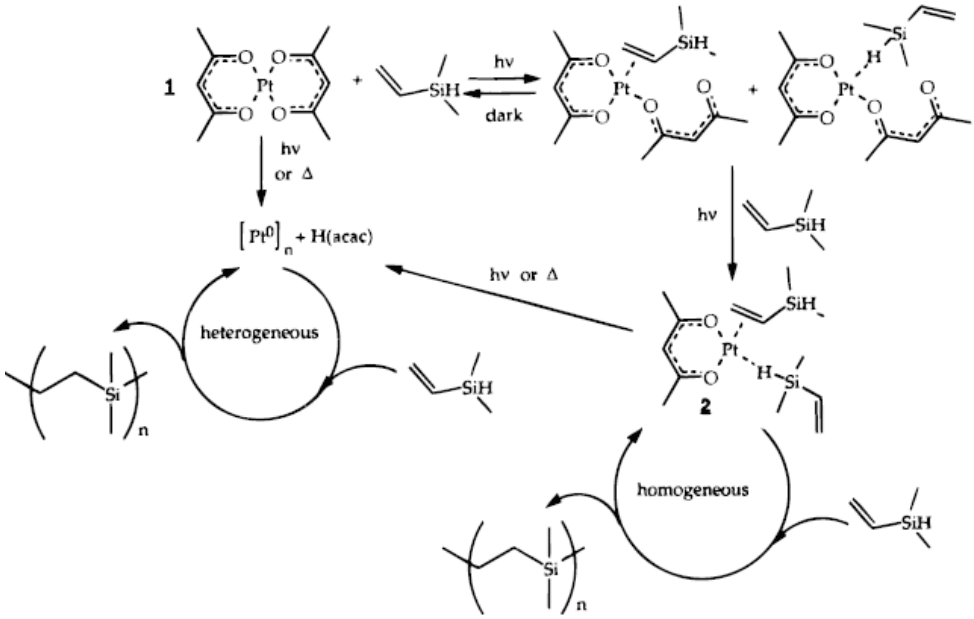

Figure 3.7: Representation of UV-induced hydrosilation reaction

Photoinitiated reactions can be employed for the polymerization of vinyl-silanes [24],[25] as shown in Figure 3.8. After a brief induction period, vigorous consumption of the silane monomer occurs resulting in complete conversion of the monomer to low molecular weight polymers and small amounts of dimers. Experiments conducted in this manner exhibited such vigorous exothermic reaction that the sealed reaction tubes burst.

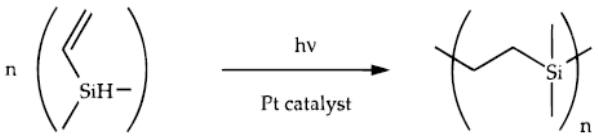

Figure 3.8: Polymerization of vinyl-silane

In the absence of either $Pt(acac)_2$ or light, only minor amounts of monomer conversion occurred and negligible amounts of products resulted. Because of the difficulty to control the above reactions, most of the experiments were conducted at lower concentrations which slowed the reaction rates compared to neat monomer. Dichloromethane was used because it readily dissolves $Pt(acac)_2$ and does not inhibit platinum catalysis.

The consumption of 2 M vinyldimethylsilane under irradiation and the concomitant production of dimers are reported in Figure 3.9. An initial shoulder on the monomer consumption curve shows that there is an induction time of about 5 min. This is attributed to the photochemical formation of a homogeneous active catalyst consisting of a $Pt(acac)_2$ and silicon hydride or olefin complex (**2**) which subsequently mediates hydrosilation. Complete conversion of the monomer to polymer and dimers takes approximately 20 min at 2 M initial concentration.

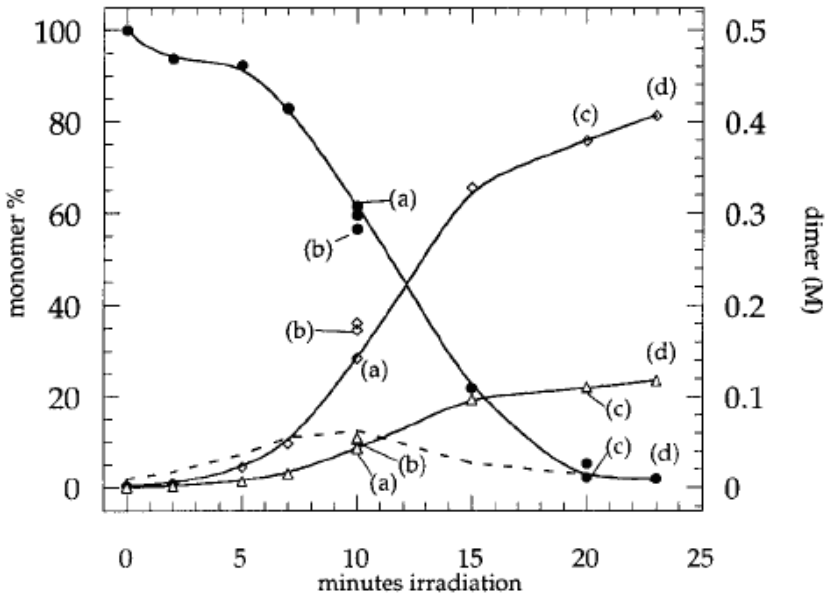

Figure 3.9: Gas Chromatography results of 336 nm irradiation of 2M vinyldimethylsilane in CH_2Cl_2 with $5*10^{-3}$ M $Pt(acac)_2$. ●: 1,1,2,3,3-pentamethyl-1,3-disilacyclopentane, ◇: 1,1,4,4-tetramethyl-1,4-disilacyclohexane, △: transiet dimmer, - - - - - - - - Argon bubbled, (a) oxygen bubbled, (b) freeze/pump/thaw degassed, (c) Hg drop added.

This polymerization is a step reaction which takes place on the photogenerated platinum centers. The molecular weight of the polymer, shown in Table 3.2, is about 50% higher when produced with 10 min of irradiation than with 20min. This is expected since fewer activated catalytic sites resulting from less complete photoactivation in a given concentration of monomer should produce longer polymer chains. These activated centers remain with the polymer after formation, producing chain growth linearly from vinyl and hydride end-groups even after the monomer is completely consumed. This apparently takes place by addition of polymer chains to one another.

Table 3.2: PDMVS molecular weight prepared from 2M monomer

Hv (min)	Aged[a] (months)	Mw	PD	Polym. yield (%)
10	0	5500	2.5	61
10	6	12300	3.4	55
20	0	3700	2.1	74

[a]Each was held for 40 min in the dark at 25°C postirradiation

The molecular weight of polymer measured six months after irradiation of the monomer solution (Table 3.2) is more than two times the molecular weight immediately after illumination. Brown color due to platinum colloids appears in the photoactivated solutions about one day after irradiation. The colloids could not be removed by filtration and are probably responsible for hydrosilation of the polymer during aging. As discussed previously, heterogeneous catalysis may be responsible for the increase in the polymer molecular weight during aging, while homogeneous catalysis by the complex (**2**) is probably active during the initial reaction of the monomer (Figure 3.7).

Bubbling the solutions with oxygen or argon prior to irradiation had no significant effect on the reaction rates or product distributions compared to samples prepared in air (both with 2 M and 0.5 M vinyldimethylsilane concentrations). This is in contrast with the findings of Lewis et al. who determined that hydrosilation addition reactions catalyzed by the secondary photoproduct were inhibited by oxygen.

Rigorous removal of dissolved gases by freeze/pump/thaw prior to irradiation did not significantly alter the course of the reaction either. These results demonstrate that oxygen does not function as a reactant, co-catalyst, or significant inhibitor of this polymerization reaction.

If the complex (**2**) is the main catalyst during monomer consumption (Figure 3.6), the absence of oxygen inhibition in hydrosilation reaction might means that the polymerization of vinyldimethylsilane is competitive with oxygen coordination at the catalytic surfaces. Alternatively, if this complex is not a major player and instead the reaction is primarily heterogeneous, early polymerization may take place before Pt(0) colloids large enough to scatter light (and be detected by absorption) are formed. Platinum colloids of this small size are likely to produce relatively fast hydrosilation reactions.

In absence of light, solutions containing platinum (II) bis(β-diketonate), hydrosilane and olefin are stable indefinitely at 25°C but undergo slow adduct formation at 80°C. Rapid hydrosilation is observed when a dichloromethane solution containing $5x10^{-4}$ M $Pt(acac)_2$, 0.5 M Et_3SiH and 0.5 M $Et_3Si(vinyl)$ is either irradiated continuously or irradiated for a short period of time and then placed in the dark.

Irradiation of Et_3SiH and $Et_3Si(vinyl)$ in the presence of several catalysts such as Pt(II) β-diketonates, $Pd(acac)_2$ and $Ni(acac)_2$ has also been investigated. The time dependence of adduct formation with $Pt(acac)_2$, $Pt(ba)_2$ (ba= benzoylacetonate), $Pt(dmb)_2$ (dmb= dibenzoylmethanate) and $Pt(hafac)_2$ (hafac= hexafluoroacetylacetonate) is shown in Figure 3.10. The rates of reaction at $5x10^{-4}$ M catalyst concentration are similar when $Pt(acac)_2$, $Pt(ba)_2$and $Pt(dmb)_2$ are used, but the rate for $Pt(hafac)_2$ is lower. Irradiation of Et_3SiH and $Et_3Si(vinyl)$ in the presence of $Ni(acac)_2$ or $Pd(acac)_2$ results in formation of Hacac and precipitated metal but fails to produce detectable hydrosilation adduct, even after prolonged irradiation.

The generation of an active hydrosilation catalyst requires the presence of a Pt β-diketonate and either Et_3SiH or $Et_3Si(vinyl)$ during the irradiation. Thus irradiation of $5x10^{-3}$ M $Pt(acac)_2$ and 0.5 M Et_3SiH in deareated dichloromethane

solution followed by the immediate addition of Et_3Si(vinyl) (0.5 M) results in adduct formation. Similar results are obtained upon immediate addition of Et_3SiH (0.5 M) to an irradiated solution of $5x10^{-3}$ $Pt(acac)_2$ and 0.5 M Et_3Si(vinyl).

However, irradiation of $5x10^{-3}$ M $Pt(acac)_2$ and 0.05 M Et_3SiH followed by the immediate addition of Et_3SiH (0.45 M) and Et_3Si(vinyl) (0.5 M) results in only 4.1% adduct formation after 4 hours dark reaction time and 43% adduct formation after 24 hours dark reaction time.

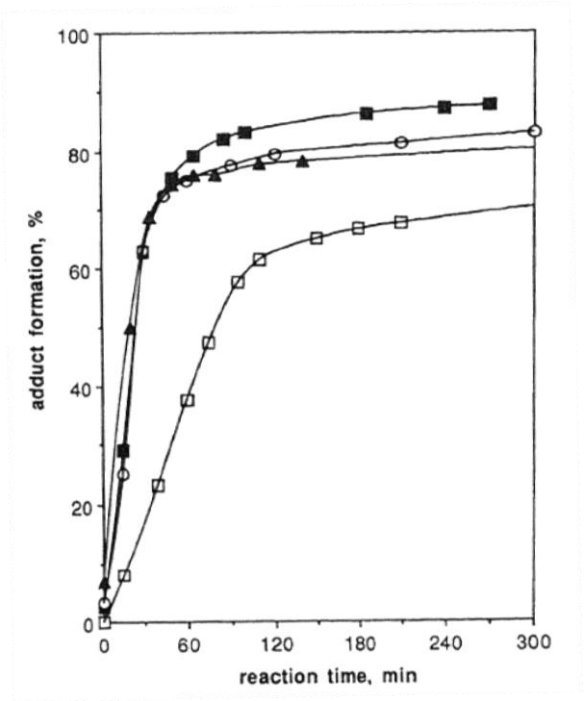

Figure 3.10: Adduct formation vs dark reaction time for deaerated dichloromethane solutions containing 0.5 M Et_3SiH and Et_3Si(vinyl) after 10 min of irradiation in the presence of $5x10^{-3}$M $Pt(acac)_2$ (○), $Pt(ba)_2$ (■), $Pt(dbm)_2$ (▲) or $Pt(hafac)_2$ (□)

3.2.2. Nature of the homogeneous catalyst

The Chalk-Harrod mechanism for platinum-catalyzed homogeneous hydrosilation involves oxidative-addition of a hydrosilane to a square-planar platinum(II)-olefine complex to form an octahedral platinum (IV) complex [10]. The mechanism is reported in Figure 3.11. A hydrid shift followed by reductive

elimination yields the hydrosilation adduct and coordination of another olefine regenerates the homogeneous catalyst.

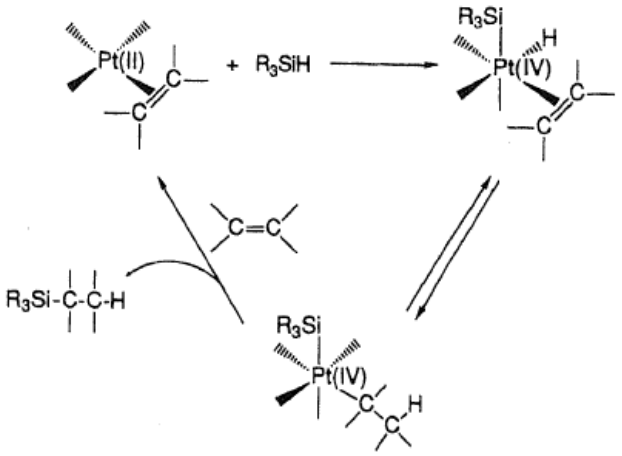

Figure 3.11: Chalk-Harrod mechanism for platinum-catalyzed homogeneous hydrosilation reaction

A variation of mechanism was proposed by Schroeder and Wrighton [25] for photoinduced hydrosilation using $Fe(CO)_5$ as catalyst precursor (Figure 3.12). Irradiation of $Fe(CO)_5$ results in loss of CO and formation of $Fe(CO)_4$ which can react with hydrosilane to yield a metal silyl hydride or with an olefine to form a metal-olefine complex. No complex was found to be a hydrosilation catalyst. However, absorption of a second photon by either complex and loss of a second CO results in the formation of the active catalyst $(H)(R_3Si)Fe(CO)_3$-(olefine).

The first step of the hydrosilation cycle is the insertion of the olefine into the metal-silyl bond (i.e. silyl migration). Immediate reductive elimination of the alkylsilane (the hydrosilation adduct) followed by the reaction with additional olefin and hydrosilane molecules results in the regeneration of the catalyst.

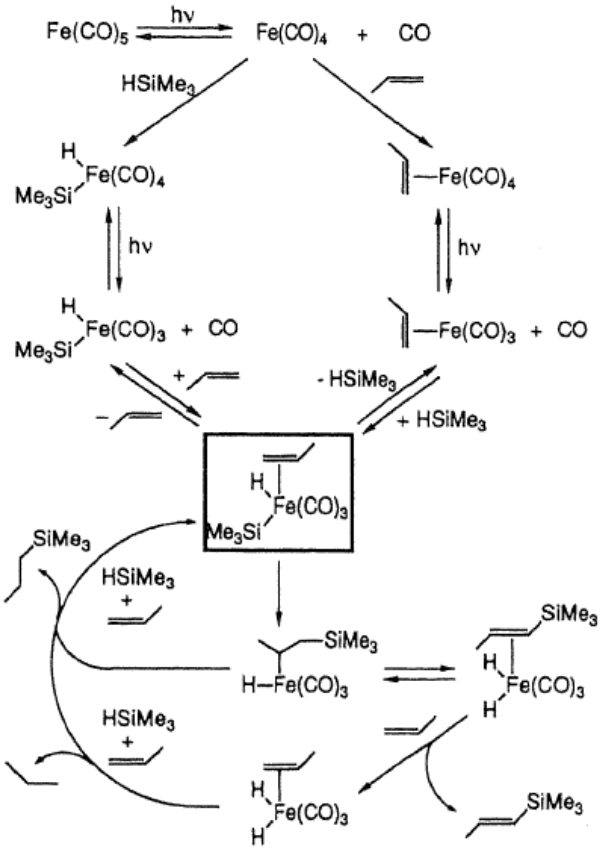

Figure 3.12: Schroeder-Wrighton mechanism for platinum-catalyzed homogeneous hydrosilation reaction

Irradiation of $Pt(acac)_2$ initially results in reversible Pt-O homolysis to yield a coordinatively-unsaturated intermediate which can subsequently be trapped by high concentration of hydrosilane or olefin (> 0.1 M) and form a primary photoproduct (Figure 3.13).

While the primary photoproducts obtained in the presence of hydrosilane and olefins have not been isolated and characterized, their UV and ^{1}H-NMR spectra are indicative of the formation of a hydrosilane or olefin complex with one chelating and one monodentate acetylacetonate (acac) ligand. The mode of metal-ligand bonding is presumably square planar for the olefine [26] and either square-planar agnostic or square-pyramidal for the hydrosilane [27].

When irradiation is terminated after the conversion of $Pt(acac)_2$ to primary product and when the complementary reactant is added; the hydrosilation is

observed and the primary product slowly reverts to $Pt(acac)_2$ upon standing in the dark. Thus, the primary products are not active hydrosilation catalysts.

However, continued irradiation results in complete loss of one acac ligand and formation of the active homogeneous catalyst. Loss of acac yields to a secondary photoproduct, presumably a coordinatively-unsaturated mono-acetyl complex capable of coordinating either two hydrosilanes or two olefins. Upon introducing the complementary reactant, the secondary photoproduct can either undergo ligand exchange or catalyze hydrosilation (Figure 3.13).

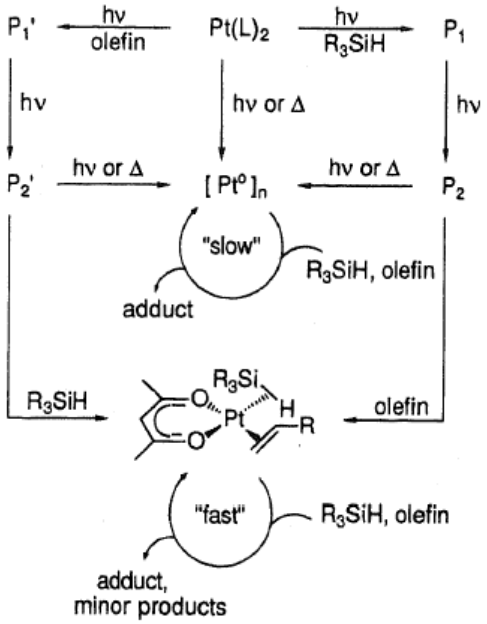

Figure 3.13: Hydrosilation mechanism with Pt catalyst

3.2.3. Metal, Hydrosilane and Olefine dependence

Irradiation of $Pt(acac)_2$ in the presence of Et_3SiH and $Et_3Si(vinyl)$ results in hydrosilation reaction whereas irradiation of $Ni(acac)_2$ or $Pd(acac)_2$ under the same condtions does not. This difference is consistent with the much larger quantum yields for conversion of $Pt(acac)_2$ to primary photoproduct in the presence of hydrosilane or olefins [28]. $Ni(acac)_2$ and $Pd(acac)_2$ have been reported to serve as catalyst precursor for thermal hydrosilation [29].

Both electronic and steric effects are known to influence the reactivity of the hydrosilane in platinum-catalyzed hydrosilation of olefins; electron withdrawing substituents increase reactivity and bulk substituents decrease reactivity [29].

Platinum-catalyzed hydrosilation is also known to be sensitive to olefin substitution. A pronounced steric dependence is indicated by the failure of internal olefins to undergo hydosilation. Electron-withdrawing halogen and alkoxy substituents decrease the rate of ethylene hydrosilation, and electron donating aromatic substituent increase the rate of styrene hydrosilation.

3.3. The limits of platinic silicones

In the last years, a significant increase in requests for formulations with platinic acceleration was observed, both for molding and extrusion. An example is the current production of silicone TSF (Italy) with approximately 40% of platinic compounds.

Despite the slightly higher price of the compounds, the economic advantages are reflected in the production field. In fact, the platinic accelerations are significantly faster than the traditional ones leading also to a better demolding with comparison to the peroxide compounds. Furthermore, the manufacturing environment is enhanced since these compounds do not emit fumes or odors during the vulcanization reaction.

Other advantages are found on the physical-mechanical characteristics of the final product, especially the tear strength (greater than 30% compared to the peroxide formulations) and the elongation at break in addition to high transparency. However, it should be noted that the crosslinked platinum compounds tend to show a worsening of the compression with respect to their peroxide counterparts. In some cases, this decay is partially offset by the reduction of demolding agents, substances whose presence in the formulations will affect the compression performances of the silicones. This type of silicone compounds offers therefore various benefits, but requires some precautions regarding their management and processing.

First, due to the higher cure speed, storage times are reduced compared to the peroxide catalyzed silicones and are adversely affected by temperature rise during summer. Secondly, platinum catalysts are very sensitive to the "poisoning" caused by amines, peroxides and sulfur products which can compromise the vulcanization: this is the reason why they must be stored and manipulated away from the traditional organic and silicone rubbers in order to reduce the risks of pollution.

3.4. Actinic radiation-activated hydrosilation reaction

Some patents report about the actinic radiation-activated hydrosilation reaction in the presence of platinum complex and a free-radical photoinitiator capable of absorbing actinic radiation [30]-[33]. A photosensitizer can also be employed in order to use longer wavelengths and transfer the actinic energy to the platinum complex or to the platinum complex/free radical photoinitiator combination. By this process it could be possible to both synthesize low molecular weight compound and cure high molecular weight polymers containing unsaturated groups. The advantage of using the free-radical photoinitiator in the actinic radiation-activated hydrosilation is due to the unexpected acceleration of the reaction with a reduction of 85% of curing time.

Different platinum catalysts were employed for the UV-Vis activation of the hydrosilation reaction. Representative examples of suitable Pt(II) beta-diketonate complexes include Pt(II) bis (2,4-pentanedionate), Pt(II) bis(2,4-hexanedionate), and Pt(II) bis(1,3-diphenyl-1,3-propanedionate).

The actinic radiation-activation avoids the reaction composition to react prematurely or readily in the absence of actinic radiation. As heat is not required, the addition reaction can be carried out on the surface of a heat-sensitive substrate without adversely affecting the substrate. Moreover, actinic radiation curing requires less energy than does thermal curing. Because visible light can be used, the reaction can be conducted so as to provide greater safety than is possible with compositions that require ultraviolet radiation.

The β-dicarbonyl platinum complexes, which structure is reported in Figure 3.14, were first synthesized in 1928 by Menzies [34]. The use of the trimethyl (β-dicarbonyl) platinum(IV) complexes as photohydrosilation catalysts was analysed later on [35].

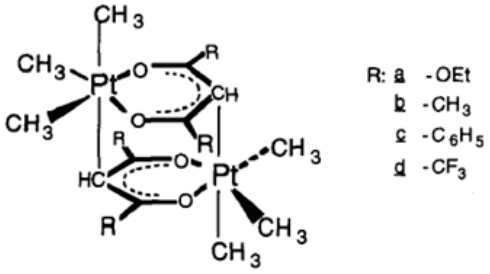

Figure 3.14: Dimeric structure of the trimethyl(β-dicarbonyl) platinum (IV)

The efficiency of these compounds as catalysts for hydrosilation reaction were checked by using a model mixture of silicone polymers containing Si-H and Si-vinyl parts. The observed reactivity of the complexes as photohydrosilation catalysts follows the trend a > b > d > c. Under irradiation the complexes are decomposed via a triplet excited state and a radical stage into an active hydrosilation catalyst and finally into less reactive colloidal platinum.

In the presence of sensitizers such as benzophenone or Michler's ketone the reaction rate is increased and the induction time shortened (Figure 3.15).

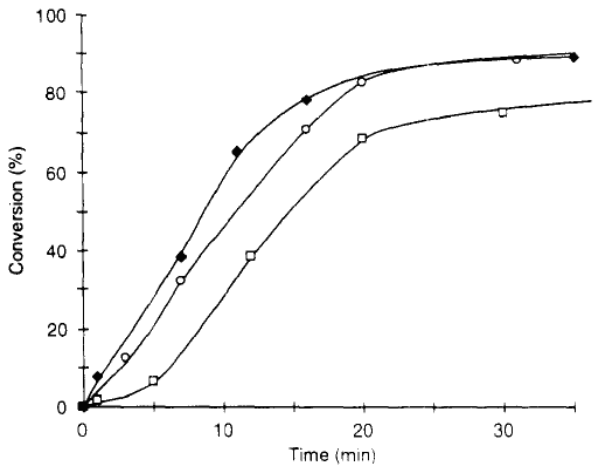

Figure 3.15: Hydrosilation under irradiation with 366 nm light: □ without sensitizer, with Michler's ketone○ in air, ♦ in argon, and 400 ppm catalyst platinum equivalent

References

[1] L.H. Palys, P.A. Callais. Rubber World 229 (**2003**) 35.

[2] P.R. Dluzneski. Rubber Chem. Technol. 74 (**2001**)451.

[3] A. Colas J. Curtis.Biomaterial Science. (Eds: B.D. Ratner, A.S. Hoffman, F.J. Schoen, J.E. Lemmons) Elsevier, Inc.(**2004**) 80.

[4] D. Troegel, J. Stohrer. Coordi. Chem.Rev. 255 (**2011**) 1440.

[5] J.L. Speier, J.A. Webster, G.H. Barnes. J. Am. Chem. Soc. 79 (**1957**) 974.

[6] J.C. Sam, J.L. Speier. J. Am. Chem. Soc. 89 (**1958**) 4104.

[7] B. Marciniec.Appl. Organomet. Chem. 14 (**2000**) 527.

[8] J.A. Reichl, D.H Berry.Adv. Organomet. Chem. 43, (**1998**) 197.

[9] T.D. Tilley. The chemistry of organic silicon chemistry (Eds: S. Patai, Z. Rappoport). John Wiley, Chichester. (**1989**) 1415.

[10] A.J. Chalk, J.F. Harrod. J. Am. Chem. Soc. 87 (**1965**) 16.

[11] I. Ojima, Z.Y. Li, J.W. Zhu. Recent Advances in the Hydrosilylation and Related Reactions. (Eds: Z. Rappoport, Y. Apeloig) (**2003**) 1687.

[12] B. Marciniec, J. Guliński. J. Organomet.Chem. 446 (**1993**) 15.

[13] B. Marciniec. Applied Homogeneous Catalysis with Organometallic Compounds (Eds: B. Cornlis, W. Hermann) (**1996**) 487.

[14] S.H. Bergens,P. Noheda, J. Whelan, B. Bosnich. J. Am. Chem. Soc. 114 (**1992**) 2128.

[15] S. Duckett, R.N. Perutz. Organomet. 11 (**1992**) 90.

[16] M. Brookhart, B.E. Grant. J. Am. Chem. Soc. 115 (**1993**) 2151.

[17] B. Marciniec. Comprehensive handbook on hydrosilylation. Pergamon, Oxford (**1992**).

[18] L.H. Sommer, E.W. Pietrusza, F.C. Whitmore. J. Am. Chem. Soc. 69 (**1947**) 188.

[19] A.M. Bueche.J. Polym. Sci. 15 (**1955**) 105.

[20] F.D. Lewis, G.D. Salvi. Inorg. Chem. 34 (**1995**) 3182.

[21] F. Wang, D.C. Neckers, J. Organomet. Chem. 665 (**2003**) 1.

[22] L.D. Boardman. Organomet. 11 (**1992**) 4194.

[23] J.L. Speier. Adv. Organomet. Chem. 17 (**1979**) 407.

[24] M.S. Wrighton,M.A. Schroeder. Am. Chem. Soc.96 (**1974**) 6235.

[25] M.A. Schroeder, M.S. Wrighton.J. Organomet. Chem. 128 (**1977**) 345.

[26] U. Schubert.Adv. Organomet. Chem. 30 (**1990**) 151.

[27] B. Marciniec, H. Maciejewski. J. Organomet. Chem. 454 (**1993**) 45.

[28] F.D. Lewis, A.M. Mille, G.D. Salvi. Inorg. Chem. 34 (**1995**) 3173.

[29] A.K. Roy. Adv. Organomet. Chem. 55 (**2007**) 1.

[30] B. Marciniec.Silicon Chem. 1 (**2002**) 155.

[31] J. Boardman, D. Larry, Oxman, D. Joel. U.S. Patent. 6,046,250 (**1990**).

[32] R.P. Eckberg. U.S. Patent. 4,670, 531 (**1986**).

[33] T.J. Drahnak U.S. Patent. 4,530, 879 (**1983**).

[34] R.C. Menzies. J. Chem. Soc. (**1928**) 565.

[35] D. Burget, T. Mayer, G. Mignani, J.P. Fouassier. J. Photochem. Photobiol. A: Chem. 97 (**1996**) 163.

4. MATERIALS AND METHODS

4.1. Materials

The hydrosilation reaction was achieved between a polydimethylsiloxane vinyldimethylsiloxane terminated (PDMS-V) and a polymethylhydrosiloxane trimethylsiloxy terminated (MH-PDMS) using a platinum catalyst. The scheme of the reaction was reported in Figure 4.1.

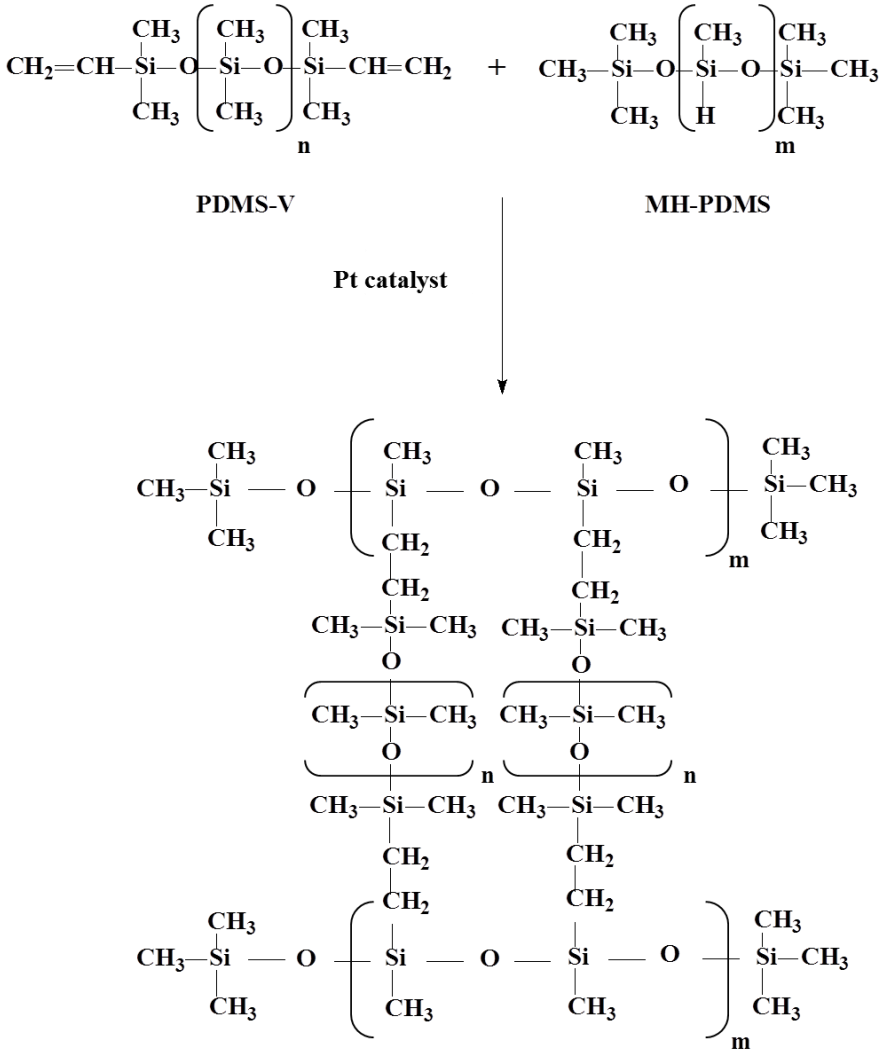

Figure 4.1: Scheme of hydrosilation reaction

The following materials were purchased from ABCR (Karlsruhe, Germany) and employed as received:

- Polydimethylsiloxane vinyldimethylsiloxane terminated (**PDMS-V**) having different molecular weights (Table 4.1) which structure was reported in Figure 4.2.

Table 4.1: Properties of the PDMS-V used

Formulation Name	Molecular Weight (g.mol^{-1})	Vinyl-Eq/kg
A	17 200	0.11 – 0.13
B	6 000	0.33 – 0.37
C	800	2.4 – 2.9

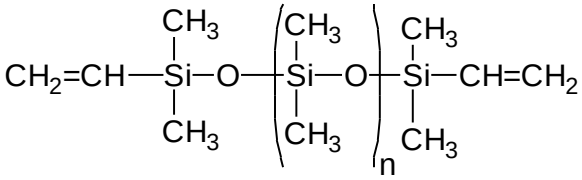

Figure 4.2:PDMS-V structure

- Polymethylhydrosiloxane trimethylsiloxy terminated (**MH-PDMS**) with molecular weight of 2250 g.mol^{-1}and Si-H equivalent weight of 64 which structure was reported in Figure 4.3.

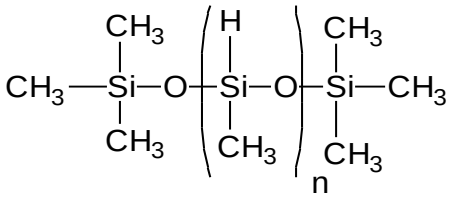

Figure 4.3: MH-PDMS structure

The reactivity of two different platinum catalysts was investigated for the UV-hydrosilation:

- Platinum carbonyl cyclovinylmethylsiloxane Pt(cvms) was purchased from ABCR (Karlsruhe, Germany) and used as received. This complex was at a concentration of 1.85-2.1% in vinylmethylcyclosiloxane. The structure of the catalyst was reported in Figure 4.4.

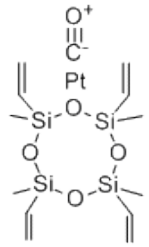

Figure 4.4: Pt(cvms) structure

- Platinum (II) acetylacetonate $Pt(acac)_2$ was purchased from ABCR (Karlsruhe, Germany) and dissolved in 1,3-dioxolane (purchased from Sigma Aldrich) at a concentration of 2.4%. The structure was reported in Figure 4.5.

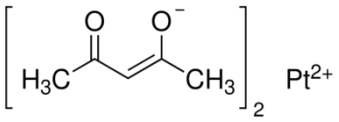

Figure 4.5: $Pt(acac)_2$ structure

After defining the best conditions suitable for the UV-activated hydrosilation, different micro-sized fillers were loaded to the formulations in order to improve the properties of the material. Two different silica oxides, named in the following $1SiO_2$ and $2SiO_2$, were purchased from Quarzwerke (Frechen, Germany). Aluminum oxide and aluminum trihydrate fillers were also used in the investigation and were purchased from Albemarle (Bergheim, Germany).
Two different nano-sized fillers were also employed:

- Zeosil 1165 from Rhodia (Courbevoie, France)
- Aerosil 200 from Evonik (Essen, Germany)

The fillers were previously dried for 2h at 80°C in order to remove adsorbed water and then dispersed into the formulations by using a Speed Mixer (Speed Mixer^{TM} DAC 400.1 FVZ).

The in-situ generation of silica, aluminum oxide and titania were obtained from their respective precursors: Tetraethyl ortho silicate (TEOS), aluminum iso-propoxide Al(OPr-i)$_3$ and titanium n-butoxide (TBO) purchased from Sigma Aldrich and used as received. Their structures were reported in Figure 4.6.

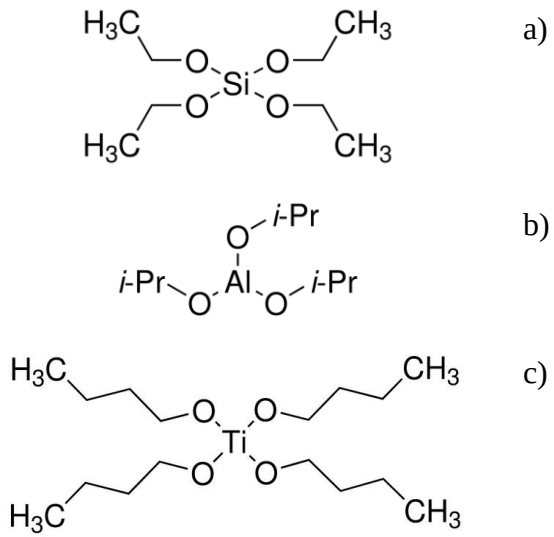

Figure 4.6: Structures of the precursors used for the in-situ generation of inorganic particles

The trimethyl(methylcyclopentadienyl) platinum(IV) complex, named in the following (Me-Cp)Pt(Me)$_3$,was used to study the hydrosilation reaction activated by blue light radiation. This catalyst was purchased from ABCR (Karlsruhe, Germany) and the structure was reported in Figure 4.7.

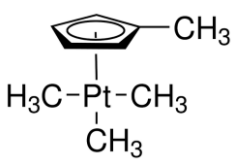

Figure 4.7: Structure of the (Me-Cp)Pt(Me)$_3$ catalyst

The sensitizer 2-chlorothioxanthen-9-one from Sigma Aldrich was employed as received and its structure was reported in Figure 4.8.

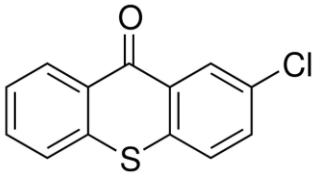

Figure 4.8:2-chlorothioxanthen-9-one used for the visible activated hydrosilation reaction

4.2. Methods

The photopolymerization was achieved with a medium pressure mercury lamp (Helios Italquartz, Milano) in air. The light intensity on the surface of the sample was about 50 mW/cm^2 (measured with EIT instrument).

When the fillers were loaded to the formulations the dispersion was achieved by using a Speed Mixer (Speed Mixer^{TM} DAC 400.1 FVZ) for 1minute at 2000 rpm. The Pt-catalyst was then solubilized in 1,3-dioxolane, added to the formulation and mixed again at 2000 rpm for 1 additional minute.

Granulometric analyses were performed by using a laser granulometer (Fritsch model Analysette 22 Compact). Measurements were done after dispersing the powder in ethanol (concentration of about 0,015 %). The diameters detected by this apparatus ranged between 1.9 μm and 188 μm. The distribution weight were reported as a function of agglomerate size.DLS measurements were performed with a Zetasizer Nanoseries ZS90 (Malvern Instruments Ltd, England). UV-visible spectra were performed using a UV-Vis spectrophotometer ATI Unicam UV2.

The kinetics of UV-curing were determined by FTIR spectroscopy employing a Thermo-Nicolet 5700 FTIR device. The decrease of the peak area centered at 2160 cm^{-1},characteristic of the silane bond, was followed during the irradiation in real-time. The formulations were coated on silicon wafer and the thin layer had a thickness of 50 μm. The photopolymerization was induced using a medium pressure mercury lamp equipped with an optical guide (Hamamatsu, LC8). The

light intensity on the surface of the sample was about 50 mW/cm^2 (measured with EIT instrument).

ATR real-time measurements were performed on thick samples (several cm) using the same instrument on the non-incident side (bottom surface) while irradiation was done on the topside.

Conversion curves as a function of time were calculated using the equation :

$$\% \text{ Conversion } (t) = 100*(A(t)-A_0)/A_0$$

where A(t) is the peak area of the silane bond measured at different times and A_0 is the area of the silane bond peak in the starting, unirradiated formulation.

The gel content was determined on the cured films by measuring the weight loss after 24h extraction with chloroform at room temperature according to the standard test method ASTM D2765-84 [1].

Thermogravimetric analyses (TGA) were performed with a TGA/SDTA 851 instrument (Mettler Toledo, Switzerland) between 20 °C and 800 °C at a heating rate of 10 °C.min^{-1} in air. The TGA were previously performed on the pure oxides fillers in order to verify their thermal stability in this temperature range.

Dynamic mechanical thermal analyses (DMTA) were performed with a Triton Technology (Mettler Toledo) instrument, at a frequency of 1 Hz in the tensile configuration. The samples prepared for these analyses had a thickness of 5 mm and dimensions of 100*50 mm.

DSC measurements were achieved using a DSC 30 (Mettler Toledo, Switzerland) apparatus equipped with a low temperature probe at a heating rate of 10°C.min^{-1}). The exothermicity of the reaction was recorded while irradiating the sample by photo-DSC experiments using a medium pressure mercury lamp equipped with an optical guide (Hamamatsu, LC8) in combination with the DSC instrument. The light intensity on the surface of the sample was about 50 mW/cm^2(measured with EIT instrument).

Curing depths measurements were performed using PVC tubes (13mm of diameter and 20mm in length) closed on one side and filled with formulations. The curing depth was measured as a function of UV light exposure time (up to 300s). The cured silicones were then demolded 30 minutes after irradiation in order to let the dark curing proceed.

The polymerization front was detected by an optical pyrometer PCE-JR 911 (PCE Group, Italy). The experiments were conducted in small-scale cylindrical reactors (inner diameter: 14mm, length: 50mm). The optical pyrometer was placed along the axial direction of the tubes to measure the temperature of the reacting system during the curing process. Temperature data were collected at a rate of 1 measurement per second and downloaded to a PC for analysis. The UV-curing was induced with a medium pressure mercury lamp equipped with an optical guide (Hamamatsu, LC8) for 30s at a distance of 4cm. The schema of the procedure was reported in Figure 4.9.

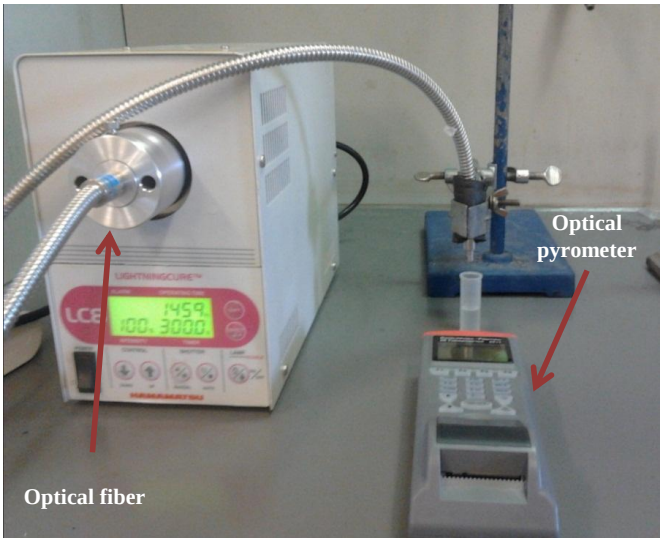

Figure 4.9:Measurement of sample temperature by optical pyrometer during irradiation

Dry Arc Resistance tests were performed according to ASTM D495-99 standards [2]. This test covers the differentiation among similar materials with respect to their resistance to the action of a high-voltage low-current arc close to the insulator surface. This arc intends to form a conducting path therein or to induce the material to become conductive due to the localized thermal and chemical decomposition and erosion. The test applies, at different interval of time, a voltage of 12.5 kV with a limited current arc discharge of 10 mA across the specimen surface between two electrodes separated by 6.35 mm. The total time to failure is recorded in seconds without reference to the sequence of tests in which it occurred. Higher values indicate greater resistance to breakdown along the surface

due to arcing or tracking conditions. Samples dimensions were 30*30 mm and 4 mm of thickness. The measurements were performed four times for both sides in order to control the homogeneity of the samples and verify that no sedimentation effects occurred (especially for filled samples). The schema of the experiment was reported in Figure 4.10.

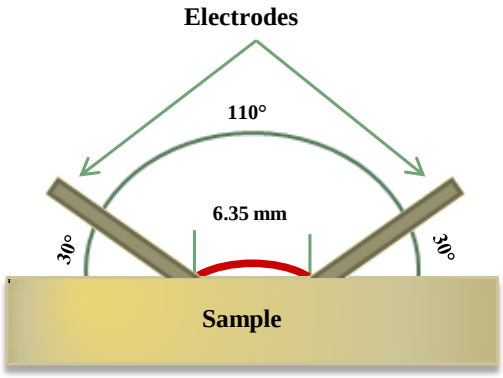

Figure 4.10: Dry Arc Resistance measurements

Dielectric spectroscopy investigations were carried out by means of a Novocontrol Alpha analyzer. The measurements were performed isothermally with the temperature being controlled by a Novocontrol Quatro cryosystem (temperature stability better than 0.1K). Samples of about 1 mm thick were fixed between two golden plated electrodes forming a parallel plate capacitor of 20 mm in diameter. An AC voltage of 1 V_{rms} was applied and the response of the system was studied. Both relative permittivity and dielectric loss factor with respect to frequency were carried out [3].

The complex dielectric function is given by the relation (1):

$$\varepsilon^*(\omega) = \varepsilon'(\omega) - i\,\varepsilon''(\omega) \qquad (1)$$

The relative permittivity ε' of a material is related to the stored energy within the medium while the dielectric loss factor is related to the dissipation energy. The measurement of the loss tangent (tan δ) is used to quantify the inherent dissipation of electromagnetic energy and is related to the angle between the resistive component (lossy one) of an electromagnetic field and its reactive component (lossless one).

Morphological analyses were conducted by Scanning Electron Microscopy (PEI PHILIPS-Quanta inspect 200 LV). The measurements were operated at 15 kV in a ultra high vacuum (10^{-7}bar). The surface fracture of the cured samples was also investigated with a FE-SEM Supra 40 (Zeiss, Germany) microscope with the in-lens detector placed above the objective lens, in order to directly detect the beam path and collect images at very low acceleration voltages (1.5–5 kV). In this way the effects due to the accumulation of local charges on the surface of nonconductive materials, that otherwise can significantly deteriorate the imaging quality, were minimized.

An optical microscope Leica (Geosystems, Germany) was used to investigate the formation of inorganic particles in the formulations prior curing.

The visible activated hydrosilation reaction was reached by means of a blue light emitting diode(an Astralis 5 gun lamp from Ivoclar Vivadent) with an intensity of approximately 500 mW/cm^2 and a wavelength range in between 380-515 nm.

References

[1] ASTM D2765-84, Standard Test Method for Determination of Gel Content and Swell Ratio of Crosslinked Ethylene Plastics.

[2] ASTM D495-99, Standard Test Method for High-Voltage, Low Current, Dry Arc Resistance of Solid Electrical Insulation.

[3] F. Kremer, A. Schönhals. Broadband Dielectric Spectroscopy, Springer-Verlag Berlin Heidelberg (**2003**).

5. INVESTIGATION ON THE HYDROSILATION REACTION

The hydrosilation reaction was studied by evaluating the UV-curing conditions suitable for the preparation of a crosslinked silicone polymer. The influence of the catalyst nature, the ratio between vinyl and silane and the temperature were evaluated.

A model UV-curable system was chosen based on a polydimethylsiloxane vinyldimethylsiloxane terminated (PDMS-V) (structure reported in Figure 4.2) having different molecular weight and a polymethylhydrosiloxane trimethylsiloxy terminated (MH-PDMS) (structure reported in Figure 4.3). The UV-curing conditions and the properties of the cured silicone materials were investigated showing the versatility of this curing method.

5.1. Influence of catalyst/ temperature /Vinyl-Silane ratio

In this section, which aims to provide the best conditions for the curing of silicone, only the PDMS-V with highest molecular weight was used. The influence of the nature of catalyst, the temperature and the ratio between vinyl and silane groups were evaluated.

5.1.1. Nature of the catalyst

In order to evaluate the influence of the nature of the catalyst on the hydrosilation reaction, two different platinum catalysts were investigated: the platinum carbonyl cyclovinylmethylsiloxane Pt(cvms) and the platinum (II) acetylacetonate $Pt(acac)_2$. The UV-visible spectra of the two platinum catalyst were studied to determine the wavelength of the maximum absorption (Figure 5.1). For the $Pt(acac)_2$, which was dissolved in 1,3-dioxolane (concentration of 2,4 wt %), the spectra showed an absorbance peak near 290 nm with a shoulder at around 350 nm.

For the platinum catalyst Pt(cvms), dissolved in vinylmethylcyclosiloxane (concentration of 1.85-2.1 wt %), the peak of higher absorbance was observed near 280 nm but no apparent shoulder at around 350 nm was evidenced. It was possible to suppose that the $Pt(acac)_2$ catalyst could be slightly more efficient in UV-induced hydrosilation because of the absorbance shoulder at around 350 nm. In any case, both absorption spectra were characterized by peaks at wavelengths compatibles with the medium-pressure mercury UV lamp used for the curing.

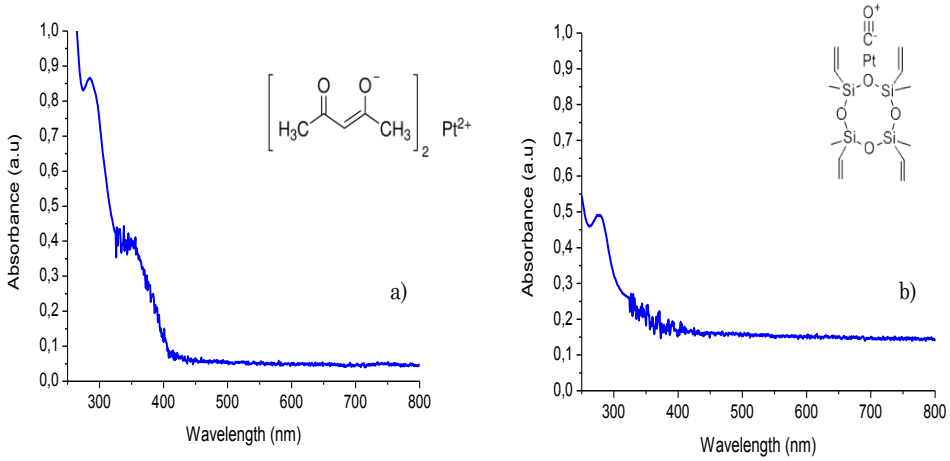

Figure 5.1: UV-Vis spectra of the a) Pt(acac)2 catalyst and b) Pt(cvms) catalyst

The kinetics of reaction were evaluated by FT-IR analyses for the two systems. Formulations were prepared in order to have a 1:1 molar ratio of the reactive groups and a concentration of Pt catalyst in the range between 500 and 1000 ppm. The conversions were evaluated following the decrease of the silane bond as a function of irradiation time (Figure 5.2).

A difference in reactivity was evidenced by comparing the two kinetics of polymerization with same amount of catalyst. The $Pt(acac)_2$ catalyst presented a faster rate of curing and higher final silane conversion than the Pt(cvms) by comparing the values obtained with 500 ppm of catalyst. A slight increase of the photopolymerization rate by increasing the amount of the Pt(cvms) catalyst up to 1000 ppm was observed. Nevertheless, the final conversion was kept unmodified around 75%.

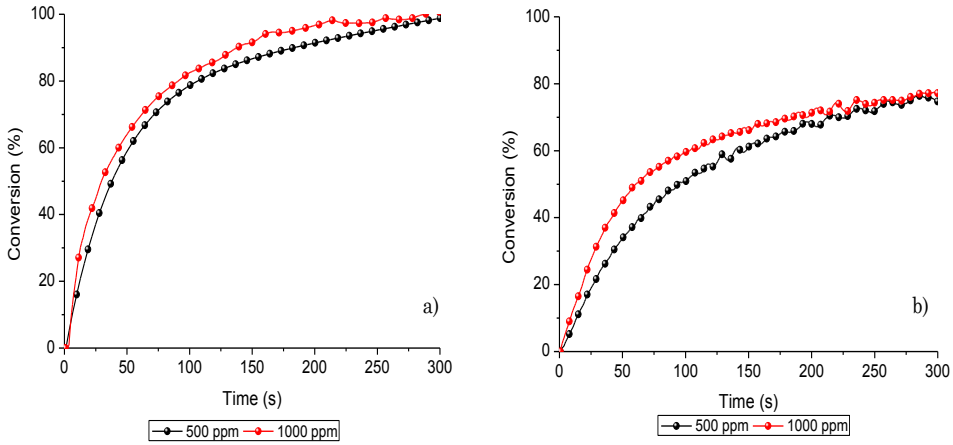

Figure 5.2: Silane conversion as a function of irradiation time for different amount of a) $Pt(acac)_2$ and b) Pt(cvms) catalyst for the 1:1 equimolar system PDMS-V/MH-PDMS

To evaluate the effect of the catalyst content, the same formulations were cured in the presence of 1000 ppm of Pt-catalyst $Pt(acac)_2$. It was evident that the increase of catalyst content did not significantly enhance neither the conversion rate nor the final conversion (Figure 5.2 a).

By decreasing the Pt-catalyst content below 500 ppm, it was not possible to achieve a fully cured tack-free sample. Therefore, there is a lower catalyst content below which the curing process is not efficient anymore. This behavior is similar to what was observed previously in literature [1].

It was therefore concluded that the lower amount sufficient to obtain a UV induced crosslinking of silicone material was 500 ppm and the $Pt(acac)_2$ catalyst was chosen for the future investigations.

5.1.2. Temperature effect

In order to evaluate the combined action of UV light and heat during the curing process, samples containing 500 ppm of $Pt(acac)_2$ in a mixture of PDMS-V/ MH-PDMS (molar ratio between vinyl group and Si-H group 1:1) were evaluated at different temperatures. The conversions during irradiation were followed at room temperature, at 60 °C and 80 °C. The FT-IR spectra of the samples were collected at different time and the area of silane group was evaluated in order to follow the reaction. The results reported in Figure 5.3 showed that a significant improvement

of the conversion could be obtained by increasing the temperature. In fact, the silane conversion after one minute of irradiation was 3 times higher at 80°C than at room temperature.

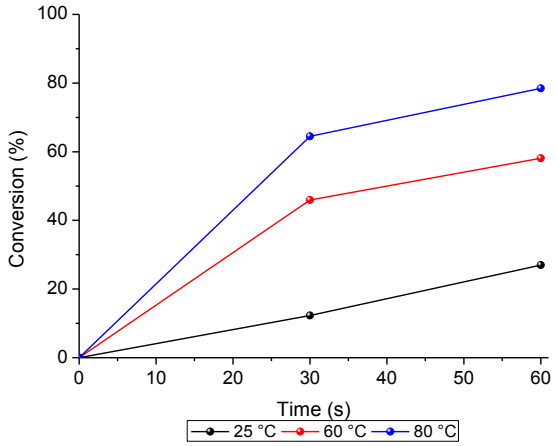

Figure 5.3: Silane conversion as a function of irradiation time for curing at room temperature (black line), 60°C (red line) and 80°C (blue line)

This was an expected behavior since the Pt-catalyst was usually thermally activated to catalyze the hydrosilation reaction. Therefore, by increasing the temperature there was a synergistic activation of the catalyst, both thermally and via UV-irradiation.

5.1.3. Vinyl-Silane ratio effect

The molar ratio between PDMS-V and MH-PDMS was varied from 25-75 to 75-25 (Vinyl-Silane ratio). The catalyst content was always kept at 500 ppm. FT-IR analyses were performed on the 25-75 and 50-50 formulations as the 75-25 formulation did not show evident silane conversion. The results were reported in Figure 5.4.

As expected, the higher silane conversion was reached when equimolar amount of vinyl and silane was used. Surprisingly, a conversion of 70% was achieved for the formulation containing molar ratio of vinyl-silane of 25-75 while theoretically maximum conversion should be 33% (taking into account the vinyl content in the

formulation). It could be supposed that silane groups (which present high reactivity) could form other chemical products in the presence of platinum catalyst that could not be predictable.

No improvement of the kinetic of polymerization could be reached by varying the vinyl-silane molar ratio and it was therefore possible to conclude that formulation containing an equimolar ratio was the best candidate to give a fully cured network.

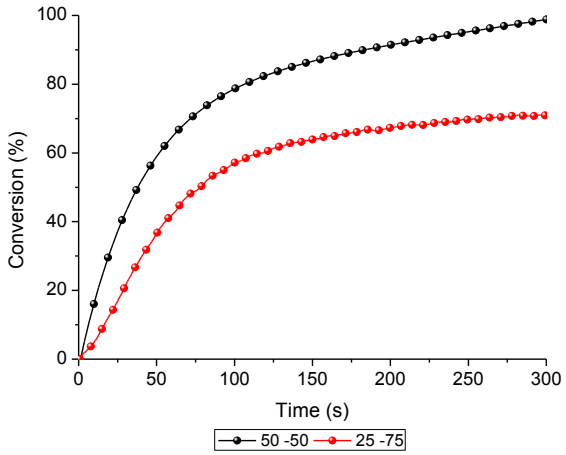

Figure 5.4: Silane conversion as a function of irradiation time for different Vinyl-Silane ratio

5.2. Influence of the vinyl oligomer molecular weight

Three different PDMS-V having molecular weight ranging from 17.200 to 800 $g.mol^{-1}$ (Table 4.1) were used to evaluate their effect on the UV-curing conditions and the properties of cured silicone materials.

5.2.1. Sample preparation

The mixtures were prepared by adding an equimolar amount of vinyl and silane reactive groups. The Pt-catalyst was solubilized in 1,3-dioxolane and added to the formulation at a content of 500 ppm. The formulations were stirred and either

coated on a substrate (leading to a thin silicone layer of about 50 µm) or poured into a mold (for the preparation of thick samples) and cured in air for 5 minutes with a medium pressure mercury lamp (intensity 50 $mW.cm^{-2}$).

5.2.2. Photocuring process and properties

The UV-activated hydrosilation process was studied by means of FTIR analyses. In Figure 5.5 the Si-H conversion curves as a function of irradiation time were reported for the photocurable formulations in which the different vinyl oligomers, with decreasing molecular weight, were employed. The catalyst content was always 500 ppm and the thickness of the samples was about 50 µm.

It was evident that by decreasing the molecular weight of the vinyl oligomer (from oligomer type A to B and C) there was a level off of the final Si-H conversion to lower values. This could be attributed to a lower mobility of the polymeric chain induced by an increase of crosslinking density (due to the decrease of molecular weight between two neighbor crosslinked) which could hindered the diffusion of the growing polymeric chains.

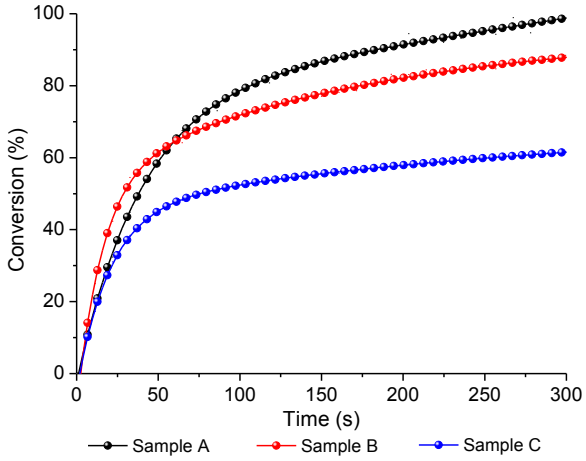

Figure 5.5: Silane conversion curve as a function of irradiation time for formulations containing the vinyl oligomer A (Mw 17,200), B (Mw 6,000), C (Mw 800) with 500 ppm of $Pt(acac)_2$ catalyst

Cured materials of about 50 µm thickness were achieved by irradiating for 5 minutes different formulations containing 500 ppm of catalyst. It was observed that the gel content increased by decreasing the molecular weight of the vinyl oligomer (data reported in Table 5.1). The cured materials obtained by using the vinyl oligomer with the highest molecular weight (oligomer A) showed a gel content of 74%. By using the oligomer B, the gel content of cured material slightly increased to 78%. Complete insoluble cured material was obtained with a gel content of 99% by using the vinyl oligomer with the lowest molecular weight (oligomer C with a molecular weight of 800 $g.mol^{-1}$). It seemed clear that by increasing the crosslinking density, a tight crosslinked polysiloxane network completely insoluble was achieved and that increasing the molecular weight would decrease the crosslink probability with subsequent decrease of the crosslinked material.

Table 5.1: Properties of UV-Cured Materials

Formulation Name	Molecular Weight ($g.mol^{-1}$)	Gel content (%)[1]	Tg (°C)[2]	Tm (°C)[2]	Tg(°C)[3]
A	17 200	74	-130	-50	-108
B	6 000	78	-120	-40	-110
C	800	99	-110	--	-106

[1]Determined after 24h extraction in chloroform, [2]Determined by DSC analyses, [3]Determined by DMTA analyses

The glass transition temperature was determined by DSC analyses for all the cured samples. The DSC curves were reported in Figure 5.6. It was observed that by decreasing the molecular weight of the vinyl oligomer (from A to C) an increase of the Tg value was achieved. This shifted from -130°C for the cured material obtained in the presence of the vinyl oligomer with the highest molecular weight, up to -110°C when the vinyl oligomer with lowest molecular weight (Mw of 800 $g.mol^{-1}$) was used.

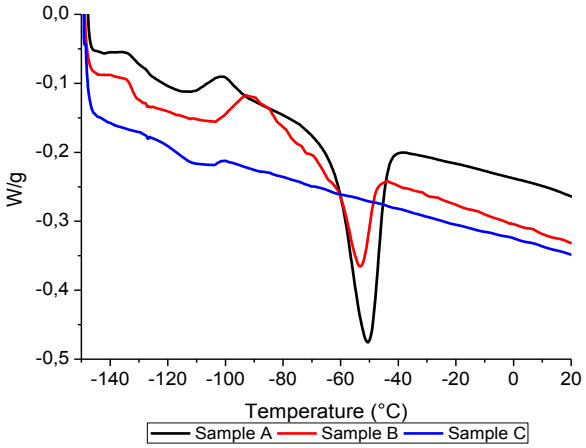

Figure 5.6: DSC curves for cured materials obtained from equimolarPDMS-V/MH-PDMS mixture obtained with the vinyl oligomer A (Mw 17,200), oligomer B (Mw 6,000) and oligomer C (Mw 800)

The Tg increase was attributed to the increased crosslinking density due to higher reactive groups present on oligomer C. In fact it is very well known that by increasing the crosslinking density there is an extension of the elastic modulus to higher temperatures with a consequent shift of the viscoelastic glass transition to higher temperatures. This was further confirmed by DMTA analyses performed on these cured materials in which an increment of the Tg value, by decreasing the molecular weight of the vinyl oligomer, was observed (Figure 5.7).

Furthermore, by shortening the distance between two crosslinks, a lower mobility of the chain-ends is induced, so that constrains are too high to allows enough mobility which is needed to get the necessary chain-folding for the crystalline structure formation.

A progressive decrease of crystallinity (Table 5.1-Figure 5.6) became also evident by decreasing the molecular weight of the vinyl oligomer. A complete disappearance of the crystallinity was achieved when the vinyl oligomer with lowest molecular weight was used (oligomer C).

As a final result, the cured materials obtained by using the vinyl oligomer with the lowest molecular weight is characterized by higher Tg value, higher mechanical performances and absence of any crystallinity (Figure 5.6).

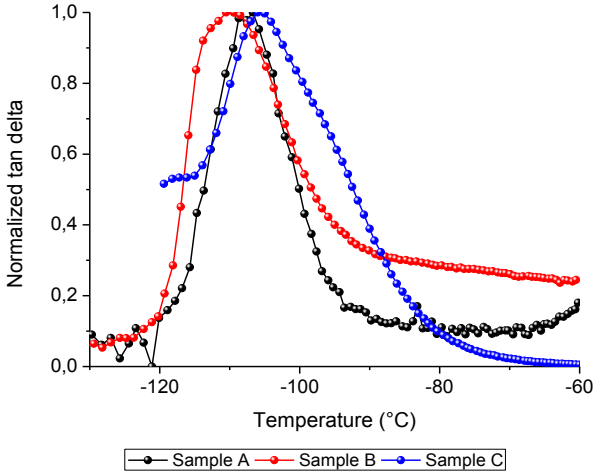

Figure 5.7: DMTA curves for cured materials obtained from equimolar PDMS-V/MH-PDMS mixture obtained with the vinyl oligomer A (Mw 17,200), oligomer B (Mw 6,000) and oligomer C (Mw 800)

An increase of final residue by decreasing the molecular weight of the vinyl oligomer was observed by TGA analyses (Figure 5.8) with an increase from 27% (oligomer A) to 37% (oligomer B) and subsequently to 67% (oligomer C). The degradation of the unfilled silicone occurs by a depolymerization reaction of the PDMS chains leading to volatile cyclic oligomers, preferentially those which consists of three Si-O groups [2]. This could be associated to a first weight loss at temperatures above 290°C. At higher temperatures, oxidation proceeds through peroxidation mechanism initiated by radicals (weak links or impurities scission) giving primary hydroperoxides that decompose eliminating hydrogen. Later on, the breakdown of the crosslinked material begins at about 400°C and occurs by molecular splitting of cyclic oligomers with an higher rate of decomposition in air with respect to nitrogen atmosphere [3].

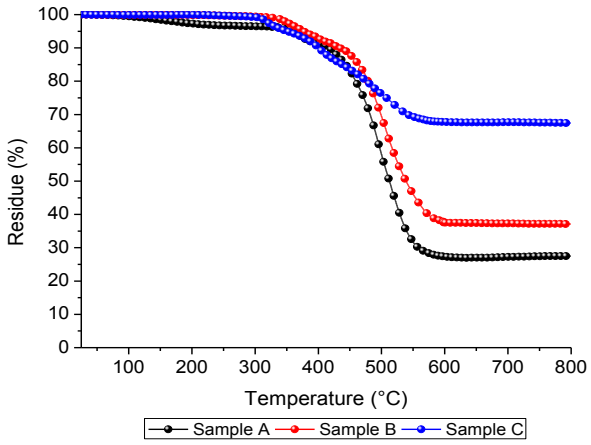

Figure 5.8: TGA curves for cured materials obtained from equimolarPDMS-V/MH-PDMS mixture obtained with the vinyl oligomer A (Mw 17,200), oligomer B (Mw 6,000) and oligomer C (Mw 800)

The results showed that these UV-curable systems were versatile and that it was possible to prepare materials characterized by different properties changing the molecular weight of the starting components.

5.2.3. Evaluation of dark-curing process

One important advantage of the UV-curing technique is that the crosslinking reaction can be trigged by a short UV irradiation and can further proceed slowly in the dark.

In order to evaluate the extent of the dark curing process, a mixture of PDMS-V (oligomer C with the lowest molecular weight) and MH-PDMS with 500 ppm of Pt catalyst was investigated by FTIR. The proceeding of dark curing was followed as a function of silane conversion during time after a short irradiation time. The thickness of the sample was about 50 µm. The results were reported in Figure 5.9 for formulations previously UV-irradiated for 10, 30, and 60s. A significant increase of Si-H conversion in the dark was evidenced as a function of UV-irradiation length. The dark curing was more pronounced for the oligomer A as higher diffusion of the growing polymer chain is possible by increasing the molecular weight of the components.

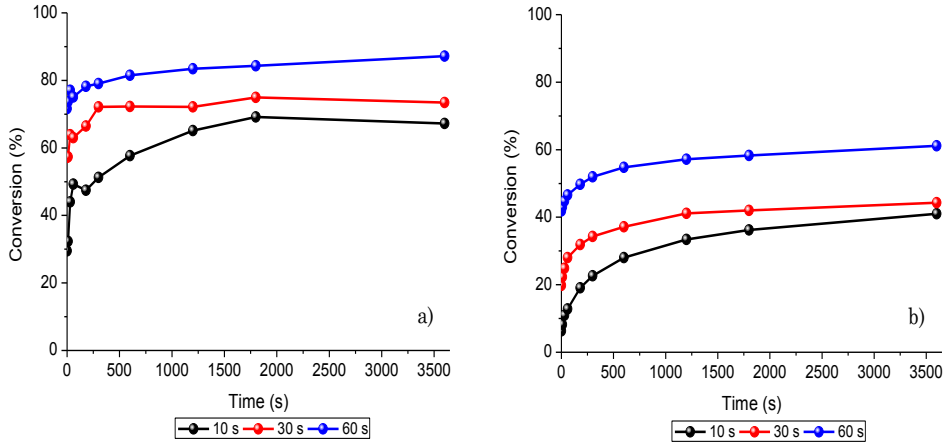

Figure 5.9: Evaluation of dark-curing after different time of UV-irradiation of equimolar PDMS-V/MH-PDMS mixture obtained with a)the vinyl oligomer A (Mw 17,200) and b)the vinyl oligomer C (Mw 800)

These data were in agreement with the literature [4],[5]and showed that high conversion could be reached by a very short irradiation time and a relatively short dark post-curing.

The data reported in literature [4] correlated the results of hydrosilation reaction and the spectral changes which accompanied irradiation of $Pt(acac)_2$ in the presence of Et_3Si-H or Et_3Si(-vinyl). It indicated that the irradiation time required to generate the active hydrosilation catalyst correspond to the time required for essential complete disappearance of the long-wavelength UV absorption band of the $Pt(acac)_2$ and for the formation and destruction of primary photoproduct (detected both by UV and ^{1}H-NMR spectroscopy). However, the complete photodecomposition of $Pt(acac)_2$ to liberate both ligands and form colloidal platinum did not occur during this brief irradiation period. These observations made postulate that a short period of irradiation results in the formation of homogeneous hydrosilation catalyst which could be slowly converted to a less active heterogeneous catalyst similar to that formed upon thermal decomposition of $Pt(acac)_2$. The heterogeneous catalyst was supposed to be the one responsible of the proceeding of the reaction in the dark as well as in depth, leading to the formation of thick crosslinked materials.

The reported results of achievement of thick cured silicone materials is therefore of high interest since this photocured silicones could be made both for thin film as well as for bulk applications. Highly UV-crosslinked silicones could be achieved with higher rate of polymerization with respect to thermal activation leading therefore to a reduction of energy consumption and an enhancement of productivity.

5.2.4. Curing into depth

On the basis of the preliminary investigations, samples were prepared in plastic molds with a thickness ranging from 1 to 4 cm using an equimolar mixture of PDMS-V/ MH-PDMS using the vinyl oligomer C (lowest molecular weight) and adding an actual content of Pt-catalyst of 500 ppm. The irradiation time was fixed at 5 minutes.

The ATR spectra, recorded on the non-incident side (bottom part) of the formulations after 5 min of irradiation were reported in Figure 5.10. For all the samples (with 1–4 cm in thickness) a certain residual amount of Si-H was always evident and the residual amount of Si-H increased with sample thickness. Nevertheless, all the investigated thick samples were tack-free and completely insoluble with a gel content value around 98–99%.

These data were particularly interesting for UV-curing process since in the classical UV-initiation polymerization there is a well-known thickness effect with a strong decrease of conversion by increasing thickness of photocurable formulation. As a matter of fact, in the classical UV-induced polymerization reaction the thickness limit is very low (usually homogeneous curing are achieved for coatings of about 50–100 μm). Because of the occurrence of a UV intensity gradient by increasing the penetration depth, UV-curing is usually applied only for thin coatings. The possibility to achieve a thick cured material must be explained with a different curing process, which could probably involve at the same time a homogeneous and a heterogeneous catalytic mechanism, as described above on the basis of the literature data (see 5.2.3).

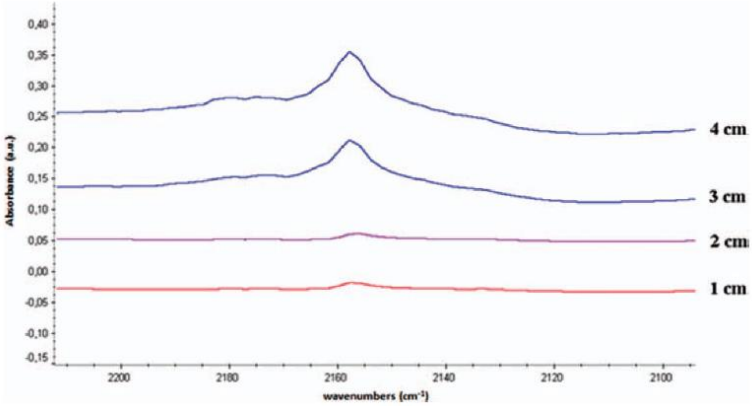

Figure 5.10: ATR spectra recorded on the non-incident side (bottom part) of the equimolar mixture PDMS-V (oligomer C)/MH-PDMS after 5 min of irradiation.

Real time ATR spectra were recorded on the non-incident side (bottom part) of formulations C with different thicknesses after 2 and 5 minutes of irradiation (Figure 5.11). The proceeding of the reaction was followed monitoring the decrease of the Si-H peak centered at around 2160 cm^{-1}, both during and after the irradiation. An increase of Si-H conversion in the dark was evidenced and homogeneous 3cm thick samples could be obtained after 30 min of post-curing.

These data are in agreement with the literature [4]-[6] and the previous dark-curing investigation, and clearly show the possibility to get thick fully crosslinked silicone polymers after a short irradiation time followed by a short post dark-curing.

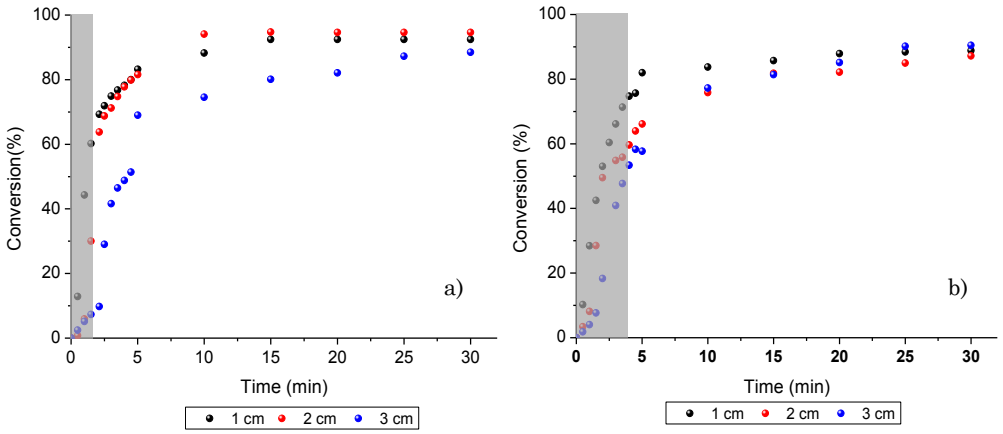

Figure 5.11: Real time ATR for formulation C after a) 2 minutes and b) 5 minutes of irradiation and 30 minutes of dark-curing

5.3. Frontal polymerization

An important dark-curing reaction of the silicone formulation C, which showed the continuation of the crosslinking process after short irradiation time, was previously reported. This behavior was particularly peculiar for UV-cured samples since, if the hydrosilation reaction would really occur just considering the pure UV contribution, a strong UV-gradient in the penetration depth should be observed and it would not be possible to cure homogeneously 3cm thick samples.

On the contrary, it can be supposed that the UV-irradiation initially yields a highly active homogeneous catalyst species by loss of one bidentate ligand. Subsequently, the exothermal heat generated by the polymerization reaction occurring at the surface of the sample is able to convert the homogeneous Pt-catalyst to a colloidal Pt-heterogeneous catalyst which is efficient in catalyzing the hydrosilation reaction in the dark and in the bulk after the short irradiation. In the following, the evaluation of the enthalpy of reaction and the demonstration of a frontal propagation (FP) in the system is reported.

In FP [7], a spatially localized reaction zone propagates through the reactive monomers or oligomers, which leads in consequence to a crosslinked solid polymer (Figure 5.12). It is a self-sustaining process controlled by the curing enthalpy of the reactive monomers or oligomers. A high exothermicity of the polymerization reaction and an Arrhenius dependence for the polymerization rate are the most important requirements to support a front.

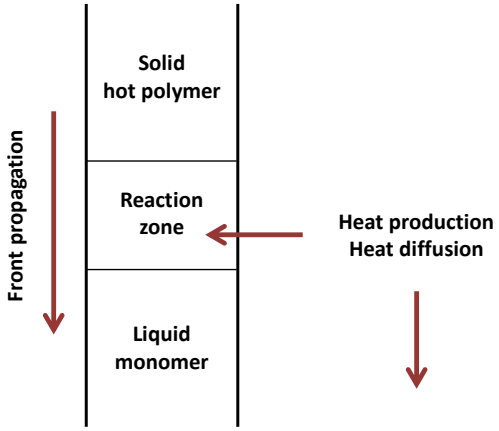

Figure 5.12: Scheme of frontal polymerization

In classical bulk polymerizations, heat is uniformly provided during the entire cure cycle to the whole surface of the reactive monomers thus promoting their reaction. Conversely, during FP, heat is applied only to a small area of the sample and for a limited time interval that is short if compared with the total cure time for the sample. The local increase in temperature triggers the polymerization of the monomers (or reactants) within the heating region of interest and the heat released by the curing process is transferred to the surroundings, promoting the creation of a hot reaction front that propagates in the rest of the monomers, converting them into polymer.

Front velocity and front temperature are strictly dependent on the enthalpy of the cure reaction, on the reaction kinetics, on the thermal conductivity of the resin, and on the resin heat capacity. The usual means of starting or "igniting" FP is to apply a localized heat source to a small portion of the reaction mass. Recently, it was shown that both free radical and cationic frontal polymerizations can be ignited by UV irradiation in the presence of an appropriate photoinitiator [8],[9].

The UV-induced FP mechanism can exhaustively explain the possibility to obtain a thick UV-cured silicone sample and the occurrence of a dark post-curing. Both these phenomena can be attributed to the thermal dark decomposition of the Pt-catalyst to colloidal platinum triggered by the UV-activated hydrosilation reaction which starts a heat propagation front.

5.3.1. Enthalpy of reaction

Photo-DSC were performed on the three different mixtures of PDMS-V/MH-PDMS (with oligomers A,B and C) in order to evaluate the difference in reactivity and their enthalpy reaction. The amount of Pt catalyst was fixed at 500 ppm and the measurements were done at 20°C. The formulations were irradiated for 4 minutes and the variation of enthalpy during the reaction was recorded by the photo-DSC instrument (Figure 5.13). The oligomer C resulted to be the most reactive with an high peak of enthalpy just after starting the UV-irradiation leading to the hypothesis that this system could have a frontal propagation.

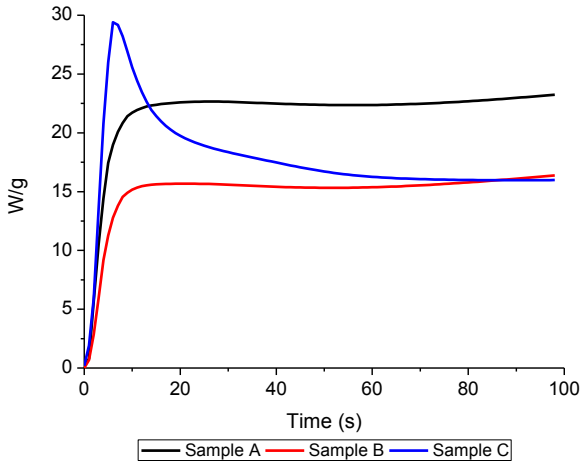

Figure 5.13: Photo-DSC of equimolar PDMS-V/MH-PDMS mixture obtained with a)the vinyl oligomer A (Mw 17,200) and b)the vinyl oligomer C (Mw 800)

In order to evaluate the effect of the catalyst amount on the exothermicity of the reaction, photo-DSC were performed for both 500 and 1000 ppm with the formulation containing the oligomer C (Figure 5.14). The increase of catalyst did not significantly modify the reactivity of the system as the reaction rate remained unvaried and the enthalpy of the two formulations were comparable. These data confirmed that the optimum catalyst content could be fixed at 500 ppm as it was already defined in previous experiments.

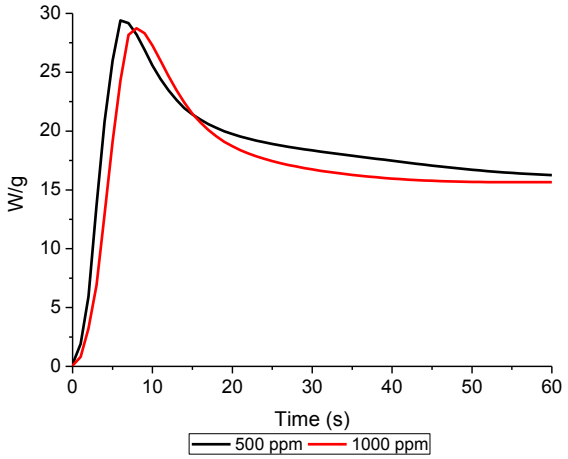

Figure 5.14:Photo-DSC with 500 and 1000ppm of Pt catalyst for the equimolar PDMS-V/MH-PDMS mixture with the vinyl oligomer C (Mw 800)

From photo-DSC measurements, the curing enthalpy for the investigated silicone system C was estimated at about 70J.g^{-1} (Figure 5.13). This relatively high value could provide the heat and high temperature during the hydrosilation reaction allowing to thermally activate the Pt-catalyst also in the deeper layer of the formulations where the light intensity would not be enough to photo-activate the catalyst. The enthalpies related to the oligomers A and B were relatively low and not comparable to the one obtained for the oligomer C (measured enthalpies of about 7 J.g^{-1} for both systems).

DSC performed at 10°C.min^{-1} on cured system C showed a residual enthalpy of about 36 J.g^{-1} necessary to complete the polymerization of the system (Figure 5.15). From these data, it was possible to conclude that the total enthalpy of the reaction was about 106 J.g^{-1} in the case that all the Si-H bonds react with the vinyl groups. This relatively high value could explain the noticeable warm and high temperature released during the hydrosilation reaction and let suppose a frontal propagation that could allow the curing of thick samples.

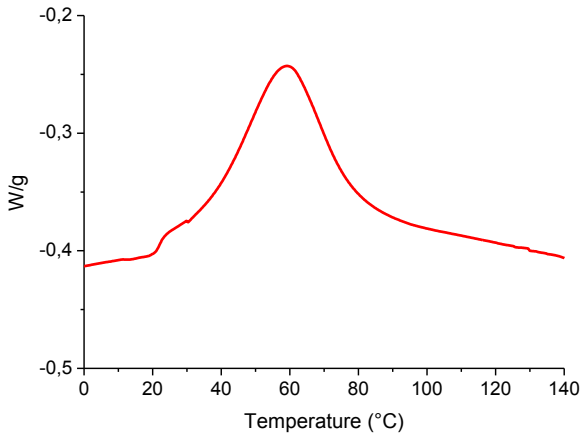

Figure 5.15: DSC for the mixture PDMS-V/MH-PDMS with oligomer C performed after 4 minutes of UV-irradiation

It is important to note that the total enthalpy of the system C will be likely higher than the one calculated experimentally. Indeed, from the DSC experiment, it is possible to observe that a temperature above 20°C can start the thermal cure and that most probably the sample continued the curing between the two analyses (Photo-DSC and subsequent DSC). However, this data did not mean that it would

be possible to achieve a cured sample by thermal curing at 20°C with the same crosslinking density as it could be obtained with UV light curing. If the thermal curing was performed at 20°C, the viscosity of the formulation would be too high to allow the polymeric chain mobility necessary for the curing. The crosslinking would be deeply reduced and the properties of the final material would not be comparable to the ones obtained by UV curing.

5.3.2. Frontal propagation in the system C

The possibility to have a frontal propagation was studied for the formulation C. The polymerization front was detected by optical pyrometer. The temperature profiles of four fixed points (respectively 1,2,3 and 4 cm from the top end tubes) were registered during the experiment. The results were reported in Figure 5.16. The time at which the temperature reached the maximum was taken as front time. Formulations attained high temperature up to 85°C for 1cm of thickness.

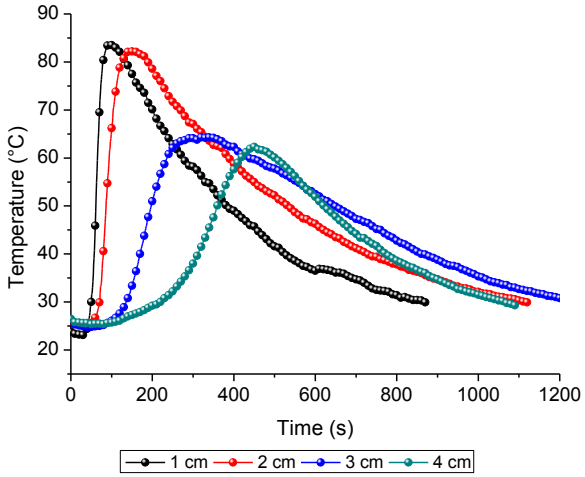

Figure 5.16: Temperature profiles of the four fixed points in the cylindrical reaction vessel

By reporting the distance of the front as a function of the highest temperature reached in the sample, it should be possible to obtain the front advancement along the axial direction [10]. Indeed, the polymerization front propagates at constant speed. The linear behavior observed for the formulation C (Figure 5.17) strongly supported the front propagation mechanism. The propagation speed calculated on

the basis of the experimental data was around 5mm/min (0,08mm.s^{-1}). This indicated that it should be possible to cure thick samples in low times of curing and dark-curing (if no dissipation heat occurs among the sample). The front propagation among sample thickness was reported in Figure 5.18.

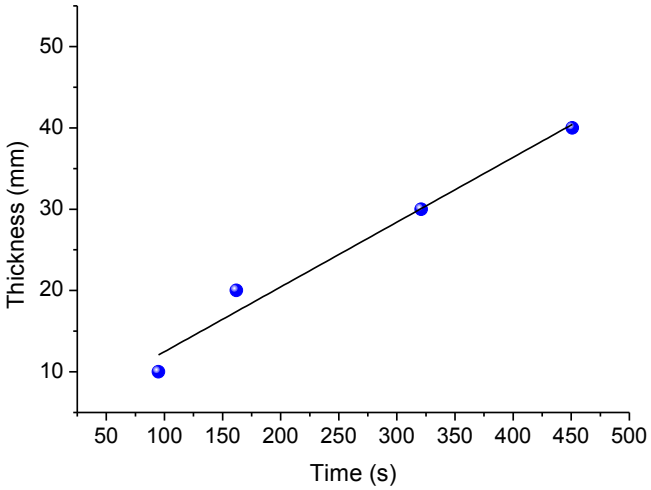

Figure 5.17: Front position as a function of time

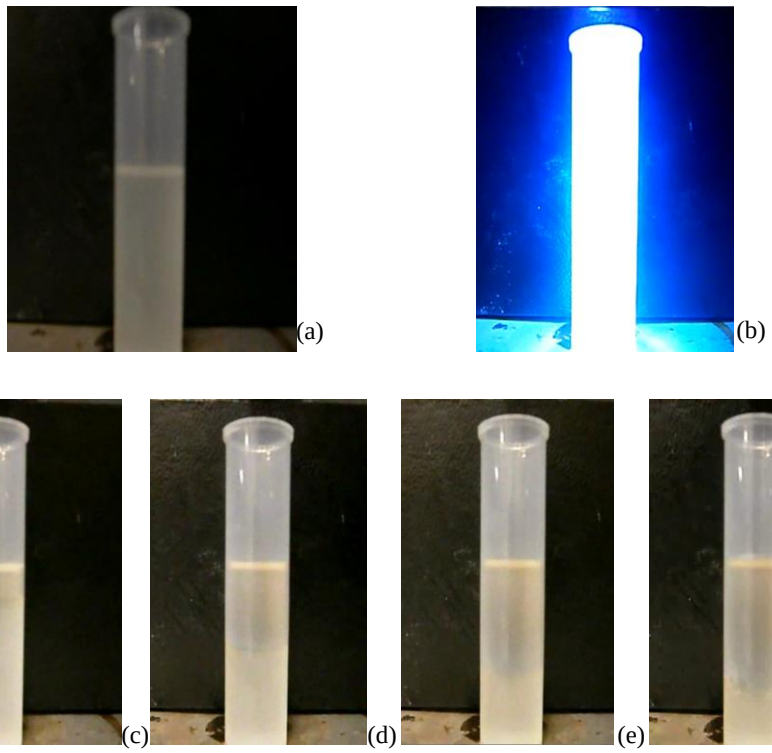

Figure 5.18: Illustration of the front propagation before (a) during (b) and 30s(c), 60s (d), 90s (e) and 120s (f) after the irradiation time of 30s.

In order to verify that the heat released was only due to frontal polymerization (and not from UV lamp), formulation without Pt catalyst (so that the reaction did not occur) was irradiated and the temperature profile was registered. The same was then performed in the presence of catalyst in order to compare the temperature profiles (Figure 5.19). It was possible to observe that without Pt the temperature still remain below 25°C even after 5min of irradiation while, for the sample with Pt-catalyst, a temperature increase up to 45°C was observed. This should demonstrate that the heat in the formulation was due to the enthalpy of hydrosilation reaction and not to the heat generated by the lamp.

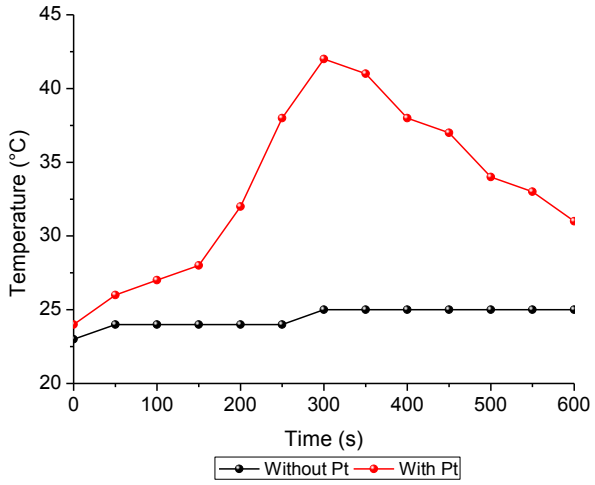

Figure 5.19: Temperature profiles of the formulation with and without Pt catalyst

It was therefore possible to strongly conclude that the UV-activated hydrosilation proceeds by a frontal propagation across the sample. The Pt-catalyst was allowed to be activated also in the deeper layer of the formulations where the light intensity would not be enough to photo-activate the catalyst.

5.4. Conclusions

The UV-activated hydrosilation reaction was investigated evaluating the influence of the catalyst nature, the temperature used for the reaction and the ratio between the vinyl and silane oligomers. The best suitable conditions for the reaction were therefore established.

The photocuring process was then evaluated by varying the vinyl oligomer molecular weight (from 17,200 to 800 $g.mol^{-1}$) and the proceeding of curing after UV-irradiation was studied. A modulation of the final properties of the silicone material could be achieved by using different vinyl oligomers: a progressive shift of the Tg value at higher temperatures and progressive disappearance of the Tm was obtained by lowering the vinyl oligomer molecular weight.

A significant increase of the silane conversion in the dark was evidenced and the longer was the irradiation time the higher was the final conversion. The dark curing was more pronounced for the vinyl oligomer with highest molecular weight (formulation A) as the diffusion of the growing polymeric chain is promoted. ATR performed in real-time on the bottom part of thick samples indicated that homogeneous unfilled samples 3cm thick could be obtained using the formulation C after a short post-curing.

The enthalpies of reaction were calculated for the three systems and a high value of enthalpy was observed for the formulation C indicating a possible front propagation among the system. This phenomena was demonstrated by optical pyrometry measurement which evidenced an increase of temperature inside the formulation as a function of sample thickness. The front propagation velocity was estimated experimentally.

References

[1] J. Boardman, D. Larry, Oxman, D. Joel. U.S. Patent. 6,046,250 (**1990**).

[2] G. Camino, S.M. Lomakin, M. Lazzari. Polym., 42 (**2001**) 2395.

[3] S.L.B. Dal. IEEE 04CH37533. 42nd Annual International Reliability Physics Symposium, Phoenix **2004**.

[4] F. Wang, D.C. Neckers. J. Organomet. Chem. 665(**2003**) 1.

[5] F.D. Lewis, G.D. Salvi. Inorg. Chem. 34 (**1995**) 3182.

[6] J.L. Speier. Adv. Organomet. Chem. 17 (**1979**) 407

[7] J.A. Pojman. J. Am. Chem. Soc. 113 (**1995**) 6284.

[8] C. Nason, T. Ropper, C. Hoyle, J.A. Pojman. Macromolecules 38 (**2005**) 5506.

[9] A. Mariani, S. Bidali, S. Fiori, M. Sangermano, G. Malucelli, R. Bongiovanni, A. Priola. J. Polym. Sci., Polym. Chem. 42 (**2004**) 2066.

[10] E. Frulloni, M.M. Salinas, L. Torre, A. Mariani, J.M. Kenny. J. Appl. Pol. Sci. 96 (**2005**) 1756.

6. SILICONE COMPOSITES VIA TOP-DOWN APPROACH

To promote the electrical resistance of the silicone material, investigations were performed by adding either micrometric or nanometric fillers in the formulation. The curing reaction and final properties of the composites were evaluated. The study was performed using the vinyl oligomer with the lowest molecular weight (formulation C), as a front propagation was evidenced for this system, leading to the formation of thick samples suitable for outdoor applications.

6.1. Sample preparation

The mixtures were prepared by adding an equimolar amount of vinyl and silane reactive groups. The fillers were previously dried for 2h at 80°C in order to remove adsorbed water and then dispersed into the formulations by using a Speed Mixer (Speed Mixer^{TM} DAC 400.1 FVZ) for 1minute at 2000 rpm. The Pt-catalyst was solubilized in 1,3-dioxolane, added to the formulation at a content of 500 ppm and mixed again at 2000 rpm for 1 additional minute. The resulting formulations were poured into molds and the curing was carried out in air with a medium pressure mercury lamp for 5 minutes. The thickness of the samples was varied from 50 µm to 4 mm.

The amount of filler was chosen as follows: the lower limit was predetermined by avoiding sedimentation effects while the upper limit of filler content was related to the critical volume concentration. At this volume concentration there is just enough resin available to wet the pigment surface and fill the interstices

between particles. Further addition of pigment causes voids in the system because there is not enough resin to completely wet the pigment and fill the interstices thus creating a resin-starved system.

6.2. Micrometric sized fillers

6.2.1. Materials

The individual filler content used for the preparation of the samples were reported in Table 6.1 where the particles dimension indicates that respectively 90% and 95% of the distribution was below the indicated value. The amount of filler used (per hundred resin phr) and the volume fractions were also reported.

Table 6.1: List of filler used

Type	Filler amount (phr)	Filler volume fraction Vf	Particles dimension	Density ($g.cm^{-3}$)
$1SiO_2$	130 – 300	0.30 – 0.51	d_{90} = 35 µm	2.65
$2SiO_2$	130 – 350	0.30 – 0.55	d_{95} = 130 µm	2.65
Al_2O_3	80 – 370	0.11 – 0.46	d_{90} = 11 µm	4.0
$Al(OH)_3$	46 - 400	0.30 – 0.60	d_{90} = 65 µm	2.4

Two different silica oxides with different particle sizes were tested in order to evaluate the influence of the dimension on the curing and properties of the composites.

6.2.2. Granulometric analyses

The granulometric distribution of the selected fillers were achieved by dispersing the powders in ethanol. The distribution weight were reported as a

function of the particles size (Figure 6.1). The different oxides presented a narrow size distribution. A slight underestimation of the data given by the different suppliers was observed which could be due to a good dispersion of the filler in ethanol and subsequent disappearance of the agglomerates.

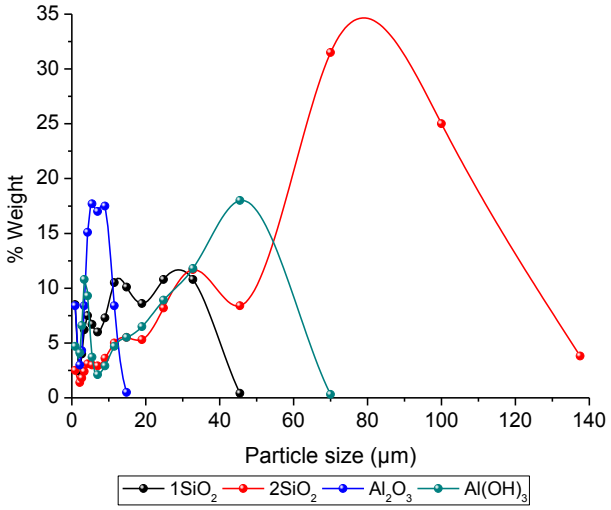

Figure 6.1: Granulometric distribution for the filler used

The particle size and distribution could be relevant to evaluate the effect of the fillers on the curing process and to determine the suitable amount of particles that could be added to the formulation without reaching the critical volume fraction. Moreover, the size of the filler needed to be well known as it also influence the final properties of the composites.

6.2.3. FT-IR analyses

The effect of the type and amount of fillers on the curing process was studied by means of real-time FTIR analyses. The Si-H conversion curves as a function of the irradiation time for the different fillers were reported in Figure 6.2.

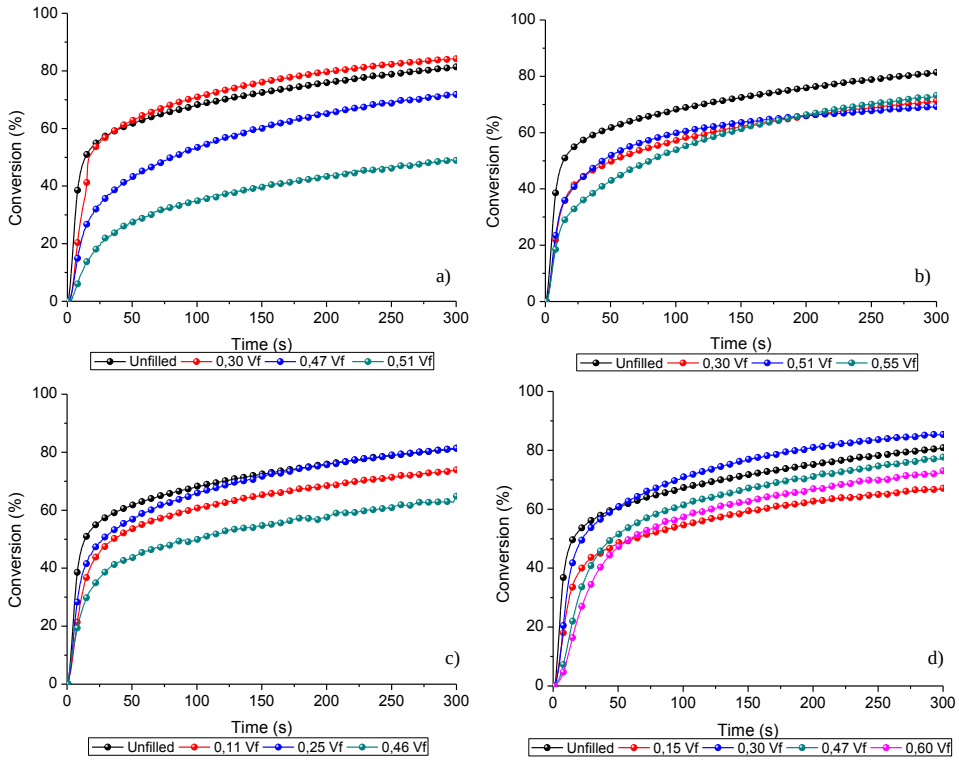

Figure 6.2: Silane conversion as a function of irradiation time for different amount of: a) $1SiO_2$, b) $2SiO_2$, c) Al_2O_3, d) $Al(OH)_3$

It became evident that the presence of fillers lead to a progressive decrease of the system reactivity. This was evidenced by a decrease of the initial slope and the final conversion of the silane increasing the filler content.

This phenomena could be attributed to a lower mobility of the polymeric chains induced by the particles which could hinder the diffusion of the growing polymeric chains. By comparing the kinetics of the two SiO_2 oxide ($1SiO_2$ and $2SiO_2$) with different particle sizes (Figure 6.2a-b), it resulted that lower final conversions were achieved for the smallest particles ($1SiO_2$). This could be due to an higher specific surface area by decreasing the particles dimension (from 1300 $cm^2.g^{-1}$ for $2SiO_2$ to 4200 $cm^2.g^{-1}$ for 1 SiO_2 0), leading to an higher viscosity of the formulation. That reduced the polymeric chains mobility inducing a decrease of final conversion. This also occurred for Al_2O_3 where the curing was highly reduced by progressive addition of filler. On the contrary, by using $Al(OH)_3$ that presented larger particles, the kinetic of polymerization was less affected. In fact

the final silane conversion was around 73% even in the presence of high amount of particles (Table 6.2).

Table 6.2: Conversion and gel content of UV-cured samples after 300s of UV irradiation

Type	Volume fraction Vf	FT-IR Conversion (%)	Gel content (%)
Unfilled	/	81	99
1SiO_2	0.30	84	99
	0.47	71	99
	0.51	48	99
2SiO_2	0.30	71	98
	0.51	69	99
	0.55	73	99
Al_2O_3	0.11	73	98
	0.25	81	99
	0.46	65	99
$Al(OH)_3$	0.15	67	99
	0.30	85	99
	0.47	77	99
	0.60	73	99

Gel content measurements were performed on thick samples (4mm). The experiments showed values higher than 98% for all the samples (Table 6.2) indicating that they reached a high degree of conversion all along their thicknesses. These data clearly demonstrated that UV-activated hydrosilation is an efficient curing technology which works perfectly to cure silicones also in the presence of inorganic fillers.

6.2.4. TGA analyses

Thermogravimetric analyses were performed in air for all the cured samples and the influence of the amount and type of filler was evaluated (Figure 6.3). The presence of silica fillers 1SiO_2 and 2SiO_2 (Figure 6.3a-b) lead to an increase of the thermal stability of the composites. In fact T_{10} (temperature for 10% weight loss) was shifted from approximately 400°C to 540°C due to the presence of fillers

(that are inert for temperatures even higher than 800°C). When the silica content was too high (for example 0.40 Vf of $1SiO_2$ Figure 6.3a); the thermal stability started to decrease. This was probably associated to a lower curing degree of the sample confirmed by FT-IR experiments (Figure 6.2a). For the samples containing Al_2O_3 filler (Figure 6.3c), a progressive increase of the thermal stability was achieved by increasing the filler content.

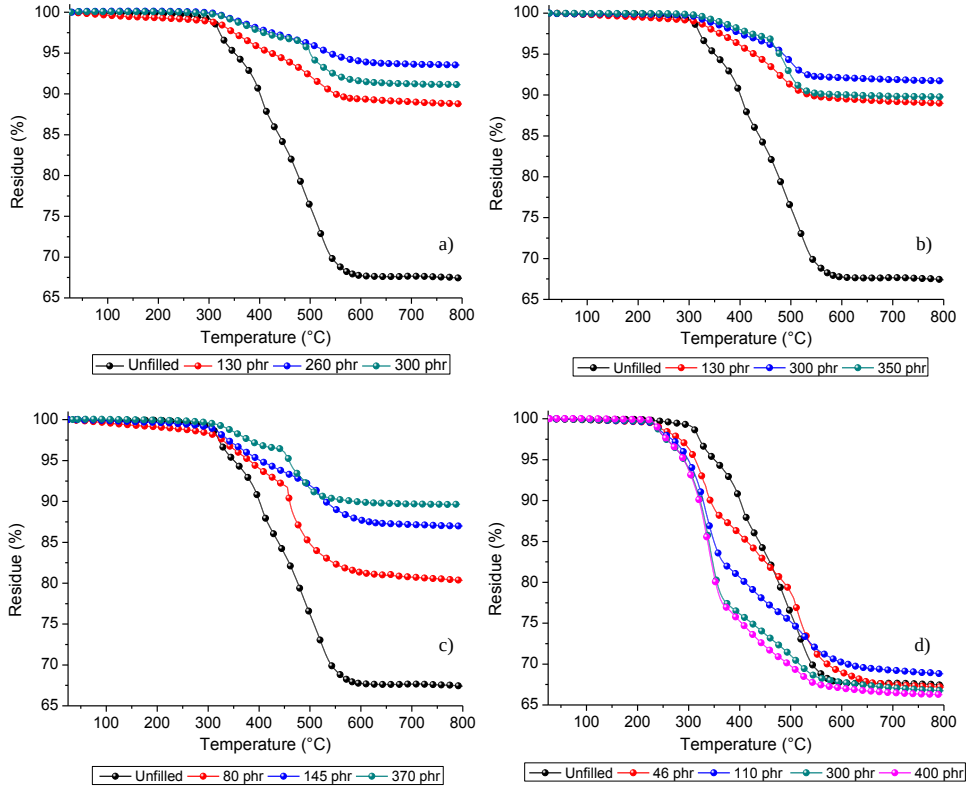

Figure 6.3: TGA analyses for samples with different amount of: a) $1SiO_2$,b) $2SiO_2$, c) Al_2O_3, d) $Al(OH)_3$

The distinct step at 480°C obtained for samples containing silica or alumina filler was due to the shift of the crosslinked PDMS breakdown to higher temperatures as a result of the fillers reinforcing effect. On the contrary, when $Al(OH)_3$was used (Figure 6.3d), a decrease of the final thermal properties was evidenced. It is well known from literature that polymer composites containing $Al(OH)_3$ fillers do not show an improvement of the thermal stability. $Al(OH)_3$ starts to degrade at around 190°C by release of water and progressive formation of

boehmite until 380 °C. At this temperature the boehmite decomposition into alumina starts and this reaction is responsible for the second step of weight loss up to 550°C [2]. The $Al(OH)_3$ decomposes according to the reaction: $2Al(OH)_3 \rightarrow Al_2O_3 + 3H_2O$. The detailed mechanism was summarized in Figure 6.4.

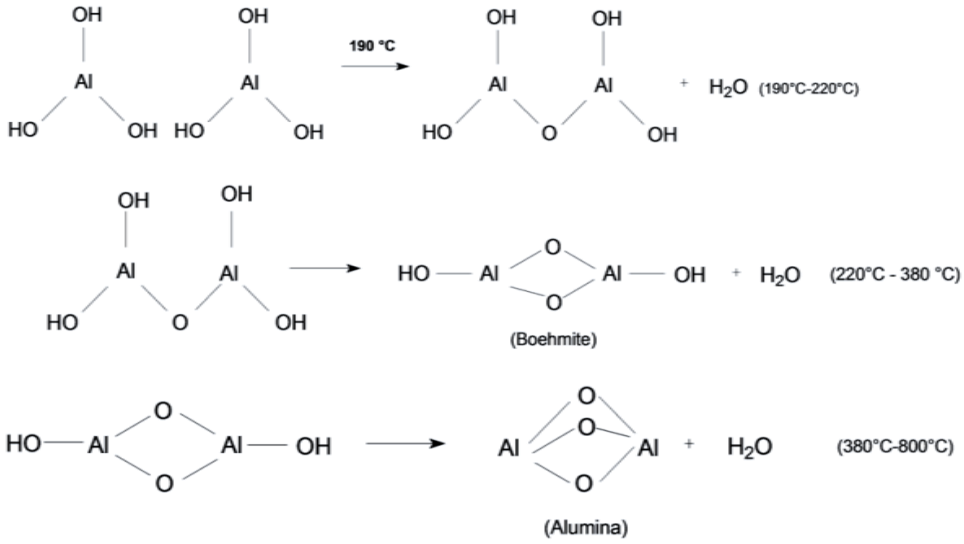

Figure 6.4: $Al(OH)_3$ thermal decomposition mechanism

6.2.5. DMTA analyses

Dynamic mechanical thermal analyses were performed on cured samples with different amount of fillers. The maximum value of tan δ is related to the transition from a glassy to a rubbery state. The tan δ curves for samples containing different fillers were reported (Figure 6.5a SiO_2, Figure 6.5b $Al(OH)_3$). All the samples showed an increase of the Tg values with respect to the unfilled PDMS attributable to the presence of the inorganic fillers. The nature of the filler had an influence on the Tg increase (Table 6.3). In fact, aluminium trihydrate composites presented lower Tg than silica ones even for high amounts of fillers. This was due to an higher increase of viscosity by the presence of particles that hindered the complete curing of the polymeric matrix with a consequent decrease of crosslinking density.

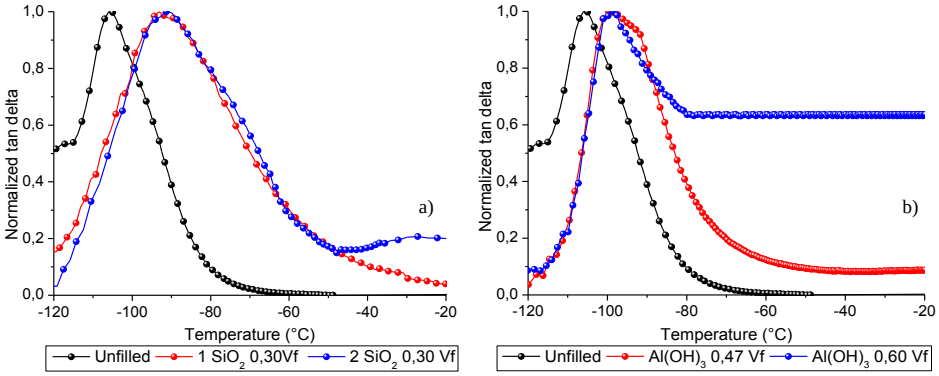

Figure 6.5: Tan delta values for: a) Silica filler, b) $Al(OH)_3$ filler

Table 6.3: Tg values of PDMS composites

Sample	Unfilled	0.30 Vf $1SiO_2$	0.30 Vf $1SiO_2$	0.47 Vf $Al(OH)_3$	0.60 Vf $Al(OH)_3$
Tg value (°C)	-108	-93	-94	-99	-98

6.2.6. Dry Arc Resistance

A voltage was applied on the samples surface until a conducting path across the entire surface of the specimen occurred; indicating the end-point of the measurement. Failure of silicone materials has an end point that is usually quite definite and a noticeable change in sound of the applied voltage is recognizable. Higher values indicate greater resistance to breakdown along the surface due to arcing or tracking conditions. Preliminary conclusions of change in structure and composition of the material can be obtained with this analysis without the complicating influence of environmental conditions. The dry arc resistance values for the PDMS composites were reported in Table 6.4.

The measurements were performed four times for both sides in order to control the homogeneity of the samples and verify that no filler sedimentation occurred. Samples dimensions were 30*30mm and 4mm thick. The values obtained for the unfilled PDMS (120s) were in accordance with those usually obtained for silicone grease with a dry arc resistance value of 80-150s [3]. In the presence of fillers (independently of the nature of the filler) this value was progressively increased to

180s when sedimentation effect was avoided (recognizable by different values between top and bottom sides as for example with 0.30 Vf of $2SiO_2$). By dispersing higher amount of fillers inside the polymeric matrix, a further increase up to 240s could be reached independently of the filler nature. No significant improvement of the dry arc resistance values were observed by a further increase of the filler content.

Table 6.4: Dry Arc Resistance Values for the PDMS composites

Type	Volume fraction Vf	Amount phr	Top side (s)	Bottom side (s)
Unfilled	/	/	124	123
$1SiO_2$	0.30	130	181	182
	0.47	260	242	242
	0.51	300	242	242
$2SiO_2$	0.30	130	124	187
	0.51	300	243	243
	0.55	350	241	241
Al_2O_3	0.11	80	182	182
	0.46	370	244	244
$Al(OH)_3$	0.30	110	183	183
	0.47	300	239	235
	0.60	400	247	246

It is somehow important to underline that the dry arc resistance time could be doubled by addition of the inorganic fillers.

6.2.7. Dielectric Spectroscopy

The relative permittivities (ε') for the pure PDMS and their various composites were reported in Figure 6.6 as a function of frequency (at 40 °C). The dielectric constant of the pure PDMS was flat (independent on frequency)that is a typical behavior for non-polar polymers. The addition of the various fillers, all having dielectric constant values higher than the PDMS, induced an overall increase in ε'. The observed increase was systematic in most cases with the filler content. Only the specimen containing 0.51 Vf of $1SiO_2$ deviated from the above trend. This

could be attributed to air intrusion inside the formulation during mixing owing to the high viscosity at such high filler loadings. An increase at the low frequency side could be also noticed in the composites due to the rise of an interfacial slow relaxation owing to a difference in permittivities among matrix and fillers (so called Maxwell-Wagner-Sillars relaxation). In this case charges could be blocked at the internal phase boundaries causing a strong increase in ε' with frequency decrease.

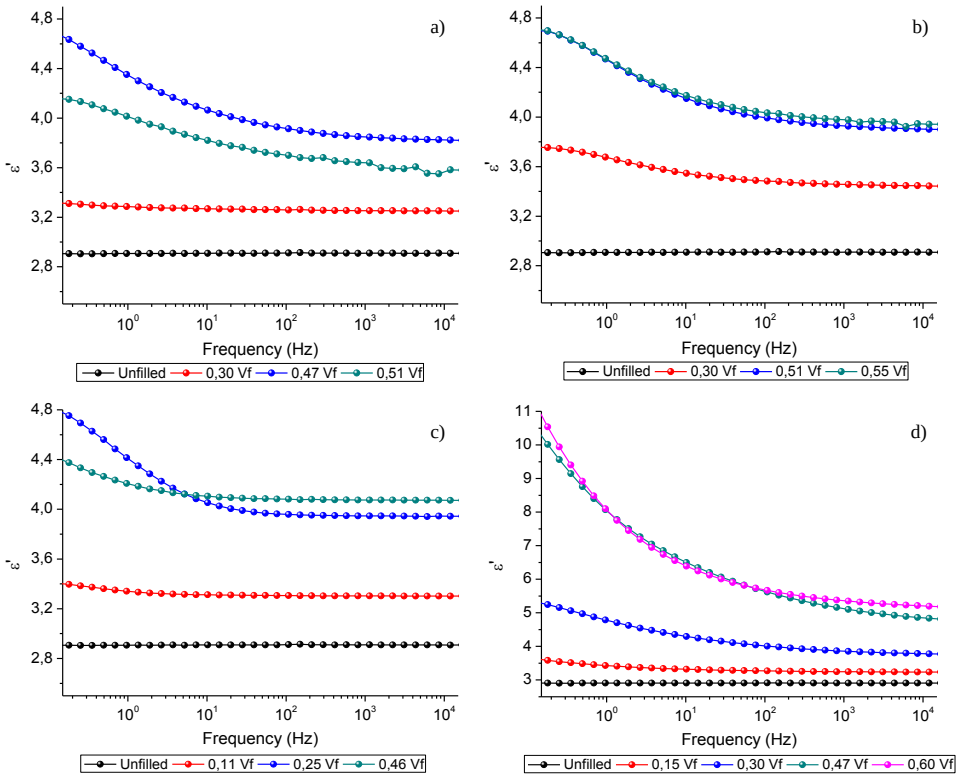

Figure 6.6: Relative permittivity for samples with different amount of: a) $1SiO_2$, (b) $2SiO_2$, c) Al_2O_3, d) $Al(OH)_3$

The dielectric loss factor were reported for all the fillers used (Figure 6.7). For the unfilled system, the losses were below the sensitivity of the instrument (less than 10^{-3}) and therefore were not reported in the different curves. The increase of filler content lead to a shift of the relaxation process (that is the return of a perturbed system into equilibrium characterized by a decrease of relative permittivity and a peak in the dielectric loss factor) at higher frequencies. This

phenomenon was observed for all the fillers under investigation and could be due to the polymer-filler interaction [4],[5].

The high values of relative permittivity for the $Al(OH)_3$ (Figure 6.6d) could be attributed to electrode polarization as no peak were present in the dielectric loss factor at the same frequencies (Figure 6.7d).

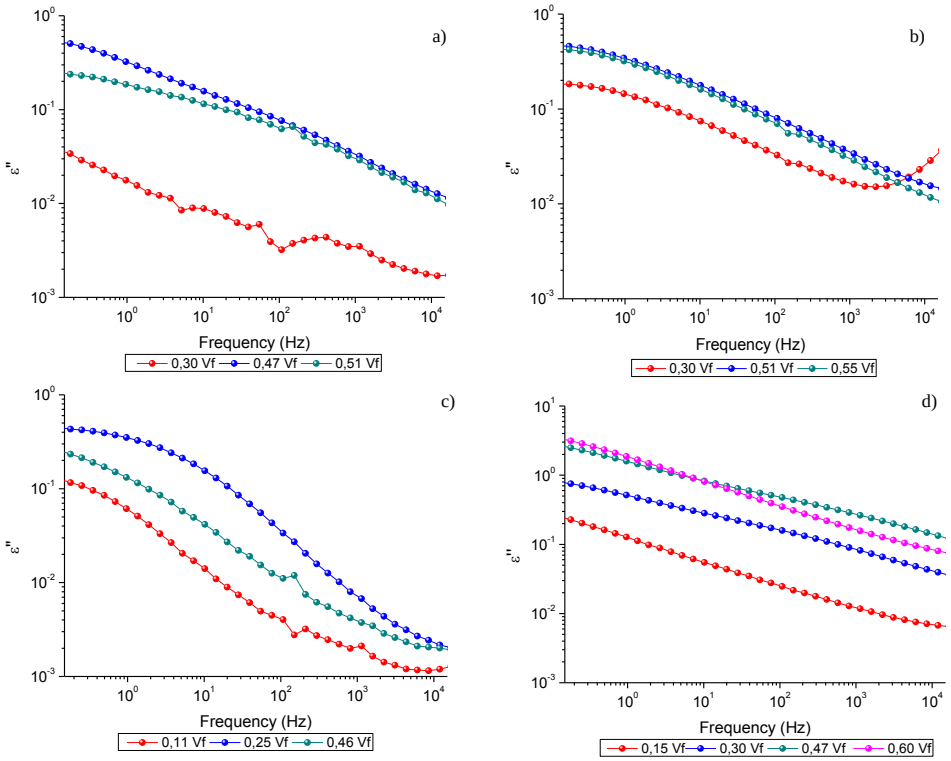

Figure 6.7: Dielectric loss factor of samples with different amount of: a) $1SiO_2$, (b) $2SiO_2$, c) Al_2O_3, d) $Al(OH)_3$

6.2.8. Prediction of composites relative permittivity

One of the problems inherent in composite systems is to predict their macroscopic properties using the properties of the constituents. Many theoretical investigations on binary systems were performed in regard to the dielectric and elastic constants[6]-[8]. The equations here used to calculate theoretical values of the real part of the relative permittivity are based on previous investigations [9],[10] where it was shown that Lichtenecker (LE) mixing rule or the logarithmic

mixing rule for random media provided the best fitting prediction of effective relative permittivity. The equation was given below:

$$(\boldsymbol{V_1 + V_2})\,\boldsymbol{\log \varepsilon_{eff}} = \boldsymbol{V_1 \log \varepsilon_1 + V_2 \log \varepsilon_2} \quad (2)$$

where V and ε represent respectively the volume percent (V_1+V_2=1) and the dielectric constant;the subscript 1 is referred to the PDMS and 2is referred to the filler under investigation.

The other different equations used in this part are given as follows:

Furukawa equation (FE) or equation from the effective medium theory modified by Hashin-Shtrikman [11]:

$$\boldsymbol{\varepsilon_{eff}} = \frac{\boldsymbol{\varepsilon_1[(1\ +\ 2f)\varepsilon_2 + 2\varepsilon_1(1-f)]}}{\boldsymbol{\varepsilon_2(1-f)\ +\ (2+f)\varepsilon_1}} \quad (3)$$

where f is the volume fraction of the filler.

Jayasundere-Smith equation (J-SE) [12]:

$$\boldsymbol{\varepsilon_{eff}} = \frac{\boldsymbol{[\{\varepsilon_1 f_1\ +\ \varepsilon_2 f_2(3\varepsilon_1/(\varepsilon_2+2\varepsilon_1))\}\{1+3f_2(\varepsilon_2-\ \varepsilon_1)/(\varepsilon_2+2\varepsilon_1)\}]}}{\boldsymbol{[\{f_1+\ f_2(3\varepsilon_1/(\varepsilon_2+2\varepsilon_1))\}\{1+3f_2(\varepsilon_2-\ \varepsilon_1)/(\varepsilon_2+2\varepsilon_1)\}]}} \quad (4)$$

Knott equation (KE) [13] :

$$\boldsymbol{\varepsilon_{eff}} = \boldsymbol{\varepsilon_2[1-\{(\varepsilon_2-\ \varepsilon_1)(1-f)\}/\{\varepsilon_1+\ (\varepsilon_2-\ \varepsilon_1)(1-f)^{1/3}\}]} \quad (5)$$

Modified Rother-Lichtnecker equation (MRLE) [14] :

$$\boldsymbol{\varepsilon_{eff}} = \boldsymbol{exp}[\boldsymbol{\ln \varepsilon_1 +\ f_2(1-k)\ln(\varepsilon_2/\varepsilon_1)}] \quad (6)$$

where k is a shape-dependent parameter. When f_2=1; which means that the composite is made only by the particles; the effective relative permittivity equals to $\varepsilon_{eff} = \varepsilon_1 * (\varepsilon_2/\varepsilon_1)^{(1-k)}$.Therefore, the smaller is k and the more accurate is the equation. This parameter was fixed at 0.05 in our investigation so that the values of the relative permittivity at the boundaries were close to the theoretical values of both PDMS and filler.

The relative permittivities of the fillers used were taken from literature [15] and summarized in Table 6.5. The value for the silica was referred to the quartz crystalline form. For the unfilled, system the value was obtained from the dielectric spectroscopy measurement.

Table 6.5: Relative permittivities of the unfilled system and the different fillers used

	Unfilled	SiO_2	Al_2O_3	$Al(OH)_3$
Relative Permittivity (at 25°C and 1 kHz)	2.9	4.6	10.4	8.4

The theoretical and experimental values of ε' as a function of filler volume fraction were reported in Figure 6.8. The experimental data were taken at 1kHz from the dielectric spectroscopy measurements.

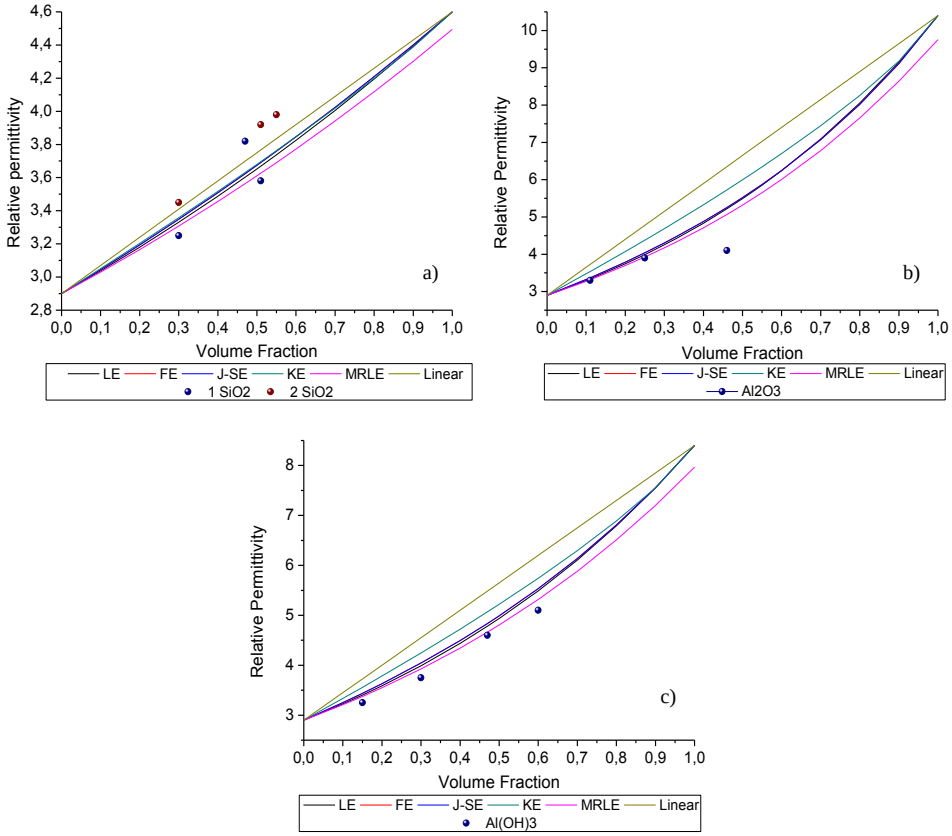

Figure 6.8: Relative permittivity at 1kHz of PDMS composites as a function of volume fraction of: a) SiO_2, b) Al_2O_3, c) $Al(OH)_3$

In the case of the silica fillers (Figure 6.8a), the theoretical equations were in accordance with the experimental data even if a slight underestimation was observed, especially in the case of the $1SiO_2$ filler. This could be due to the fact that these mixing rules do not take into account the polymer-filler interaction. For instance, an increase in system's free volume upon silica addition leads to an increase of the ε' values that is not considered in the different models.

In the case of alumina (Figure 6.8b), experimental data at low volume fraction fit well with the theoretical values from LE, J-SE and MRLE equations. At higher amount of fillers, the obtained experimental values were lower probably due to an agglomeration effect inside the composite.

All the experimental values obtained with the aluminum hydroxide were in accordance with the MRLE equation (with k=0.05) and so in this case it could be possible to predict the relative permittivity as a function of the volume fraction of the filler (Figure 6.8c).

6.2.9. Curing depth measurements

The curing depth measurements were performed using PVC tubes (13mm of diameter 20mm in length) closed on one side and filled with formulations containing different amounts of fillers. The curing depth was measured as a function of UV light exposure time (up to 300s). The cured silicone were demolded 30 minutes after irradiation in order to let the dark curing proceed.

The curing depth as a function of irradiation time was reported in Figure 6.9 for formulations loaded with 100 phr and 300 phr of SiO_2 and $Al(OH)_3$.A high reduction of the curing depth is observed in the presence of fillers. In fact, unfilled samples were obtained with thickness up to 3cm while filled systems could be cured only on few millimeters. The decrease of thickness curability was attributed to heat dissipation due to the presence of ceramic fillers. Indeed, when the heat released by the UV-activated hydrosilation reaction is dissipated by the filler, the propagation of the heat front is hindered and the thermal activation of hydrosilation in the bulk is suppressed. An increase of irradiation time resulted therefore insufficient to achieve thicker samples.

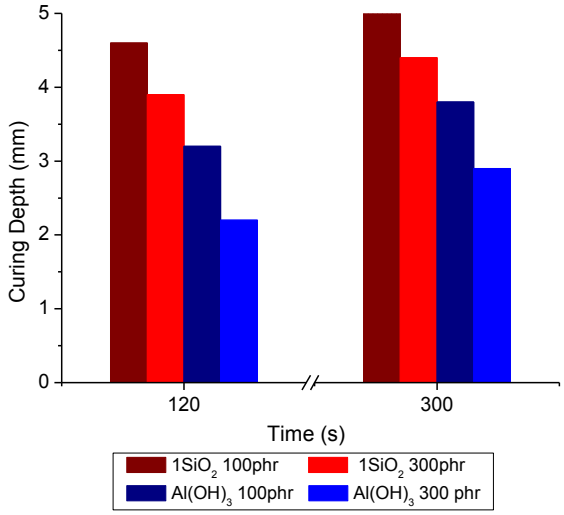

Figure 6.9: Curing depth of filled samples as a function of irradiation time

Moreover, higher cured thicknesses were achieved for silica-filled samples with respect to the same formulations containing $Al(OH)_3$. The curing depth after 90s of irradiation was reported in Figure 6.10. The difference of curing penetration could be explained by the thermal conductivities values [16]: silica particles present a thermal conductivity of about 9 $W.m^{-1}.K^{-1}$, while $Al(OH)_3$ thermal conductivity is about 2.6 $W.m^{-1}.K^{-1}$. The higher thermal conductivity for silica allowed the heat front to proceed through a longer distance, without dissipation, leading to thicker samples.

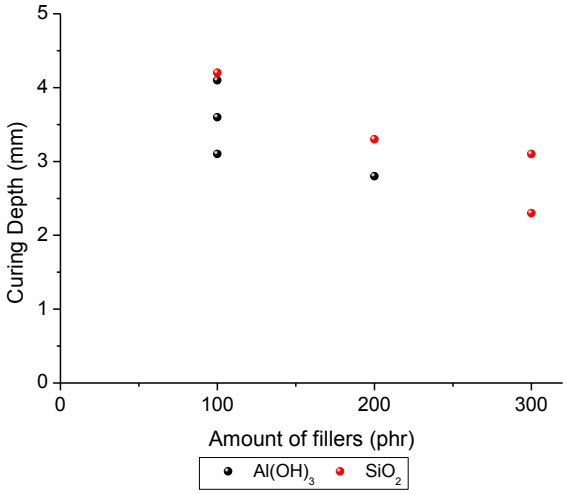

Figure 6.10: Curing depth as a function of the filler content for 90s of irradiation

An increment of Pt catalyst amount from 500 ppm to 2000 ppm was done to improve the curing depth of filled samples (Figure 6.11) but no thickness increase was achieved. This is in accordance with the catalytic nature of the process. Indeed, the catalyst is not consumed during reaction and can be recovered unchanged at the end of the reaction: when the lowest amount of catalyst is found, further addition of Pt catalyst doesn't lead to an increase of the reaction rate. This was previously observed for the pristine silicone formulations. That is the reason why by increasing the Pt catalyst, no significant increase of the thickness curability was obtained.

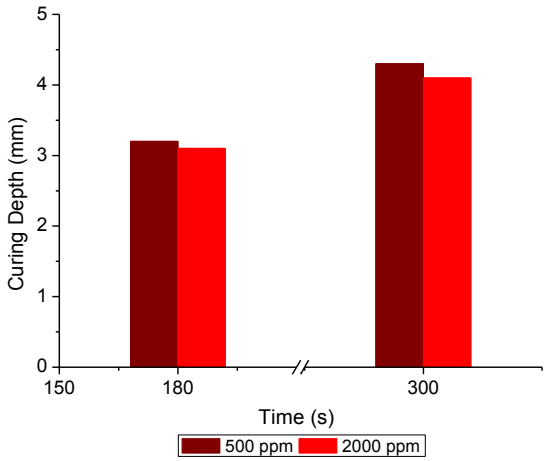

Figure 6.11: Influence of Pt catalyst amount for 300phr SiO_2 filled samples

In order to evaluate the influence of particles dimension on the thickness curability, three different $Al(OH)_3$were used at a content of 100phr. Their dimension were reported in Table 6.6.

Table 6.6: Particles dimension of the $Al(OH)_3$ used for the curing depth measurements

Name	Particles dimension
Martinal ON-904	d_{50} = 4 µm
Martinal ON-310	d_{90} = 33 µm
Martinal ON-921	d_{90} = 65 µm

No evident correlation between particle size and curing depth was observed. Therefore, an increment of thickness could not be reached by varying the particle dimension (Figure 6.12).

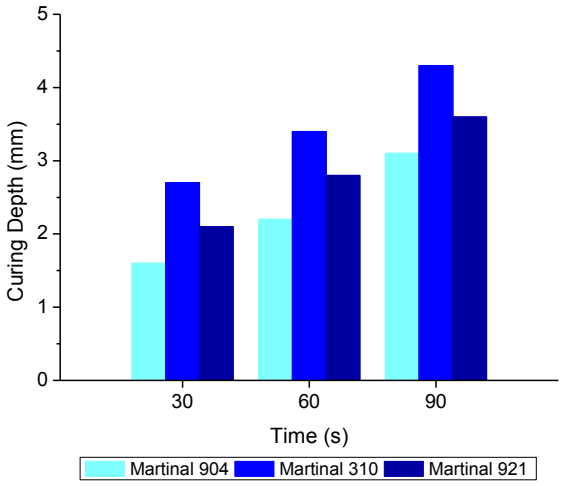

Figure 6.12: Curing depth of samples with 100phr of $Al(OH)_3$ fillers

6.2.10. SEM analyses

Morphological analyses were performed in order to evaluate the dispersion of the fillers into the polymeric matrix. The samples were 1mm thick and the results were reported in Figure 6.13-Figure 6.16. All the samples presented a good homogeneity confirming that the fillers were well distributed into the silicone polymer. The increase of particles content did not lead to any important agglomeration effect.

Regarding the silica fillers (Figure 6.13 and Figure 6.14), it resulted quite difficult to individualize the particles due to the poor contrast between the silicone matrix and the silica particles.

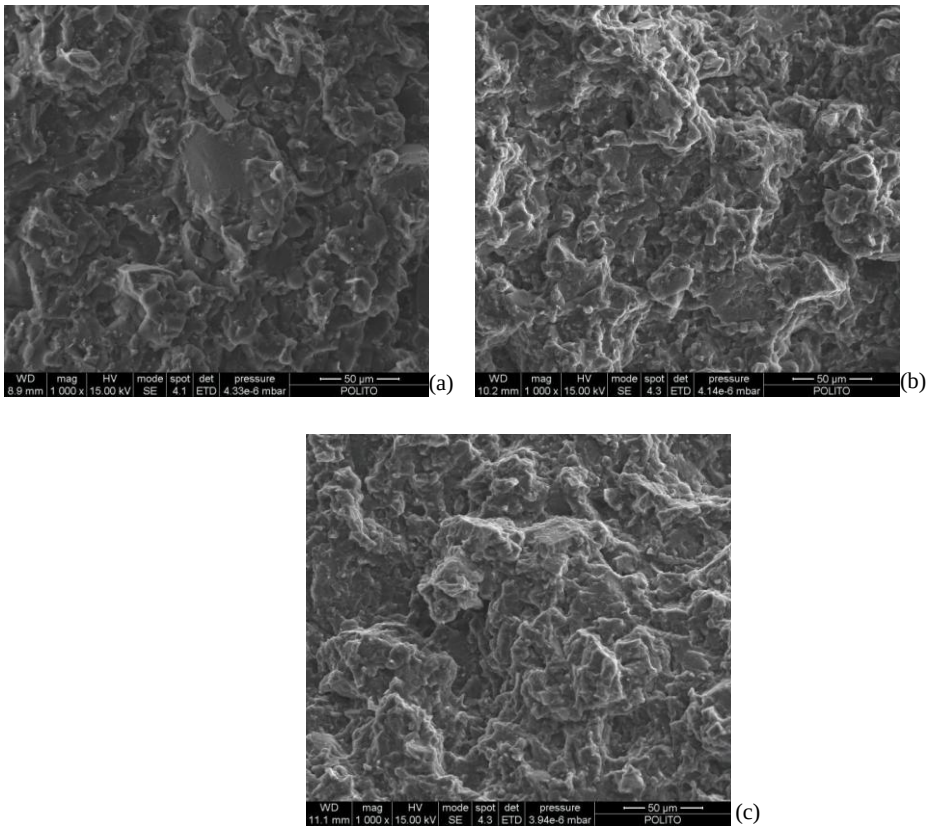

Figure 6.13: SEM analyses for samples with 130(a) 260(b) and 300(c)phr of $1SiO_2$

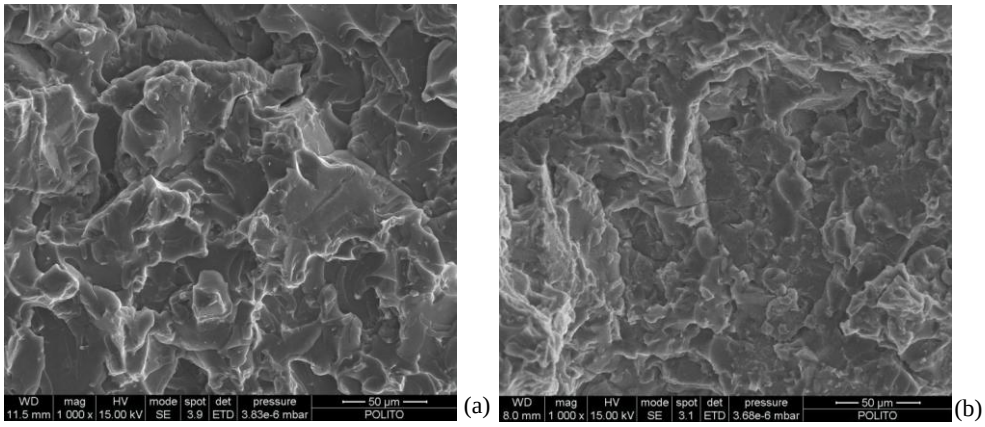

Figure 6.14: SEM analyses for samples with 130(a) and 350(b)phr of $2SiO_2$

Both Al_2O_3 and $Al(OH)_3$ fillers lead to a good dispersion inside the polymeric matrix (Figure 6.15 and Figure 6.16). It was possible to observe how the different particles resulted well embedded into the silicone matrix and that no evident agglomeration zone in the material was evidenced.

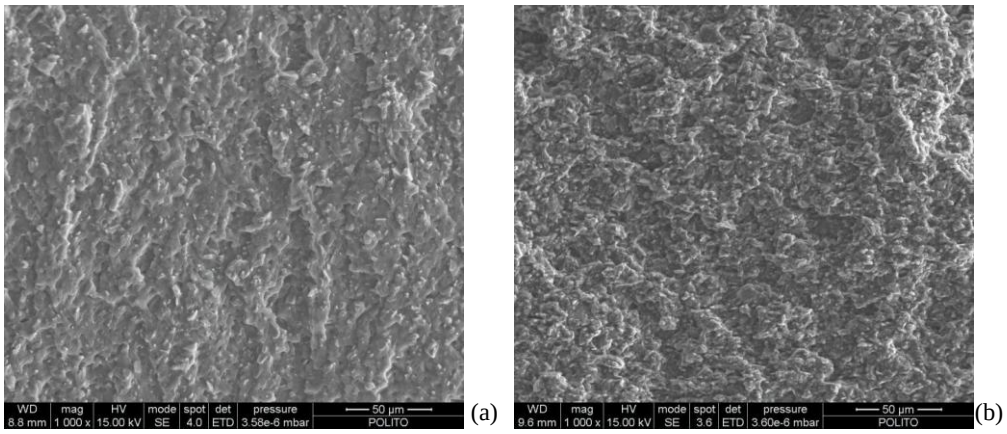

Figure 6.15: SEM analyses for samples with 80(a) and 370(b)phr of Al_2O_3

Due to the high amount and dimensions of the oxides, the cured samples were not transparent and presented a grey or white color depending on the nature of the filler used (Figure 6.17). The samples were irradiated from the top and had a thickness of 1mm.

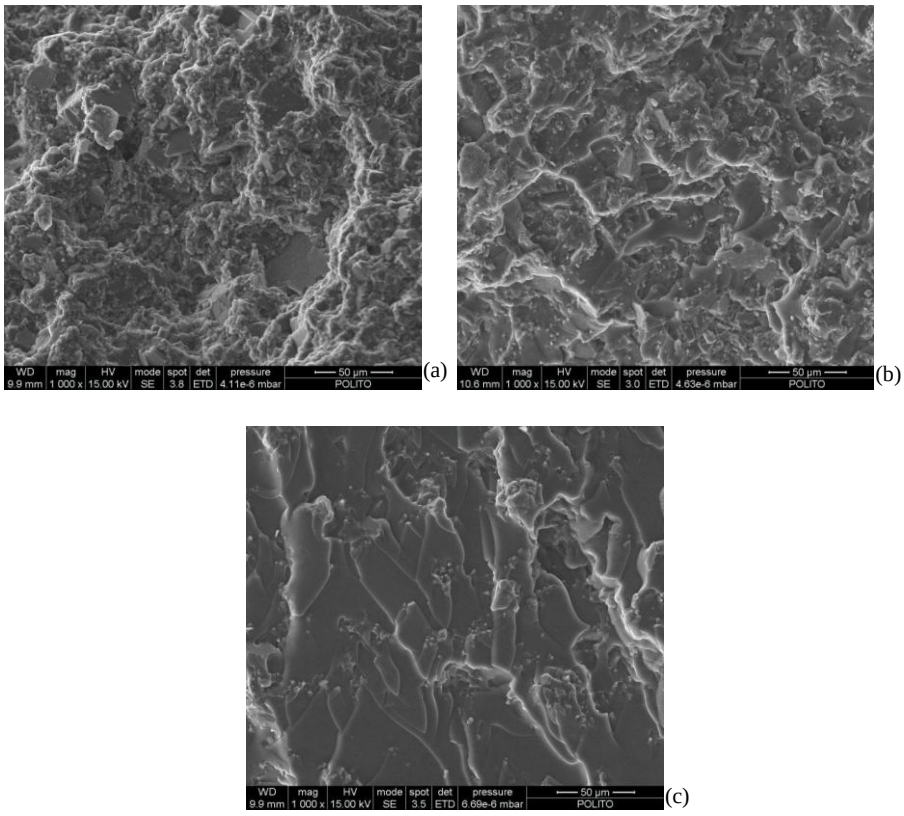

Figure 6.16: SEM analyses for samples with 46(a) 110(b) and 400(c)phr of $Al(OH)_3$

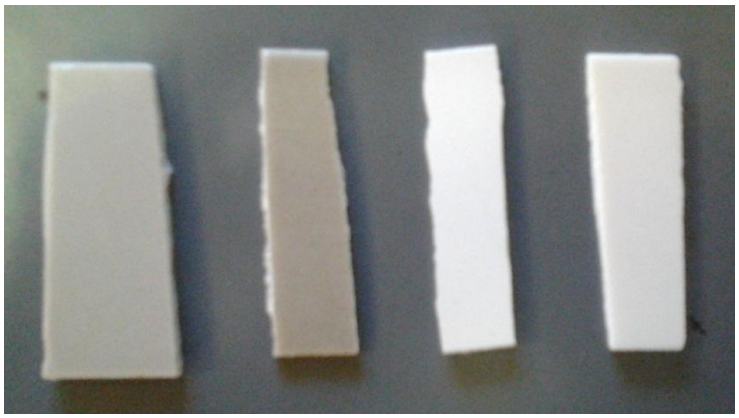

Figure 6.17: Cured samples with $1SiO_2$, $2SiO_2$, Al_2O_3 and $Al(OH)_3$ fillers (from left to right)

6.2.11. Conclusions

Micro-sized fillers were incorporated into the formulation C (with the lowest molecular weight of the vinyl) in order to improve the final electrical properties of the material. The influence of the nature and size of the fillers were evaluated.

A progressive decrease of the initial slope and final conversion were observed by increasing the filler content but gel content were still above 99% confirming that a tight crosslinked network was achieved and that almost no extractable oligomers were present.

The insertion of silica or alumina induced an increase of the composites thermal properties while the presence of aluminum hydroxide;that progressively decomposed into boehmite and alumina with progressive release of water; did not give any thermal improvement. An increase of the Tg value was observed by adding inorganic fillers inside the polymeric matrix. The dry arc resistance of filled samples could be doubled independently of the filler nature. Only the amount of filler was responsible for the increase of resistance time.

An increase of relative permittivity in the composites was observed due to higher values of filler dielectric constant with respect to the silicone matrix. However, they were still in an acceptable range. Moreover, the increase of filler content lead to a shift of the relaxation process at higher frequencies. The relative permittivity of composites could be predicted by using the MRLE equation.

SEM analyses showed a good dispersion of all the fillers under investigation within the silicone material.

The main drawback of fillers addition in polymeric matrix was the decrease of thickness curability attributed to heat dissipation by the ceramic fillers.

6.3. Nanometric sized fillers

In order to increase the thickness curability of the composites, different nanometric sized fillers were tested. The effect of nanoparticles on curing process and final properties were also evaluated.

6.3.1. Materials

The following fillers were added to the silicone precursor as received:

- Zeosil 1165 (Silica powder, d=50nm, BET=165 $m^2.g^{-1}$)
- Aerosil 200 (Fumed Silica, d=12nm, BET=200 $m^2.g^{-1}$)

The amount of nanoparticles into the formulation was selected by using quantities that do not avoid the front propagation. It was possible to prepare thick samples with Aerosil 200 (up to 7phr) and Zeosil 1165 (up to 20phr) by frontal propagation. These ranges were used for the preparation and characterization of the composites.

6.3.2. FT-IR analyses

The influence of nanofillers on the rate of polymerization was studied by following the Si-H bond conversion by means of FT-IR analyses (Figure 6.18a for Aerosil 200 and Figure 6.18b for Zeosil 1165). The thickness of the samples was about 50 µm. The final conversion and the gel content were reported in Table 6.7.

A progressive decrease of the initial slope of reaction and final silane conversion were evidenced by increasing the filler content. This could be

attributed to a lower mobility of the polymeric chain induced by the particles which could hinder the diffusion of the growing polymeric chains. However, all the samples presented high values of gel content confirming a high degree of curing.

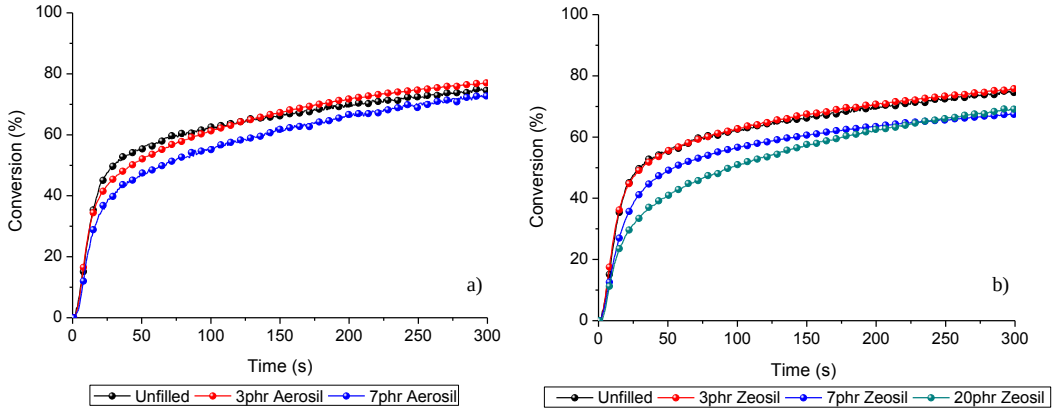

Figure 6.18: Silane conversion as a function of irradiation time for different amount of: a) Aerosil 200, b) Zeosil 1165

Table 6.7: Conversion and gel content of UV-cured materials after 300s of UV irradiation

Type	Amount (phr)	FT-IR Conversion (%)	Gel content (%)
Unfilled	/	81	99
Aerosil	3	77	99
	7	72	98
Zeosil	3	75	98
	7	67	98
	20	69	99

6.3.3. TGA analyses

Thermogravimetric analyses were performed on the cured samples and the influence of the amount and type of filler was evaluated (Figure 6.19a for Aerosil 200 and Figure 6.19b for Zeosil 1165). In the presence of nanofillers, no significant variation of thermal stability was observed but, final residues were higher for the nanocomposites with respect to the unfilled system due to the fact that fillers are inert for temperatures lower than 800°C.

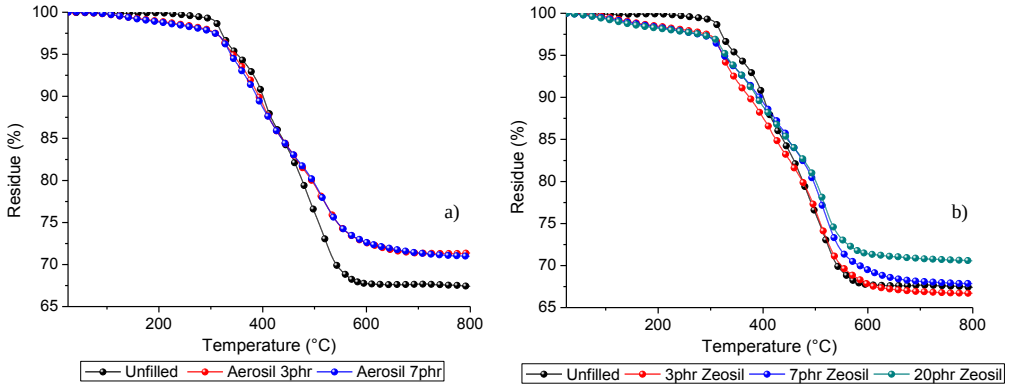

Figure 6.19: TGA analyses for samples with different amount of: a) Aerosil 200, b) Zeosil 1165

6.3.4. DMTA analyses

Dynamic mechanical thermal analyses were performed on cured samples with different amount of nanofillers. The tan δ of the different samples (Figure 6.20) showed an increase of the Tg values with respect to the unfilled PDMS. The Tg values of the different samples were reported in Table 6.8. A significant increase of the Tg valuewas achieved by using only 3phr of Aerosil 200; a further increase of filler content lead to a reduction of the value.This was probably due to a lower curing of the nanocomposites as a decrease of silane conversion was also evidenced by RT-FTIR data (Figure 6.18). On the contrary using the Zeosil filler no influence of the amount on the Tg value was observed.

It is interessant to notice that, with a few amount of nanoparticles (on the range of 3-7phr), the increase of the Tg values was comparable to whatwas achieved previously for microcomposites containing 0.22 Vf of 1SiO_2 and was also higher than what was obtained with 0.60 Vf of micro alumina trihydrate (Table 6.3). Thus confirmed that the use of smal amount ofnanofillers lead to a higher improvement of composites properties with respect to the use of micrometric fillers.

Table 6.8: Tg values of PDMS nanocomposites

Sample	Unfilled	3phr Aerosil	7phr Aerosil	3phr Zeosil	7phr Zeosil	20phr Zeosil
Tg value (°C)	-108	-92	-95	-96	-97	-96

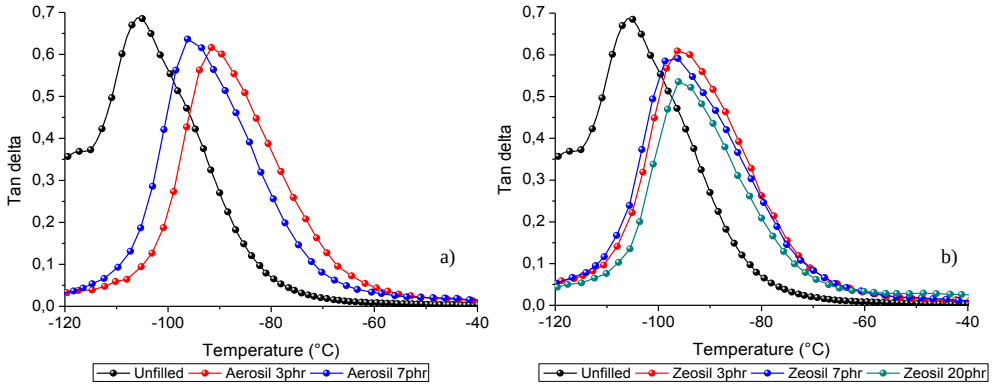

Figure 6.20: Tan delta values for different amount of: a) Aerosil 200, b) Zeosil 1165

6.3.5. Evaluation of frontal propagation

Temperature profiles were registered for filled systems by optical pyrometry measurements. Samples were prepared following the procedure reported in6.1. The formulations were subsequently let under vacuum for 15min in order to remove air coming from the dispersion phase. The temperature profiles were reported for formulations containing different amount of Aerosil 200 or Zeosil 1165 ranging from 3 to 20 phr (Figure 6.21). The measurements were performed respectively at 1cm (Figure 6.21a) and 2cm (Figure 6.21b) from the top of the formulations.

For equal amount of filler, higher temperatures inside the formulation were achieved for the composites containing Zeosil 1165. This could be explained by the lower surface area of Zeosil 1165 with respect to the Aerosil 200 filler (see 6.3.1) that enhanced the front propagation. Indeed, phenomenon of heat dissipation among samples thickness could be enhanced by increasing the surface area of powders (but also when high particles dimension are used). In fact, it was

previously observed that cured micro-sized composites presented thicknesses of some millimeters.

However, for nano-sized composites 2cm thick samples could be achieved as the front was able to propagate for these formulations (Figure 6.21). It was not possible to measure the temperature profiles for thicknesses higher than 2cmas heat dissipation avoid the proceeding of the front.

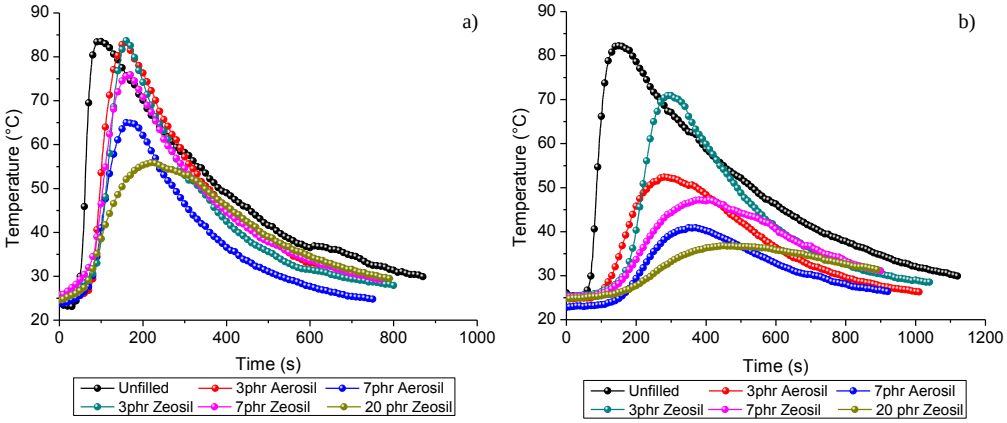

Figure 6.21: Temperature profiles at respectively a) 1cm and b) 2cm from the top for different amount of nanofillers

An increase of thickness curability was therefore achieved by reducing the particles dimension from some millimeters to 2cm thick samples.

6.3.6. Electrical properties

Dry Arc Resistance tests were performed for samples containing different amount of nanoparticles; both Aerosil 200 and Zeosil 1165. No increase on the resistance time was observed and values were still around 2 minutes as it was previously obtained for the unfilled system (Table 6.4). Moreover, a glowing channel was completed at ~2min but the arc never disappeared. The entire path was in flame in some cases and the sample cracked.

Dielectric spectroscopy measurements were performed on samples containing different amount of nanoparticles (Figure 6.22). An increase of the relative permittivity was achieved by progressive addition of Zeosil 1165 filler due to the

higher value of dielectric constant with respect to the unfilled system (as previously reported in Table 6.5) together with an increase of dielectric loss factor. On the contrary, a progressive addition of Aerosil 200 filler lead to lower values of relativity permittivity. This phenomena could be due to air intrusion in the formulation due to high viscosity but could also be a consequence of lower curing (as a decrease of the Tg was observed by DMTA analyses (Table 6.8) when the amount of Aerosil 200 was increased).

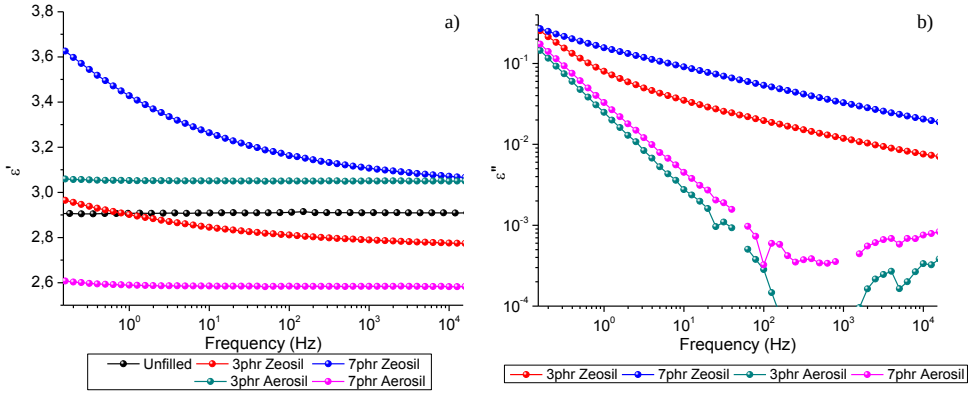

Figure 6.22: a) Relative permittivity b) and dielectric loss factor of nanocomposites

6.3.7. FE-SEM analyses

Morphological analyses were performed in order to evaluate the dispersion of the fillers into the polymeric matrix. The results were reported in Figure 6.23-Figure 6.24. It was possible to observe that all the samples present a good homogeneity confirming that the fillers were well dispersed into the silicone polymer.

The samples prepared with different amount of nanofillers were quiet transparent even in the presence of high amount of Zeosil 1165 (20phr). However, even if the formulations were put in vacuum before curing (in order to remove the air intrusion), samples prepared with Zeosil still present bubbles that were formed during the front propagation (Figure 6.25) and were therefore not removable. The brown color of some samples was due to the presence of Pt(0) colloids formed during the polymerization.

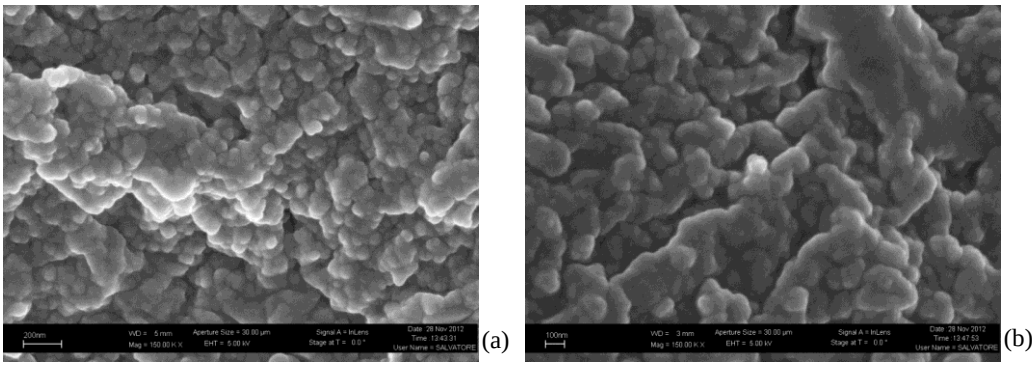

(a) (b)

Figure 6.23: FE-SEM analyses for samples with a) 3 and b) 7 phr of Zeosil 1165

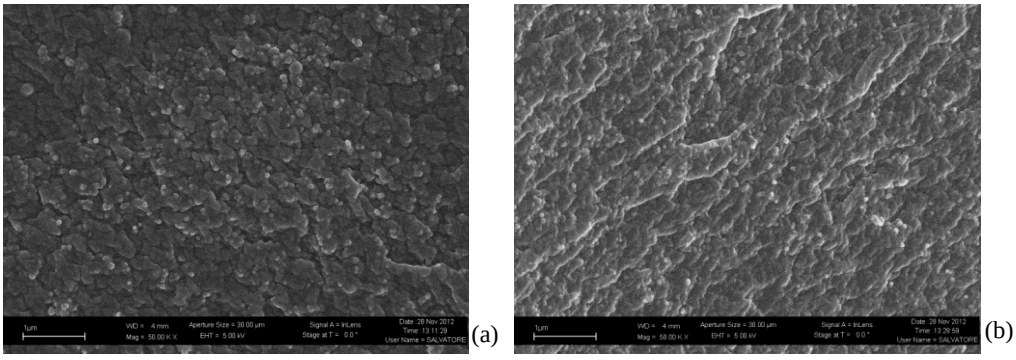

(a) (b)

Figure 6.24: FE-SEM analyses for samples with a) 3 and b) 7 phr of Aerosil 200

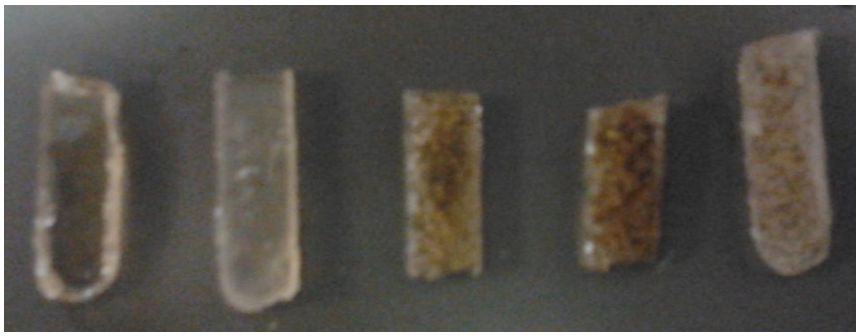

Figure 6.25: Cured samples with 3-7phr of Aerosil 200 and 3-7-20phr of Zeosil 1165 (from left to right)

6.3.8. Conclusions

In order to improve the thickness curability nano-sized particles were added into the formulation C and the properties of the filled materials were compared to those obtained for the microcomposites.

A progressive decrease of the initial slope and final conversion were observed while increasing the filler content. However, the gel content still presented values higher than 99% confirming a high degree of curing. No significant improvement of the thermal stability was observed but Tg values were comparable to those obtained with a high amount of micro-sized fillers.

The low dimensions of the particles allowed the front propagation among a thickness of 2cm with 30s of irradiation. Morphological analyses evidenced a good filler dispersion inside the silicone matrix.

References

[1] S. Sturwald, Proceedings of UHPC-2 International Symposium (**2008**).

[2] S. Hamdani, C. Longuet, J.M. Lopez-cuesta, F. Ganachaud. Polym. Degrad. Stab.95 (**2010**) 1911.

[3] E. Cherney, C. de Tourreil, D. Dumora, R. Harmon, H. Hervig, B. Kingsbury, J. Kise, T. Orbeck, K. Tanaka, R. Tay, G. Toskey, D. Wiitanen. IEEE Trans. on Power Del.10 (**1995**) 924.

[4] P. Klonos, A. Panagopoulou, L. Bokobza, A. Kyritsis, V. Peoglos, P. Pissis. Polym. 51 (**2010**) 5490.

[5] P. Klonos, A. Panagopoulou, A. Kyritsis, L. Bokobza, P. Pissis, J. Non-Cryst. Solids 357 (**2011**)610.

[6] T.R. Shrout, L.J. Bauven, W.A. Schulze. Mater. Res. Bull. 15 (**1980**) 1371.

[7] T. Furukawa, K. Ishida, E. Fukud. J. Appl. Phys 50 (**1979**) 4904.

[8] T. Yamada, T. Ueda, T. Kitayama. J. Appl. Phys 53 (**1982**) 4328.

[9] Z. Ahmad, A. Prasad, K.A. Prasad.Physica B: Condensed Matter 404 (**2009**)3637.

[10] C.F. Yang, C.C. Wu, Y.C. Chen, C.C. Su.Appl. Phys. Lett 94 (**2009**) 52905.

[11] I. Webman, J. Jortner, M.H. Cohen. Phys. Rev. B 15 (**1977**) 5712.

[12] N. Jayasundere, B.V. Smith. J. Appl. Phys 76 (**1994**) 2993.

[13] E.F. Knott. IEEE Trans. Antennas Propag. 41 (**1993**) 1167.

[14] Y. Rao, C.P. Wong, J. Qu. Proceedings of the Electronic Components and Technology Conference IEEE 616 (**2000**).

[15] D.A. Sverjensky. Geochimica et Cosmochimica Acta69 (**2005**) 225.

[16] K. Horai. J. Geophys. Res. 76 (**1971**) 1278.

7. SILICONE COMPOSITES VIA IN-SITU GENERATION OF NANODOMAINS (BOTTOM-UP APPROACH)

The in-situ generation of nanodomains by sol–gel techniques have been widely used for the preparation of organic–inorganic hybrid materials. The formation of inorganic network comes from hydrolysis and condensation reactions from metal-alkoxysilanes in alcoholic solutions. This process was used to generate nanoparticles such as silica or titania in order to enhance the dispersion within the matrix and therefore improve the final properties of the composites.

7.1. Sol-gel process

The sol-gel synthesis of oxide materials is known as an efficient method to produce a three-dimensional inorganic network by chemical reactions. The general character of the sol-gel reaction scheme is basically a condensation polymerization reaction of molecular precursors such as metal alkoxides $M(OR)_n$ where R is an alkyl group. Alkoxide molecules are usually monomers or small oligomers with low molecular weight. In principle, any precursor of a suitable compound which can be hydrolyzed could be used as precursor.

The sol-gel reaction occurs via hydrolysis of M-OR groups and formation of reactive hydroxyl groups (M-OH). Polycondensation reactions involve the group formed during hydrolysis leading to the formation of bridging oxygen. This reaction can occur between two groups formed during the hydrolysis or between a metal alkoxide (M-OR) and a reactive hydroxyl previously formed (M-OH). The chemical reactions of sol-gel process can be described schematically as follows:

Hydrolysis $\quad M–OR + H_2O \rightarrow M–OH + ROH$

Condensation $\quad M–OR + HO–M \rightarrow M–O–M + ROH \quad (a)$

$\quad M–OH + HO–M \rightarrow M–O–M + H_2O \quad (b)$

To initiate the sol-gel process water is usually externally added but, as most of the metal alkoxides are usually not miscible with water, a common solvent needs to be used, quiet often the parent alcohol [1]. Water can be also generated in situ by the condensation of carboxylic acids and alcohols. The oxide network leads progressively to the formation of oligomers, colloids and finally a solid phase.

The chemical reactivity of metal alkoxides towards hydrolysis and condensation depends on the ability of the metal ion to increase its coordination number. For example, addition of water to zirconium alkoxide leads to an uncontrolled precipitation of zirconia powder. This is due to the tendency of Zr to increase its coordination number up to 7 or 8 as in crystalline zirconia ZrO_2 [2].

TetraEthyl Ortho Silicate (TEOS) has been widely used as a precursor for silica in the sol–gel process to create the Si–O–Si bonds which are the backbone of silica-based organic–inorganic hybrid materials. Silicon alkoxides are poorly reactive and the reaction usually takes several weeks. To reduce the gelation time it is necessary to catalyze both the hydrolysis and condensation reactions usually using acids or bases. The acid catalysis mainly leads to an increase of the hydrolysis rate. The chain polymers formed are monolithic gels of low porosity. On the contrary, in basic catalysis, the condensation rates are favored, leading to highly branched species and dense spherical colloids. In any case, some M-OH groups will remain after the chemical reactions due to incomplete condensation [3]. A vacuum step for several days to constant weight the mixture is necessary to ensure the removal of any alcohol generated from the reaction [4].

The incorporation of silica by the in-situ generation is controlled by a number of parameters. They are catalyst type, amount and molecular weight of the organic component, amount of solvent and water, pH of the solution, reaction temperature and time [5]-[6].

Lower water content is considered to speed up the condensation but slow down hydrolysis which favors the growth of more extended mass fractal structures and inhibits the growth of the compact TEOS primary particles [7]. However, under conditions of high acid and high water content, the condensation rate is slow, and hydrolysis may well go to completion before any significant condensation occurs. The resulting products would be with more compact structures [8]. When the

molar ratio between water and TEOS is insufficient for complete hydrolysis, there is a dominance of larger, micro-meter-scale growth and no observed nanometer-scale growth. As reported from literature [8], molar ratio has to be higher than 3.

Also the precursor substituent has an effect on the sol-gel reaction due to steric effects: branching and increasing the chain length lower the hydrolysis rate [9]. In fact, the reactivity of the silica alkoxydes is the following:

$$Si(OMe)_4 > Si(OEt)_4 > Si(OnPr)_4 > Si(OiPr)_4 > Si(OnBu)_4 > Si(OHex)_4$$

The in-situ generation of inorganic domains can also be performed by swelling a crosslinked polymer in the inorganic precursor solution and subsequent formation of inorganic phase. The most common method used for the formation of hybrid materials is the formation of particles within the formulation and subsequent curing. Other method is achieved by previous curing of the organic phase and consecutive formation of the inorganic phase by thermal treatment [10],[11]. The two first methods were used for the preparation of silicone composites and their properties were evaluated.

The scheme of the reactions were reported in Figure 7.1.The third method was not applied in our system as the release of water on the crosslinked material lead to internal stresses and cracks.

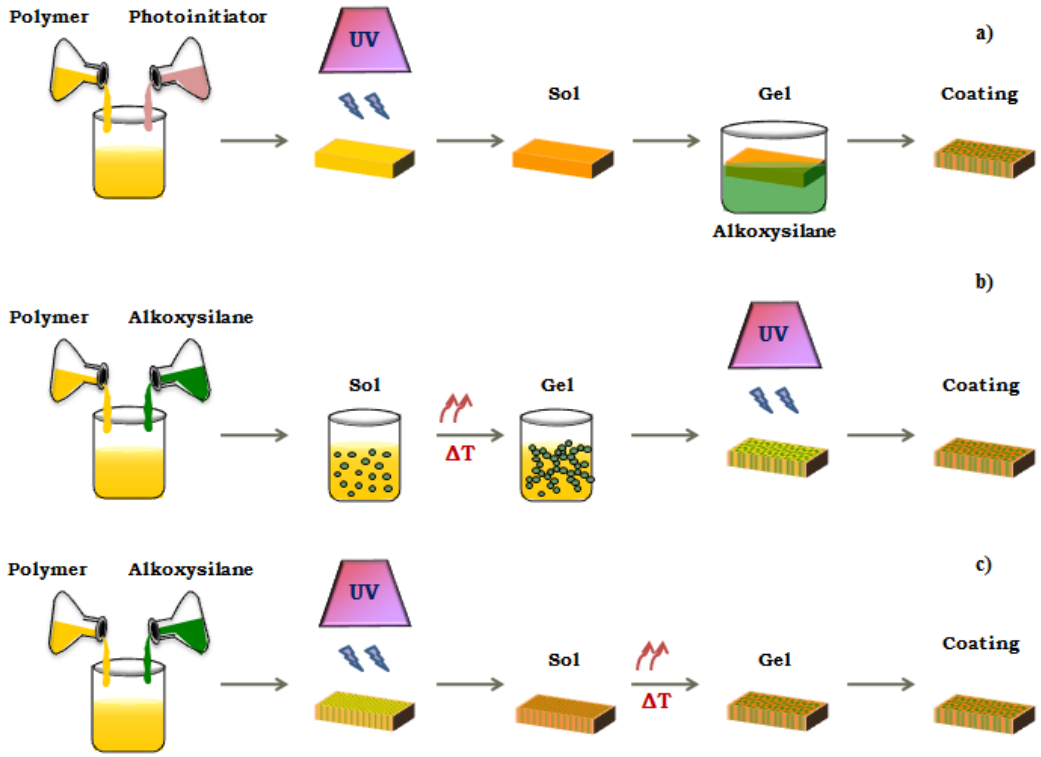

Figure 7.1: In-situ generation of nanodomains a) by swelling of crosslinked polymer b) prior curing c) after curing

7.2. Swelling of crosslinked polymer in inorganic precursor solution

The in-situ precipitation of alkoxides within the PDMS network can be carried out in the following way. The PDMS network is immersed in the inorganic precursor solution and subsequently placed into an aqueous solution containing 2 wt% of triethylamine as basic catalyst for 24h. The hydrolysis and condensation are allowed to take place for 24h at room temperature [12]-[14]. Titanium alkoxides present higher reactivity but also higher viscosity with respect of TEOS. Therefore, the rate of diffusion of titanium n-butoxide (TBO) [$Ti(OBu)_4$] in PDMS films is much longer than the TEOS. This leads, at a given swelling time, to a much lower swelling ratio of TBO [15]. ZrO_2 or Al_2O_3 particles can also be formed by using zirconium and aluminium n-propoxide respectively.

7.2.1. Sample preparation

The in-situ generation of silica clusters via sol-gel process was performed using tetraethylorthosilicate (TEOS) as silica precursor. In the simplest application, the crosslinked network is immersed for one day into a solution of TEOS. The swollen sample is then placed into an aqueous solution containing 2wt% triethylamine (called TEA) so that the hydrolysis and condensation of the precursor are allowed to take place for one day at room temperature. In the following, this method will be named method 1.

Another way to generate silica particles by swelling is to allow the PDMS to swell in TEOS solution in the presence of the catalyst (2wt% of TEA) for 1 day and then placed in water for 24h [4]-[16]. In the following, this method will be named method 2.

PDMS network was prepared using an equimolar amount of PDMS-V (with the lowest molecular weight) and MH-PDMS; and 500 ppm of the $Pt(acac)_2$ catalyst. Samples 1cm thick were prepared by UV-curing for 5 minutes. The samples were then placed in a solution of TEOS or TEOS + 2wt % TEA according to the method chosen, for one day, and successively into water + 2wt% TEA or water for another day. All the samples were then dried under atmospheric conditions for 1 day.

7.2.2. TGA analyses

Thermal analyses were performed on the samples prepared (according to the two methods of swelling) in order to control the sol gel process occurring. An increase of residue at high temperatures evidenced the formation of silica within the material. No significant increment of the thermal stability was noticed. The TGA curves were reported in Figure 7.2.

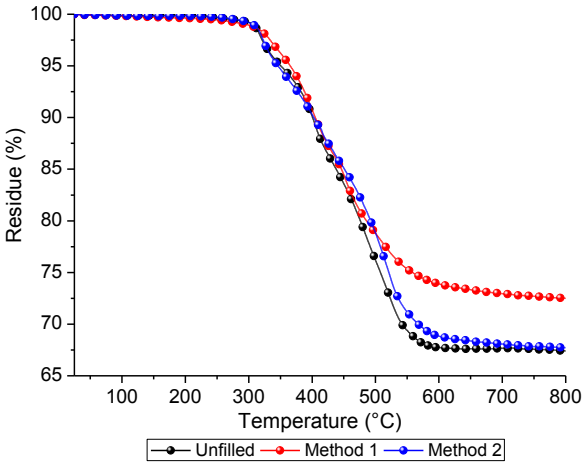

Figure 7.2: TGA of samples swelled in TEOS solution with the two different methods

The amount of filler incorporated into the network is generally calculated from the weight of the sample before and after the generation of the filler. These measurements tend to demonstrate that silica is effectively generated during the swelling due to an increase of sample weight.

The values of generated silica, both from TGA and weight difference calculation (Table 7.1), showed similar results. However, due to lower amount of silica in the method 2, it seemed that the generation of silica is preferred when the catalyst is present in water during the hydrolysis reaction.

Table 7.1: Amounts of generated silica prepared with the two swelling methods

	Method 1	**Method 2**
SiO_2 (from TGA)	15 %	5 %
SiO_2 (from weight difference)	16 %	6 %

The gel content (reported in Table 7.2) for the two methods of swelling showed high gel content values (above 99%) confirming that the swelling did not lead to a damage of the cured silicone.

Table 7.2: Gel content of samples swelled in silica precursor with the two different methods

	Reference	**Method 1**	**Method 2**
Gel content (%)	99%	99 %	99 %

7.2.3. DMTA analyses

Dynamic mechanical thermal analyses were performed on cured samples obtained with the two swelling methods. The tan δ of the different samples (Figure 7.3) evidenced an increase of the Tg values with respect to the unfilled system. The values were reported in Table 7.3. The increase of glass transition temperature was attributable to a hindering effect on the polymeric chain mobility due to the presence of silica particles generated during the swelling. The Tg was further enhanced in the case of swelling according to method 1 confirming that the generation of silica is preferred when the basic catalyst is present in the aqueous solution (as previously observed by TGA analyses). Moreover, the Tg valueswere comparable to what was obtained by incorporating nano-sized or micro-sized fillers, especially for the method 1 of swelling.

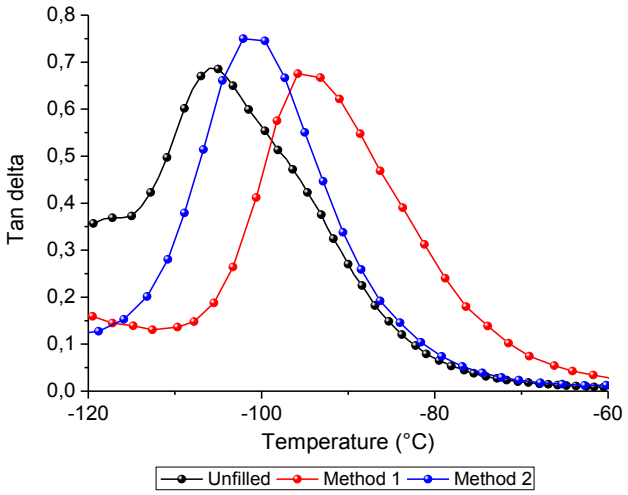

Figure 7.3: Tan delta values for the nanocomposites obtained by swelling

Table 7.3: Tg values of the PDMS nanocomposites obtained by swelling

	Reference	**Method 1**	**Method 2**
Tg value (°C)	-108	-96	-100

7.2.4. FE-SEM analyses

Morphological analyses were performed in order to evaluate the dispersion of the generated silica into the polymeric matrix (Figure 7.4). The investigations were achieved on the sample prepared according to method 1. It was possible to observe that silica particles were effectively generated and well dispersed into the polymeric matrix (Figure 7.4a) and presented dimension of about 50 nm (Figure 7.4b). These observations further confirmed that sol-gel process by swelling in silica precursor solution is an efficient way to generate in situ silica particles. This could be an easy approach to prepare thick filled samples without any influence on the kinetic of polymerization. Indeed, in a first step the unfilled material was cured and subsequently the silica particles were generated by swelling. The samples maintained their transparency as the silica clusters generated in-situ present nanometric dimension (Figure 7.5).

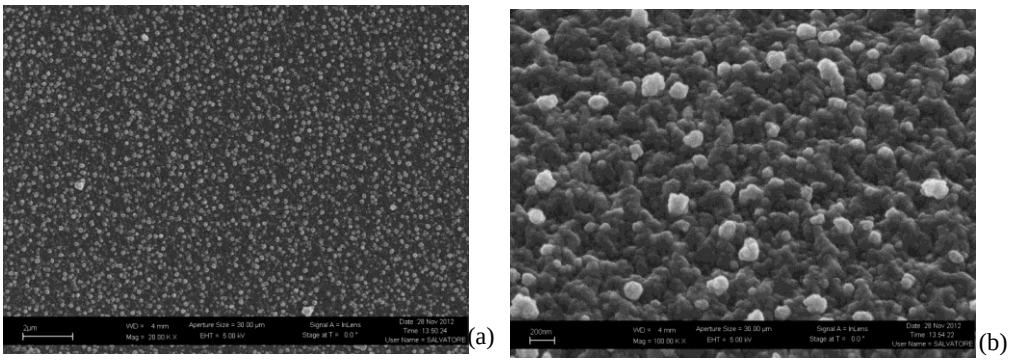

(a) (b)

Figure 7.4: FE-SEM analyses for samples prepared according to method 1

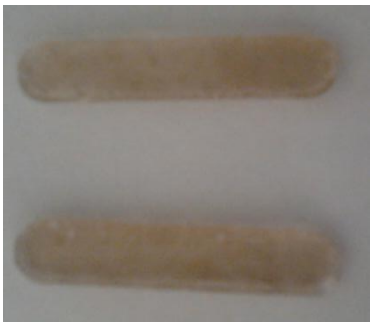

Figure 7.5: Cured samples obtained by swelling according to method 1(up) and 2 (down)

7.2.5. Electrical properties

Dry arc resistance tests were performed on the samples obtained by the two swelling methods. No increase of resistance time was observed for the swelled samples and the values were comparable to the unfilled system. The arc around the electrodes wasn't stable and a glowing path was observed before the recorded time. In some cases, a huge crack in the sample was formed during the experiment.

Dielectric spectroscopy performed on these samples didn't give any suitable trend of values as they presented so many random results especially in the lower frequencies (less than 100 Hz). This problem could come from the samples or the contact between the samples and the electrodes. It was not possible to sputtered the samples with gold as the samples broke. Therefore, the swelling of crosslinked polymer was not an efficient way to induce an increase of the electrical insulating properties of the material.

7.3. Generation of nanodomains prior curing

In the classical sol-gel process, the in-situ generation of silica particles occurs by a two steps process. Formulations containing the organic and inorganic phases are cured so that the organic phase is crosslinked. Subsequently, a thermal treatment in basic atmosphere is achieved in order to form the inorganic domain. The removal of the byproducts and unreacted alkoxydes causes a significant decrease in volume and also shrinkage which could be disadvantageous in some applications. A pratical way to avoid this difficulty is the precipitation of the inorganic particles within formulation containing the organic phase in order to give a stable polymer-filler suspension which remains capable of being end linked, subsequently, with no substantial changes in volume [19].

This method was used to obtain nanocomposites by sol-gel process in basic atmosphere as it was already performed in previous works [4] and the reactivity of

the different alkoxides was studied. Different particles were obtained such as titania, silica or aluminua according to the inorganic precursor used.

According to literature, the best results were obtained with a formulation containing PDMS, alkoxyde precursor and a small amount of catalyst stannous-2-ethyl hexanoate in a beaker placed (uncovered) into a larger covered jar containing a 2-5 wt% aqueous solution of ethylamine. The stirred mixtures were thus continuously exposed to water-ethylamine vapor. The reaction was allowed to proceed for 1 day at room temperature and the resulting formulation was then cured. However, it was observed that in the presence of the catalyst stannous-2-ethyl hexanoate the formulations were not able to cure due to an interaction with the platinum. The mixtures were then prepared without any tin catalyst.

7.3.1. Different ways of synthesis

In order to evaluate the more suitable way of generating inorganic particles three different routes were used. The investigation was performed using TEOS as silica precursor. The selected procedure will then be applied for the generation of Al_2O_3 from aluminum iso-propoxide and TiO_2 from titanium butoxide.

In the first analyses, the amount of silica precursor TEOS was fixed at 50phr with respect to the amount of PDMS in order to determine the best method for the in-situ generation of inorganic particles. The particles were first generated in the vinyl oligomer and subsequently the MH-PDMS and the Pt catalyst were added to the formulation containing the vinyl oligomer and the silica particles. The resulting mixture was then cured and the material characterized.

7.3.1.1. Use of a common solvent mixture

In order to increase the miscibility between the inorganic precursor TEOS and the water necessary for the sol-gel process, a common solvent mixture was used. The hydrolysis and condensation reactions were allowed to take place in a mixture of isopropyl alcohol (IPA) and tetrahydrofuran (THF). The solution was prepared

with 1mol THF and 4 mol IPA per mol TEOS according to the literature [8],[20],[21]. A solution of water containing triethylamine (2%wt) was added to the formulation so that the molar ratio of TEOS/water was 1/4.

The mixed solution, contained in a flask, was placed in an oil bath at 80°C. The hydrolysis and condensation reactions of TEOS proceeded for 90 min under magnetic stirring. It was observed that the silica particles were preferentially formed at the interface between the solvent and the vinyl terminated PDMS. The resulting formulation was then vacuum dried for several days in order to constant weight and also to remove both the alcohol formed during the reaction and the solvent mixture. It was then observed that the silica particles tend to agglomerate when the solvent was progressively removed and therefore it was not possible to obtain a homogeneous formulation. From the optical microscope, it was observed that the formulation presented silica agglomerates (Figure 7.6).This way of synthesis was therefore not suitable to prepare PDMS composites by in situ generation of TEOS prior curing.

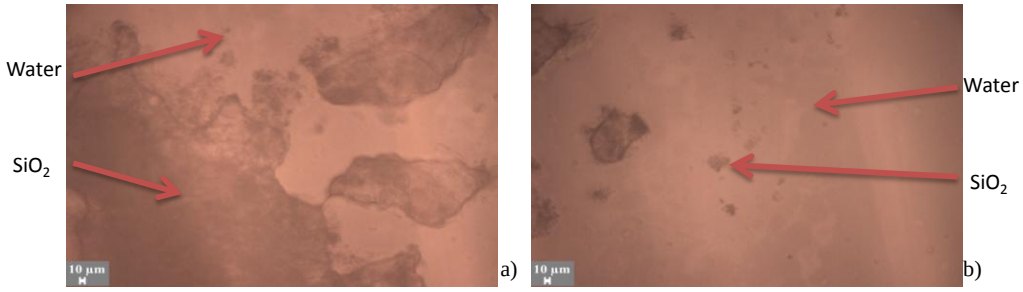

Figure 7.6: Optical images of the formulation

7.3.1.2. Direct addition of water into PDMS/TEOS formulation

It was then investigated the direct addition of a solution of water + triethylamine (2%wt) into the formulation of vinyl terminated PDMS/TEOS so that the molar ration between TEOS and water was 1/4 without using any solvent. The mixture was placed in an oil bath at 80°C and the reaction was allowed to proceed for 90 min under magnetic stirring.

The resulting formulation was a two phased mixture due to the immiscibility between water and vinyl terminated PDMS. The formulation was vacuum dried

for several days in order to constant weight. Optical microscope observations evidenced that silica particles were preferentially generated in the water phase (Figure 7.7a-b) and that a low amount of particles were obtained into the vinyl terminated PDMS phase (Figure 7.7 c).

DLS measurements were performed in order to have an indication of the particles dimension. For the vinyl terminated PDMS phase, the instrument was not able to give any information, must probably because the amount of particles was very low. On the contrary, in the water phase particles presented diameters in the range between 200-300nm (Figure 7.8).

This formulation was however not suitable to prepare PDMS composites by in situ generation of TEOS prior curing.

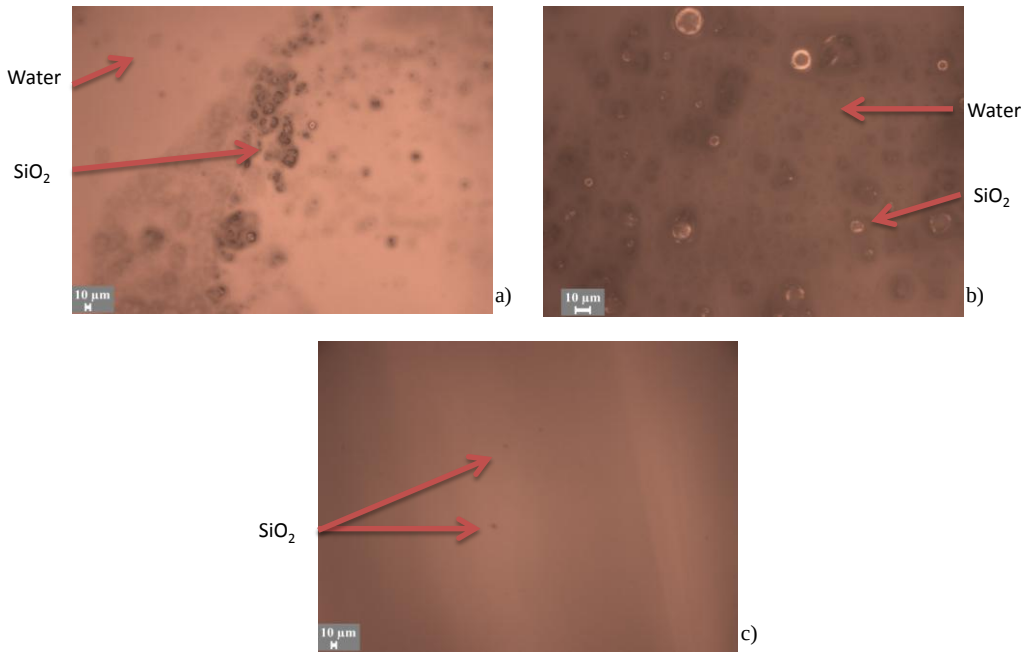

Figure 7.7: Optical images of a,b) the water phase and c) vinyl terminated PDMS phase

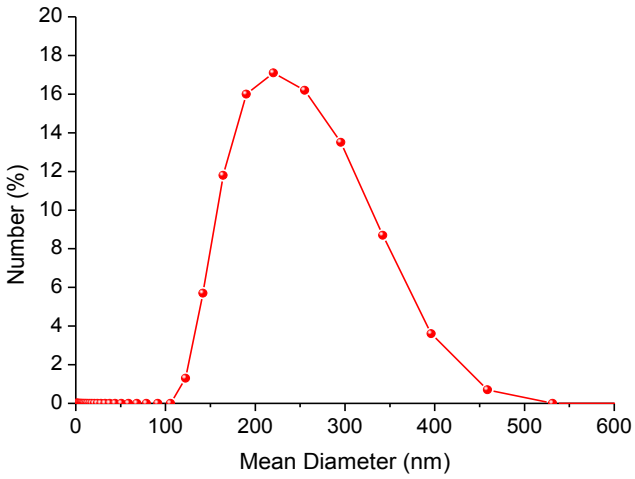

Figure 7.8: DLS in the water phase

7.3.1.3. Mixing of PDMS and TEOS in basic atmosphere

A mixture of vinyl terminated PDMS and TEOS was put uncovered in a jar containing a solution of water and 2% wt of triethylamine according to the method previously reported in literature [4]. The solution was placed in an oven at 80°C and the reaction was allowed to proceed for 90 min. The mixture resulted slightly cloudy after the reaction indicating the formation of silica particles. The resulting formulation was vacuum dried to constant weight.

The mixture was then analyzed by an optical microscope in order to evaluate the presence and dimension of silica particles (Figure 7.9). A very few amount of particles was evidenced but still confirmed that silica could be generated by using this method.

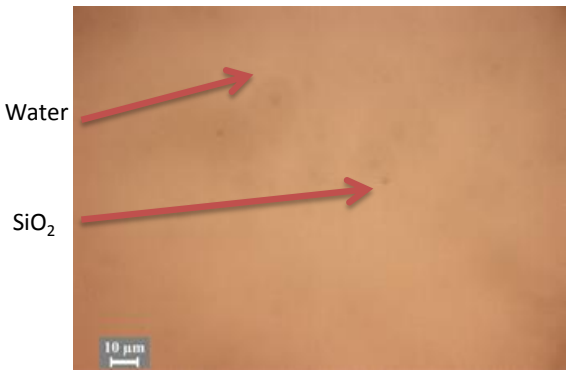

Figure 7.9: Optical images of the vinyl terminated PDMS formulation

This way of in-situ generation of silica particles in vinyl terminated PDMS was the most promising and was chosen to prepare PDMS composites by bottom-up approach.

7.3.2. In-situ generation of silica particles

The sol-gel process was performed according to the method previously described that is the mixing of vinyl terminated PDMS and silica precursor (TEOS) in basic atmosphere.

The equation was reported below :

$Si(OCH_3)_4 + 2\ H_2O \rightarrow SiO_2 + 4\ CH_3OH$

The influence of sol-gel reaction time, amount of silica precursor and basicity of the water on the final properties of the PDMS composites were studied.

7.3.2.1. Influence of sol-gel reaction time

The sol-gel reaction in the vinyl terminated PDMS was allowed to proceed for different time ranging from 1,5 to 24h at 80°C. The amount of TEOS in the formulation was fixed at 50 phr. The amount of triethylamine in the water was fixed at 2%wt. The resulting formulations were analyzed by optical microscope which confirmed that silica particles were effectively present in the formulation (Figure 7.10). An increase of the particles number and agglomerations were observed by increasing the time of sol-gel reaction.

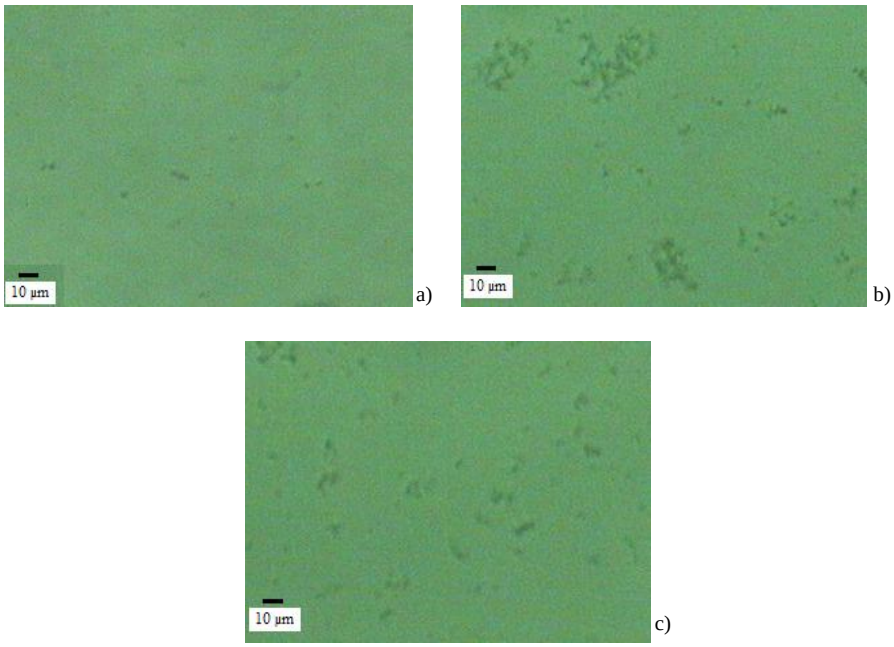

Figure 7.10: Optical images after 3h a) 6h b) and 24h c) of sol-gel reaction

DLS measurements were performed in order to study the evolution of particles dimension as a function of the sol-gel reaction time. The results were reported in Figure 7.11. A progressive increase of particles dimension from 1800 nm after 1.5h of reaction to 3800 nm after 24h was evidenced. In the latter case a bimodal distribution was observed probably due to agglomeration effect.

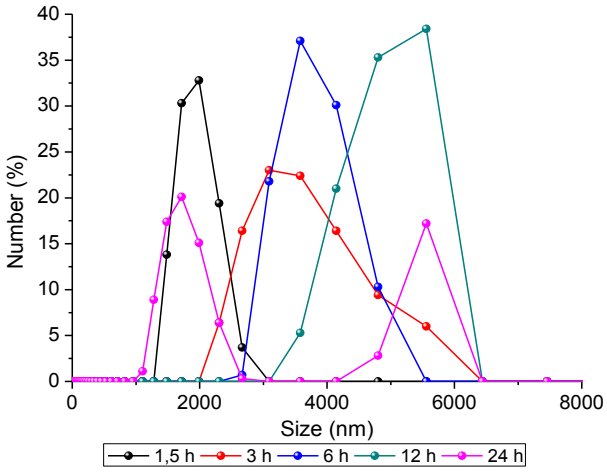

Figure 7.11: DLS of formulations after different sol-gel reaction time

The effect of sol-gel reaction time on the curing process was studied by means of real-time FTIR analyses. After the sol-gel reaction, the formulations were vacuum dried for several days in order to remove the alcohol formed. The silane (MH-PDMS) and the Pt catalyst were then added so that the final mixture had an equimolar amount between PDMS-V and MH-PDMS oligomers.

The silane conversion was followed as a function of the irradiation time for the different formulations (Figure 7.12) coated on a SiC substrate so that the samples thickness was about 50 µm. It was evidenced that sol-gel reaction time up to 6h did not have any influence on the initial slope and final conversion of the silane. On the contrary, after 24h of sol-gel reaction, the final silane conversion was slightly reduced. This could be attributed to an higher amount of generated silica particles leading to a lower mobility of the polymeric chains.

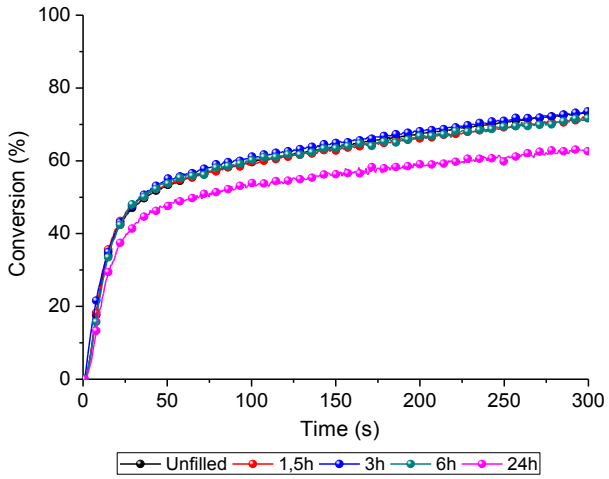

Figure 7.12: Silane conversion as a function of irradiation time for different sol-gel reaction time

Dynamic mechanical thermal analyses were performed on the cured samples prepared after different time of sol-gel reaction. The tan δ values (Figure 7.13) showed an increment of the Tg with respect to the unfilled PDMS by progressive enhancement of the sol-gel reaction time. The Tg values of the different samples were reported in Table 7.4.

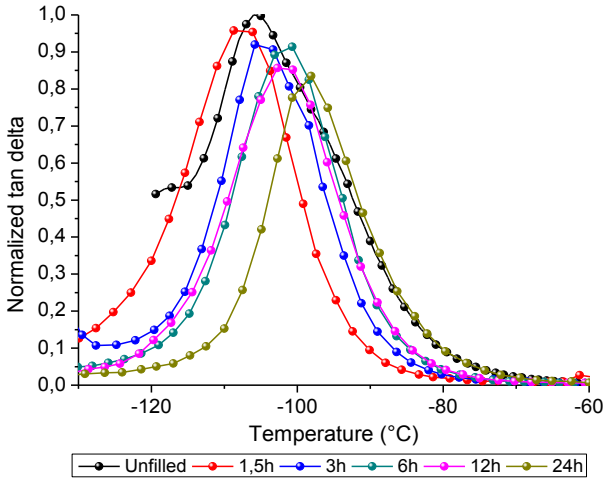

Figure 7.13: Tan delta values for samples with different sol-gel reaction time

Table 7.4: Tg values for the PDMS composites with different sol-gel reaction time

	Reference	**1,5h**	**3h**	**6h**	**12h**	**24h**
Tg value (°C)	-108	-107	-104	-100	-101	-98

TGA analyses were performed in order to evaluate the thermal stability of the PDMS composites. The results were reported in Figure 7.14. At low temperatures, the weight loss was due to the evaporation of water and the volatilization and thermal decomposition of the remnant organic compounds that were not removed during the vacuum dried time. The samples obtained after 24h of sol-gel reaction showed the higher thermal stability even if it still resulted lower than the unfilled system.

The amount of silica particles generated during the reaction was estimated from the TGA curves for all the samples and the values were reported in Table 7.5. A slight increase of the silica generated was observed from 18% after 3h to 21% after 24h.

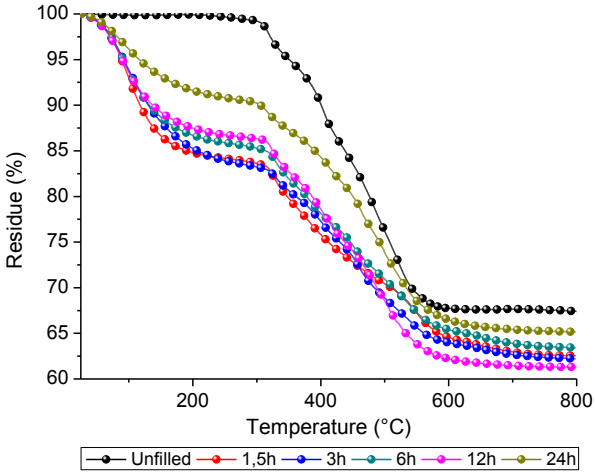

Figure 7.14: TGA analyses for samples with different sol-gel reaction time

Table 7.5: Amount of generated silica as a function of sol-gel reaction time

	1,5h	3h	6h	12h	24h
Amount of SiO_2 (%)	18	18	18	18	21

These analyses performed on PDMS composites prepared with different sol-gel reaction time evidenced that the higher Tg value and the best thermal stability were achieved after 24h of sol-gel reaction. This parameter was then kept as reference to study the influence of TEOS on the final properties of the material.

7.3.2.2. Influence of TEOS amount

As previously discussed, the sol-gel reaction in the vinyl terminated PDMS was allowed to proceed for 24h at 80°C. The amount of triethylamine in the water was fixed at 2%wt in order to evaluate the influence of the amount of silica precursor on the final properties. The amount of TEOS in the formulation was varied from 10 to 100phr.

The increment of TEOS in the formulation induced an increase of the silica particles generated into the vinyl terminated PDMS as it was observed by optical microscopy (Figure 7.15).

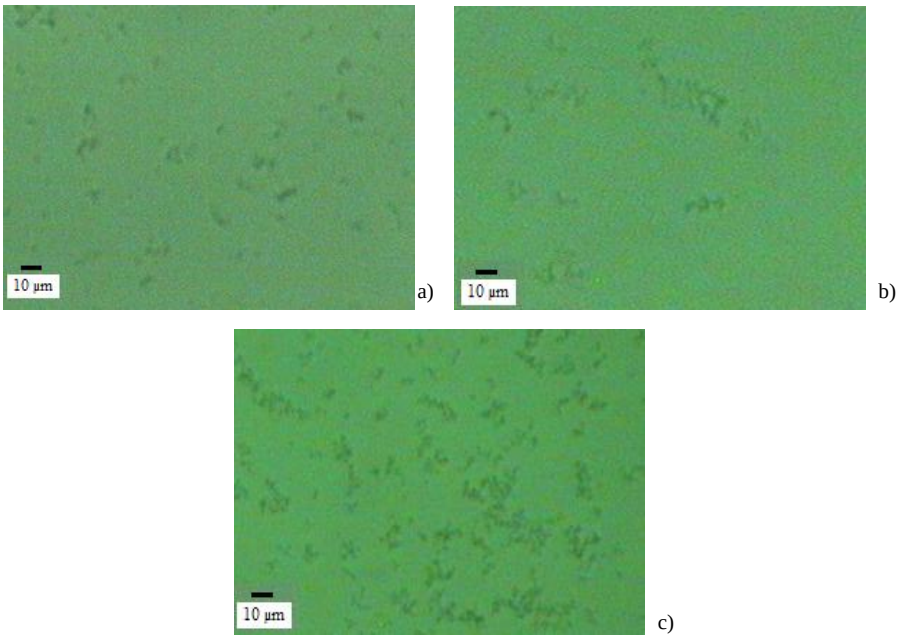

Figure 7.15: Optical images for 50phr a) 75phr b) and 100phr c) of TEOS after 24h of sol-gel reaction time

DLS measurements reported in Figure 7.16 evidenced that in the presence of low amount of TEOS (10 phr) the particles dimension was around 400 nm while increasing the amount of silica precursor higher dimensions were achieved together with a bimodal distribution. The main dimension observed was around 2000 nm (except for the 25 phr) and a second distribution was always observed at around 5500 nm (attributable to agglomeration effect).

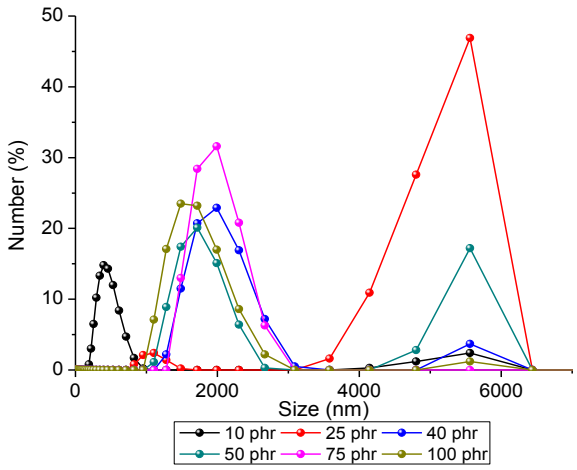

Figure 7.16: DLS of formulations with different amount of TEOS after 24h of sol-gel reaction time

The silane conversions of the different formulations were followed as a function of irradiation time (Figure 7.17). It was observed that the kinetic of polymerization (both initial slope and final conversion) was slightly affected by the presence of silica particles but the final conversions were still comparable to the unfilled system. Amounts of TEOS up to 100phr did not induce any substantial change in the reactivity of the system.

DMTA analyses performed on samples 4mm thick (Figure 7.18) evidenced an increase of the Tg value for amount of TEOS up to 50 phr (data reported in Table 7.6). At higher amount (75 and 100 phr) a progressive decrease of the value was observed most probably due to the fact that the presence of silica particles hindered the complete curing of the polymeric matrix, with a consequent decrease of crosslinking density. It could be therefore concluded that increasing the amount of silica generated particles progressively induced a decrease of the system reactivity leading to a lower crosslinking [22].

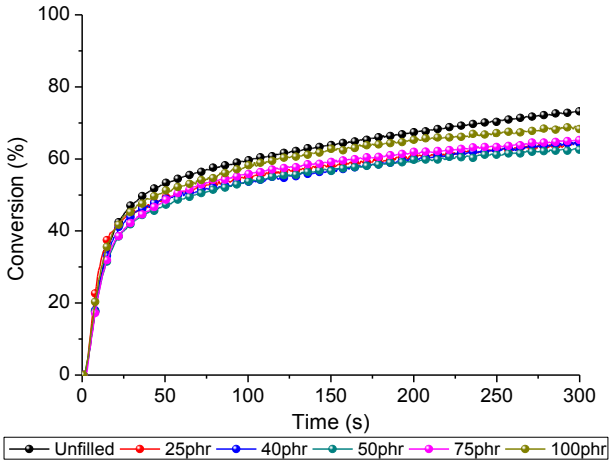

Figure 7.17: Silane conversion for different amount of TEOS after 24h of sol-gel reaction time

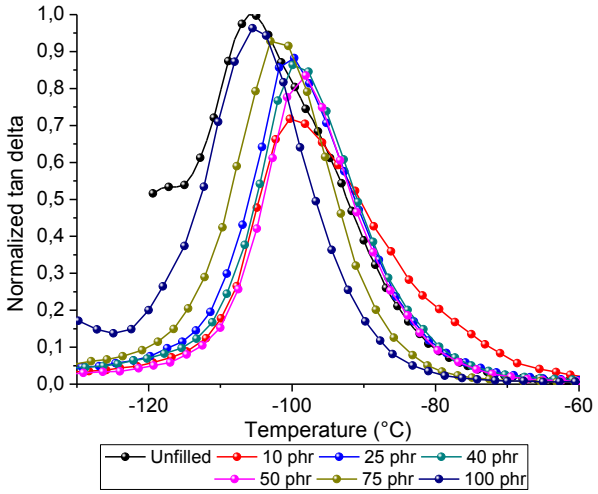

Figure 7.18: Tan delta values for samples with different amount of TEOS after 24h of sol-gel reaction time

Table 7.6: Tg values for the PDMS composites with different amount of TEOS after 24h of sol-gel reaction time

	Reference	10phr	25phr	40phr	50phr	75phr	100phr
Tg value (°C)	-108	-99	-100	-99	-98	-101	-104

TGA analyses were performed in order to evaluate the thermal stability of the composites. The results were reported in Figure 7.19 and the amount of the generated silica both from experimental and theoretical calculations were reported in Table 7.7. The initial decrease of the weight at low temperatures was due to the evaporation of water and the volatilization and thermal decomposition of the remnant organic compounds that were not removed during the vacuum dried time. An increase of the amount of TEOS effectively lead to an increase of the weight loss at low temperatures as higher amounts of alcohol are formed. The amount of generated silica into the formulation increased by progressive addition of TEOS (Table 7.7).

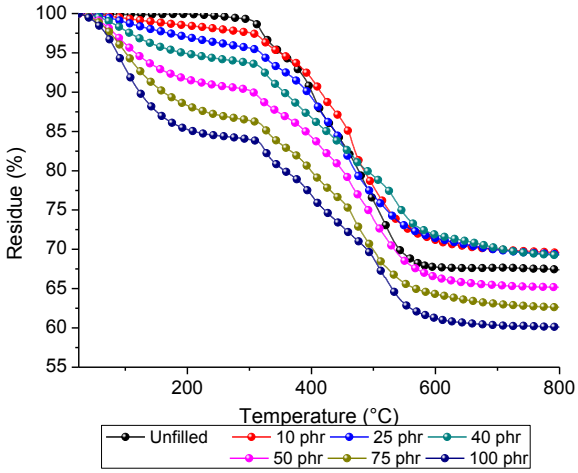

Figure 7.19: TGA analyses for samples with different amount of TEOS after 24h of sol-gel reaction time

Table 7.7: Amount of generated silica as a function of the amount of silica precursor for 24h of sol-gel reaction time

	10phr	25phr	40phr	50phr	75phr	100phr
Amount of SiO_2 (%)	8	15	20	21	24	26

Morphological analyses performed on cured sample containing 25 phr of TEOS after 24h of sol-gel reaction (Figure 7.20) evidenced that silica particles were well dispersed in the matrix and the particles presented dimensions lower than 3 µm.

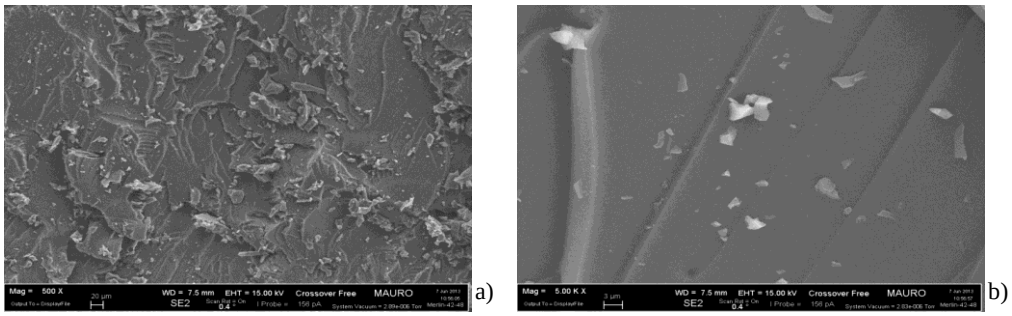

Figure 7.20: FE-SEM analyses for sample containing 25phr of TEOS after 24h of sol-gel reaction time

It was therefore possible to conclude that 24 hours of sol-gel reaction were necessary to obtain the most reinforcing effect of the particles in the composites.

The nanocomposites presented an increase of the final properties when the amount of TEOS was below or equal to 75phr. Higher quantities lead to a progressive decrement of both thermal stability and Tg value as a too high amount of unreacted TEOS remained present in the formulation inducing lower crosslinking.

7.3.2.3. Frontal propagation on thick samples

The propagation of the front among samples thickness was evaluated by optical pyrometry. Formulations containing vinyl terminated PDMS and different amount of silica precursor were put for 24h at 80°C in the presence of 2% wt of triethylamine in order to generate silica particles. The formulations were then let for one day under vacuum in order to remove any alcohol formed during the sol-gel reaction. The silane PDMS and the platinum catalyst were then added to the formulations in order to have an equimolar amount of vinyl and silane and 500ppm of platinum catalyst.

The experiments were performed in a small-scale cylindrical reactors (ID 14mm, length 50 mm). The reaction was initiated by UV irradiation on the surface of the formulation through an optical fiber at a distance of 4 cm for 30 s.

The collected points at 1cm from the top of the tube (Figure 7.21) showed that the front's velocity was not deeply slowed down for amount of TEOS up to 50phr and a maximum temperature of 75°C for 50phr of TEOS was observed (the maximum temperature for the unfilled system was 85°C). For higher amount of TEOS the front velocity was affected by the presence of silica particles and the maximum temperature reached was 50°C. The decrease of temperature was due to the heat dissipation coming from the generated silica particles. Anyway, all the samples 1cm thick were cured after the measurements.

The same measurements were done collecting the data at 2cm from the top of the tube (Figure 7.22). A decrease of the maximum temperature was observed for all the formulations, especially if the amount of TEOS was higher than 25phr. For these samples the front was not able to proceed due to the high amount of silica

particles that dissipate heat. These samples were indeed not cured after the measurements.

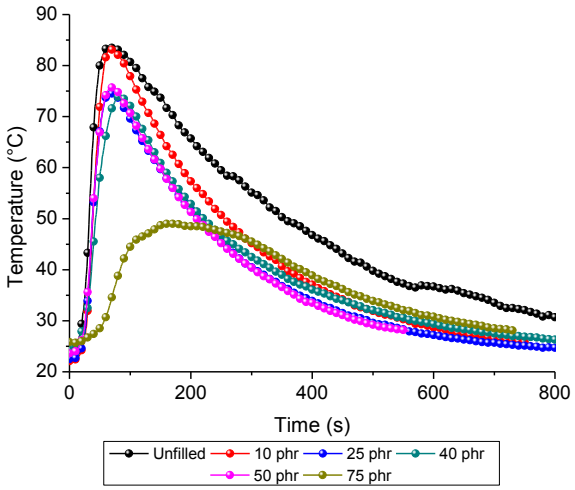

Figure 7.21: Temperature profiles for 1cm thick formulations containing different amount of TEOS

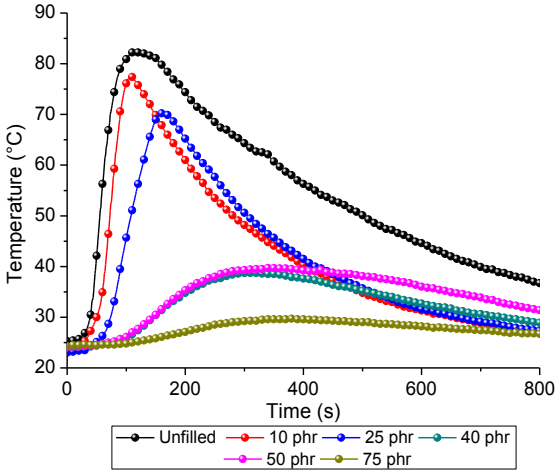

Figure 7.22: Temperature profiles for 2cm thick formulations containing different amount of TEOS

Temperature profiles for thickness up to 3cm were collected for the formulations containing 10 and 25phr of TEOS and compared with those obtained for lower thicknesses. The data were reported in Figure 7.23-Figure 7.24. It was possible to observe that a thickness of 3cm lead to a delay of the front propagation and no linear relationship between the thickness and the maximum temperature

reached was achieved. The presence of in-situ generated silica particles lead, due to heat dissipation phenomena, to a decrease of the propagation velocity. However, the samples 3cm thick were cured in both cases after the analyses even if the bottom part would need a dark-curing to complete the curing as they still resulted soft but tack-free.

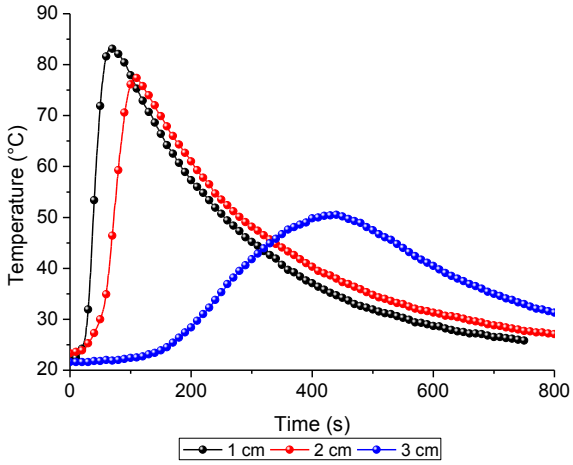

Figure 7.23: Temperature profiles for different thicknessesof formulations containing 10phr of TEOS

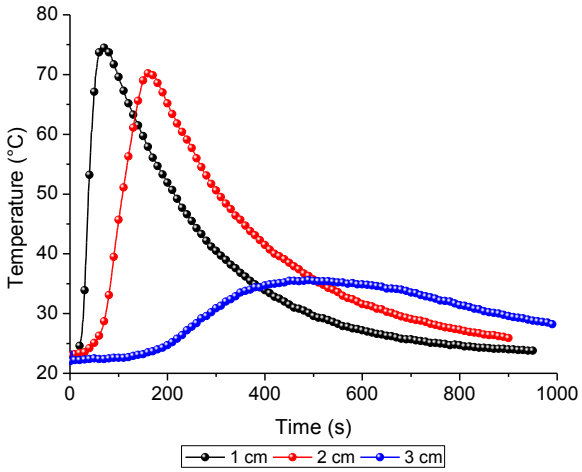

Figure 7.24: Temperature profiles for different thicknesses of formulations containing 25phr of TEOS

7.3.2.4. Electrical properties

Dielectric spectroscopy measurements were performed at 40°C on samples containing different amount of TEOS. The relative permittivity and dielectric loss factor with respect to frequency were reported in Figure 7.25-Figure 7.26.

The various composites presented a relative permittivity independent of the frequency as observed for the pure PDMS. The addition of the various amount of TEOS lead to change in the relative permittivity values but no correlation between the amount of TEOS and the ε' value was observed. However, no increase at the low frequency side was noticed in the nanocomposites indicating that no Maxwell-Wagner-Sillars relaxation (that usually appears between the matrix and the fillers) occurred.

The dielectric loss factor of the unfilled system was below the sensitivity of the instrument (less than 10^{-3}) and therefore was not reported in the curve. The increase of TEOS content lead to a progressive increase of the ε'' values; especially in the case of 75phr of TEOS. Low amount of silica precursor did not lead to any increase of the dielectric loss factor.

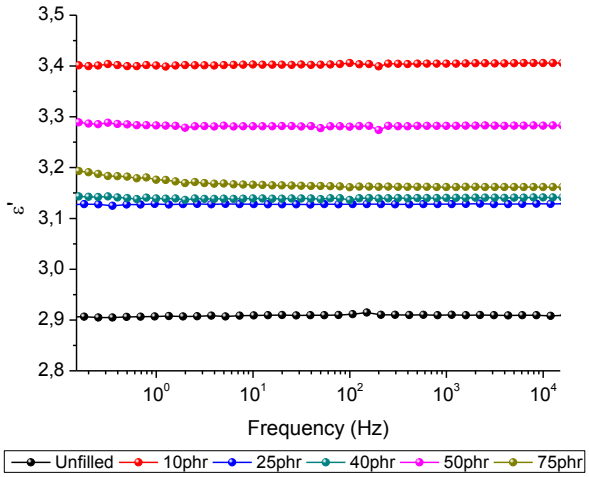

Figure 7.25: Relative permittivity of samples containing different amount of TEOS

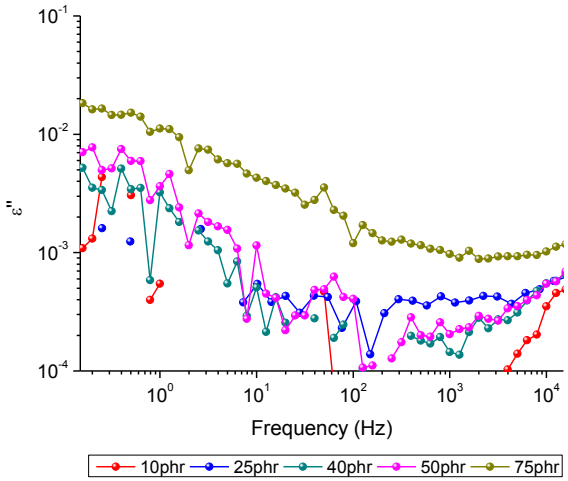

Figure 7.26: Dielectric loss factor of samples containing different amount of TEOS

Dry Arc Resistance test performed on samples containing different amount of TEOS did not indicate any improvement of the time before reaching a conducting path on sample surface. The time of resistance was still around 120s (Table 7.8)

Table 7.8: Dry Arc Resistance Values for samples containing different amount of TEOS

	Reference	10phr	25phr	40phr	50phr	75phr
Dry Arc Resistance Time (s)	123	125	123	123	125	126

In the following it has been tried to generate both aluminum oxide and titania clusters by the sol-gel process. The time of reaction and amount of inorganic precursor were studied.

7.3.3. In-situ generation of aluminum oxide

The same experimental protocol was used to in-situ generate aluminum oxide from the aluminum iso-propoxide $Al(OPr\text{-}i)_3$.

The equations of the reaction were reported below [23]:

$$Al(OPr\text{-}i)_3 + 2\ H_2O \rightarrow AlOOH + 3i\text{-}Pr\text{-}OH$$

$$2\ AlOOH \rightarrow Al_2O_3 + H_2O$$

Mixtures containing the vinyl terminated PDMS and different amount of aluminum oxide precursor were put in a jar containing a solution of water + 2

%wt of triethylamine. The formulations were placed in an oven at 80°C and the reaction was allowed to proceed for different time ranging from 3 to 24h. The resulting formulations were then vacuum dried to constant weight. The silane (MH-PDMS) and the Pt catalyst were then added to the formulation so that the final mixtures contained an equimolar amount of PDMS-V and MH-PDMS and 500ppm of $Pt(acac)_2$.The amount of inorganic precursor was first fixed at 50 phr in order to evaluate the suitable time of sol-gel reaction as TEOS and $Al(OPr\text{-}i)_3$ present different reactivities.

Thermal analyses performed on samples prepared after different time of reaction demonstrated that 24h of sol-gel reaction lead to the better thermal stability and higher final residue of the composites (Figure 7.27). DMTA analyses carried out on these samples (Figure 7.28) evidenced that no increase of the Tg occurred by increasing the time of reaction.

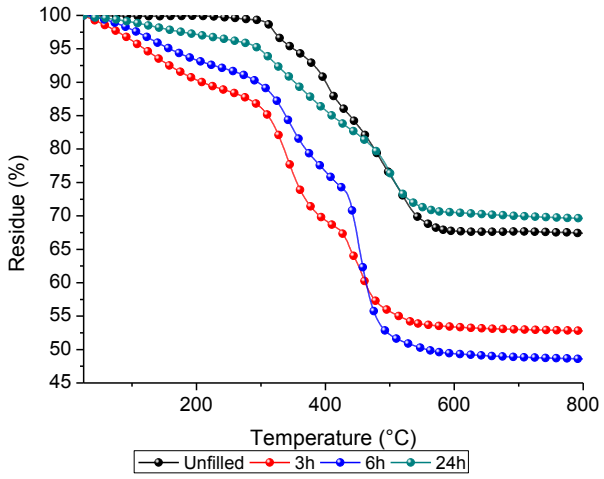

Figure 7.27: TGA analyses for samples with 50phr of $Al(OPr\text{-}i)_3$ after different sol-gel reaction time

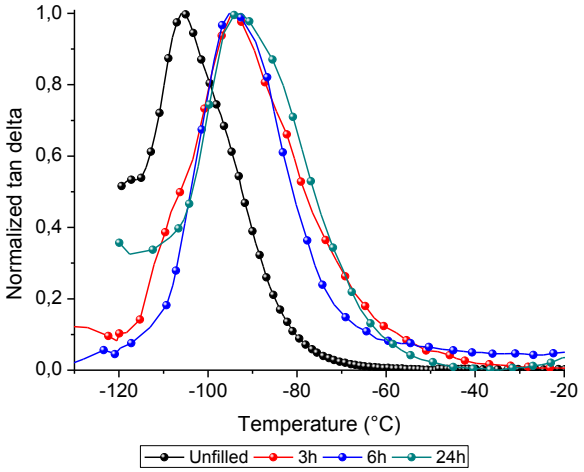

Figure 7.28: DMTA analyses for samples with 50phr of $Al(OPr\text{-}i)_3$ after different sol-gel reaction time

The time of reaction was then fixed at 24h as better thermal stability of the composites was achieved. The amount of alumina precursor was then varied between 25 and 100phr in order to evaluate the behavior of the material. The silane conversion of these formulations was followed by real-time FT-IR analysis (Figure 7.29). A progressive decrease of the silane conversion was observed by increasing the amount of inorganic precursor. This decrease of curability was attributed to the low value of thermal conductivity of aluminum hydroxide with respect to the silica (as it was previously observed in 6.2.9). Indeed, no difference of silane conversion was observed by varying the amount of silica precursor (Figure 7.17).

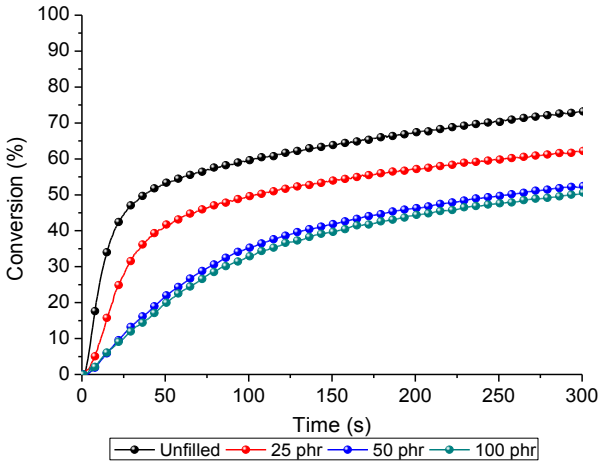

Figure 7.29: Silane conversion for samples containing different amount of Al(OPr-i)$_3$ after 24h sol-gel reaction

Thermal analyses (Figure 7.30) showed that the presence of generated alumina lead to a weight loss at low temperatures as it was already observed with TEOS. This phenomena was attributed to the evaporation of water and the volatilization and thermal decomposition of the remnant organic compounds that were not removed during the vacuum dried phase. The amount of generated alumina was reported in Table 7.9 and indicated that amount of alumina up to 40% could be formed by adding 100phr of Al(OPr-i)$_3$ in the formulation.

Table 7.9: Amount of generated alumina as a function of the amount of precursor after 24h of sol-gel reaction

	25 phr	**50 phr**	**100 phr**
Amount of Al_2O_3 (%)	10	25	40

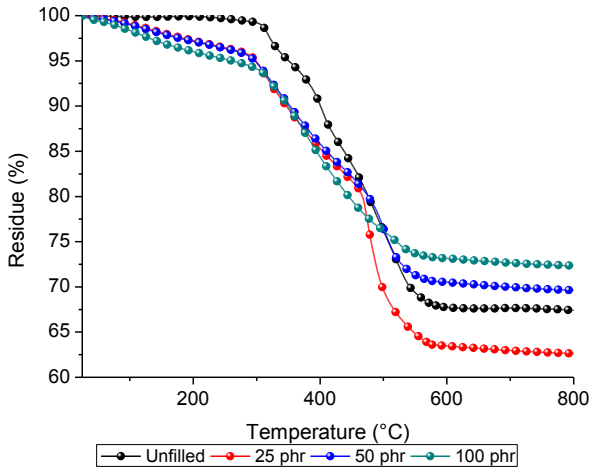

Figure 7.30: TGA analyses for samples containing different amount of Al(OPr-i)$_3$ after 24h sol-gel reaction

DMTA analyses evidenced a progressive increase of the glass transition by further addition of aluminum iso-propoxide (Figure 7.31). The Tg values were reported in Table 7.10. The increase of Tg was more pronounced in the case of in-situ generated aluminum oxide with respect to silica particles (Table 7.6).

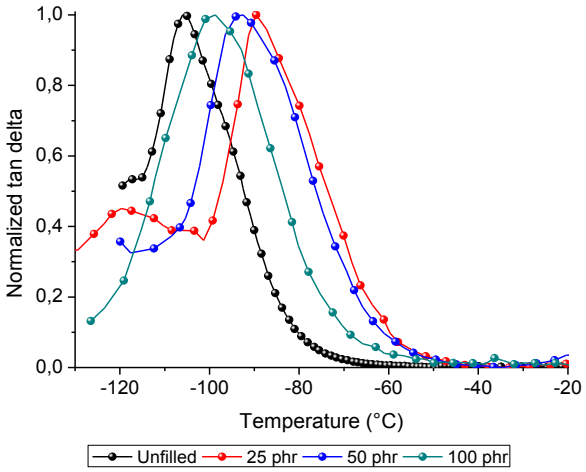

Figure 7.31: DMTA analyses for samples containing different amount of Al(OPr-i)$_3$ after 24h sol-gel reaction

Table 7.10: Tg values for samples containing different amount of Al(OPr-i)$_3$ after 24h sol-gel reaction

	Unfilled	25 phr	50 phr	100 phr
Tg value (°C)	-108	-89	-92	-99

Morphological analyses performed on the sample containing 25phr of aluminum iso-propoxide evidenced that some agglomeration occurred in the samples (Figure 7.32) and it was possible to distinguish the unfilled region. The dimensions of the particles were lower with respect to the generated silica particles (lower than 1 µm).

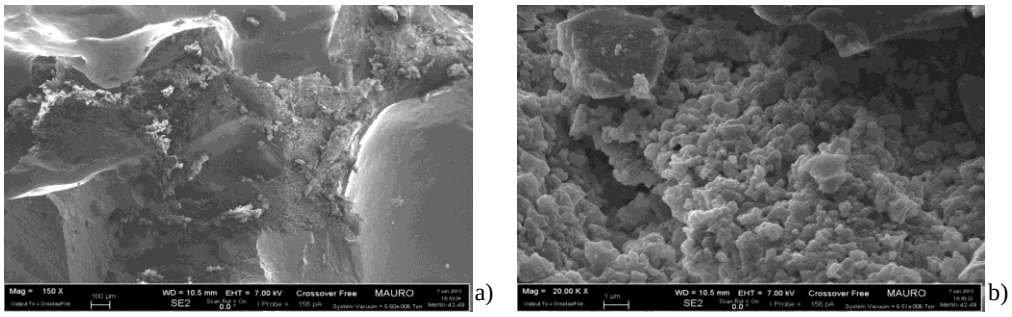

a) b)

Figure 7.32: FE-SEM analyses for sample containing 25phr of Al(OPr-i)$_3$ after 24h of sol-gel reaction

7.3.4. In-situ generation of titania

Titanium alkoxides present much higher reactivity than silicon analogues and therefore the time of sol-gel reaction is deeply reduced with respect to those used previously for the other inorganic precursors [20].Titanium n-butoxide (TBO) was used for the generation of titania particles and the reaction is the following:

$Ti(OC_4H_9)_4 + 2\ H_2O \rightarrow TiO_2 + 4\ C_4H_9OH$

Experiments performed at 80°C evidenced high agglomeration of titania particles in the formulation due to the high reactivity of its precursor. The sol-gel process was therefore performed at room temperature. It was observed that after 1h of reaction the formulation became cloudy, indicating that probably micrometric particles were generated. For this reason, the time of reaction in the study was varied between 10 and 30 min in order to get low particles dimension and avoid agglomeration.

The sol-gel process was performed by direct mixing of the vinyl oligomer and different amount of titania precursor. The mixture was let under magnetic stirring

at room temperature and the reaction was allowed to proceed for different time. The resulting formulation was vacuum dried to constant weight.

The silane (MH-PDMS) and the Pt catalyst were then added to the formulation so that the final mixtures present equimolar amount between PDMS-V and MH-PDMS and a final content of 500ppm of Pt catalyst.

In order to evaluate the suitable time of sol-gel reaction, the amount of TBO was first fixed at 10phr and the thermal stability was evaluated (Figure 7.33). It can be deduced that longer times of reaction leads to higher values of final residue indicating that higher amount of titania was generated.

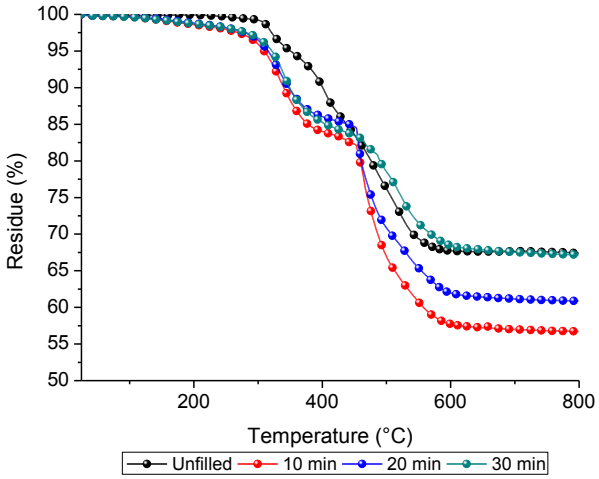

Figure 7.33: TGA analyses for samples with 10phr of TBO after different sol-gel reaction time

Silane conversion performed by real time FT-IR analyses on these formulations (Figure 7.34) demonstrated that the final conversion was not affected by the time of reaction. On the contrary, higher values with respect to the unfilled system were achieved. It was found in literature that nanosized titanium dioxide particles could be used to further promote the catalytic effect of the platinum leading to an increase of the silane conversion [24]. DMTA analyses (Figure 7.35) evidenced that the time of sol-gel reaction did not have any influence on the glass transition temperature of the composites.

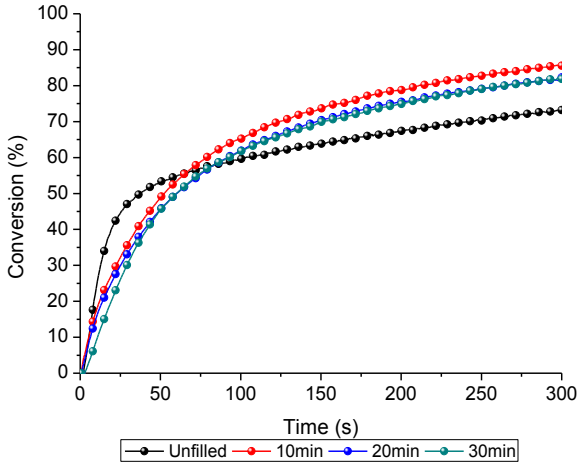

Figure 7.34: Silane conversion for samples with 10phr of TBO after different sol-gel reaction time

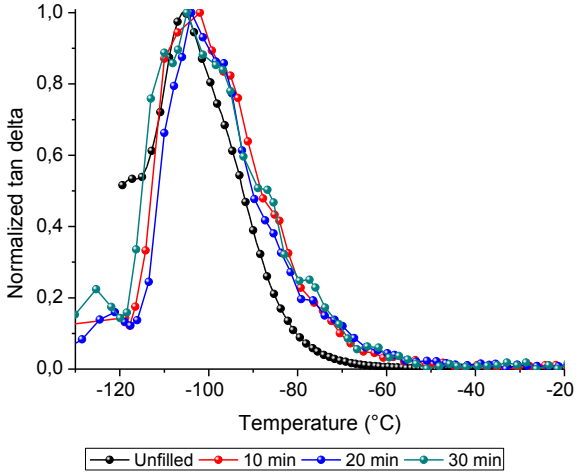

Figure 7.35: DMTA analyses for samples with 10phr of TBO after different sol-gel reaction time

In the following experiments the time of reaction was fixed at 30 minutes and the effect of amount of titania precursor on the final properties were studied. The silane conversion was followed for different amount of TBO (Figure 7.36). It resulted that the variation of TBO did not have any influence on the kinetic of polymerization. The initial slope was slower than the unfilled system but the final conversion was higher, independently of the amount of titanium precursor used.

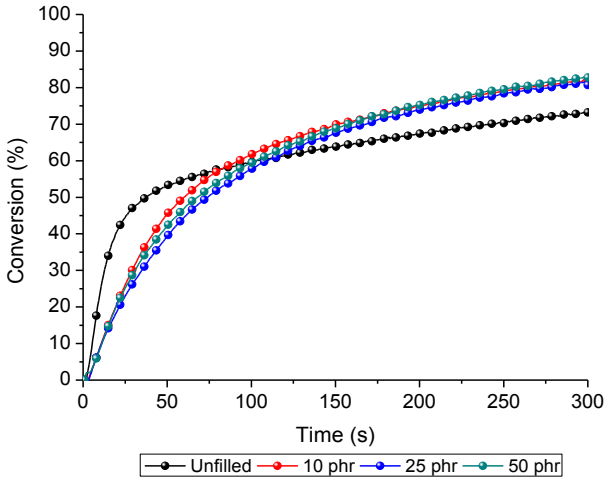

Figure 7.36: Silane conversion for samples containing different amount of TBO after 30min of sol-gel reaction

TGA analyses (reported in Figure 7.37) evidenced that amount up to 16% of titania could be obtained from 50phr of TBO (Table 7.11). Moreover, by increasing the amount of titania precursor for a sol-gel reaction of 30 min, no increase of the Tg value was evidenced by DMTA analyses (Figure 7.38).

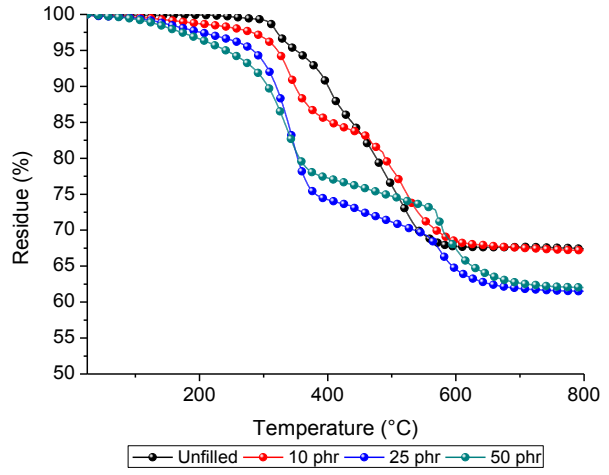

Figure 7.37: TGA analyses for samples containing different amount of TBO after 30min of sol-gel reaction

Table 7.11: Amount of generated titania as a function of the amount of precursor after 30min of sol-gel reaction

	10 phr	**25 phr**	**50 phr**
Amount of TiO_2 (%)	7	8	16

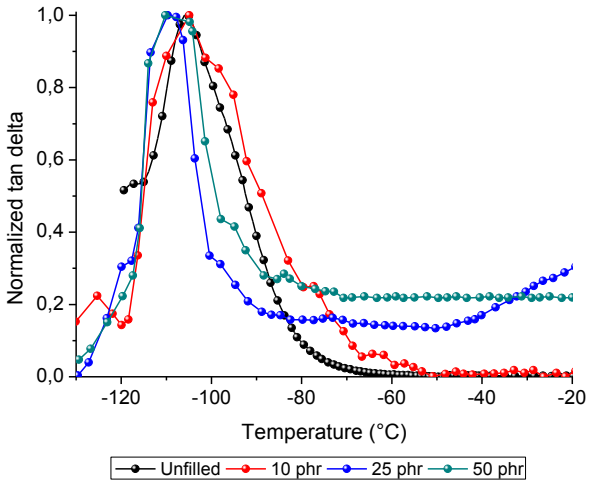

Figure 7.38: DMTA analyses for samples containing different amount of TBO after 30min of sol-gel reaction

Morphological analyses performed by FE-SEM (Figure 7.39) showed that titania particles present lower dimension with respect to silica or alumina. This could be explained by the higher reactivity of TBO that induced an increase of the condensation phase of the sol-gel reaction. The particles were well dispersed but some agglomerates were however presents in the samples. The particles presented nanometric dimension.

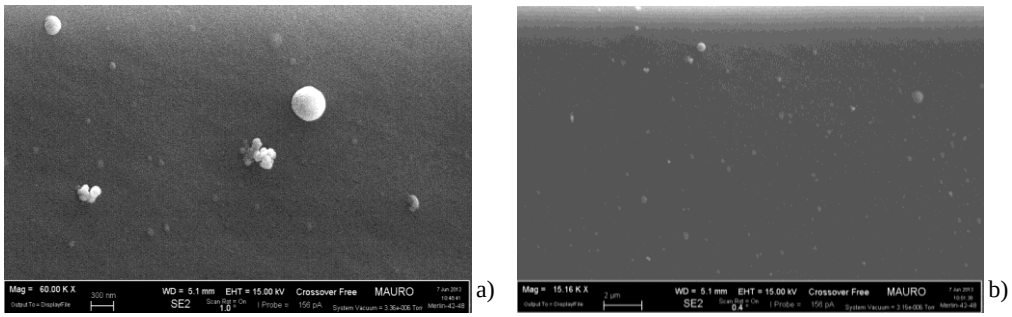

Figure 7.39: FE-SEM analyses for sample containing 25phr of TBO after 30min of sol-gel reaction

7.4. Conclusions

The in-situ generation of particles by the bottom-up approach is an efficient technique for the preparation of organic–inorganic hybrid materials. The formation of inorganic network comes from hydrolysis and condensation reactions from alkoxysilanes in alcoholic solutions.

The generation of silica particles was successfully achieved by the method of swelling of crosslinked PDMS. The presence of silica in the composite was verified by both thermal and microscopic analyses. The presence of the nanosilica clusters generated by this method lead to an improvement of the Tg values and the thermal stability of the material. However, electrical characterization did not evidenced any improvement of the electrical insulating behavior with respect to the unfilled silicone material.

The generation of silica, alumina and titania particles was achieved in the vinyl oligomer prior the hydrosilation reaction. The silane and the platinum catalyst were then added to the formulation and cured. The presence of the particles in the composite was assessed by both thermal and microscopic analyses. An increase of the particles content was observed by increasing the time of sol-gel reaction and/or the amount of inorganic precursor. The suitable conditions for the preparation of the composites were studied for the three inorganic precursors (TEOS, $Al(OPr\text{-}i)_3$, TBO). Samples thick up to 2cm were obtained in the case of silica composites while, due to lower thermal conductivity, only thin samples were obtained in the case of aluminum oxide and titania. Electrical characterization did not evidence any improvement of resistance time (Dry Arc Resistance) and dielectric spectroscopy indicated similar value of relative permittivity for the unfilled and filled samples.

References

[1] J. Livage, D. Ganguli. Sol. Energy. Mat. and Sol. Cells 68(**2001**) 365.

[2] J. Livage. Bull. Mater. Sci. 22(**1999**) 201.

[3] Y.H. Han, A. Taylor, M.D. Mantle and K.M. Knowles. J. Non-Cryst. Sol. 353 (**2007**) 313.

[4] Q.W. Yuan, J. E. Mark. Macromol. Chem. Phys. 200(**1999**)206.

[5] Y. Hu, J.D. Mackenzie. J. of Mat. Sci. 27(**1992**) 4415.

[6] H.H. Huang, B. Orler, G.L. Wilkes. Polym. Bulletin 14 (**1985**) 557.

[7] K. Chakrabarti, S.M. Kim, E.O. Oh, C.M. Whang. Mat. Letters 57(**2002**) 192

[8] L. Guo, J. Hyeon-Lee, G. Beaucage. J. Non-Cryst. Solids 243(**1999**) 61.

[9] B. Tan, S.E. Rankin. J. Phys. Chem. B. 110 (**2006**) 22353.

[10] M. Sangermano, E. Amerio, A. Priola, A. Di Gianni, B. Voit. J. Appl. Polym. Sci. 102(**2006**) 4659.

[11] M. Sangermano, G. Malucelli, E. Amerio, R. Bongiovanni, A. Priola, A. Di Gianni, B. Voit, G. Rizza. Macromol. Mat. Eng. 291 (**2006**) 517.

[12] J.E. Mark. Polym. Eng. Sci. 36(**1996**) 2905.

[13] D. Fragiadakis, P. Pissis, L. Bokobza. Polym. 46(**2005**) 6001.

[14] J.M. Breiner, J.E. Mark. Polym. 39(**1998**) 5483.

[15] L. Bokobza, A.L. Diop. Expr. Polym. Lett. 4(**2010**) 355.

[16] L. Bokobza. J. Appl. Polym. Sci. 93(**2004**) 2095.

[17] L. Dewimille, B. Bresson, L. Bokobza. Polym. 46(**2005**) 4135.

[18] G.S. Rajan, G.S. Sur, J.E. Mark, D.W. Schaefer, G. Beaucage. J. Polym. Sci. Part B: Polym. Phys. 41 (**2003**) 1897.

[19] Y.P. Ning, J.E. Mark. J. Appl. Polym. Sci. 30(**1985**) 3519.

[20] K. Morita, Y. Hu, J.D. Mackenzie. J. Sol-Gel Sci. and Techn. 3(**1994**) 109.

[21] G.D. Kim, D.A. Lee, J.W. Moon, J.D. Kim, J.A. Park. Appl. Organometal. Chem. 13(**1999**) 361.

[22] R. Bongiovanni, M. Sangermano, A. Medici, C. Tonelli, G. Rizza. J. Sol-Gel Sci. Technol 52 (**2009**) 291.

[23] H.K. Farag, M. Al Zoubi, F. Endres. J. Mater. Sci. 44(**2009**) 122.

[24] M. Hofmann, H.J. U.S. Patent 8,207,241 B2 (**2012**).

8. INVESTIGATION OF THE CYCLOPENTADIENYL TRIALKYLPLATINUM CATALYST

Several transition-metal organometallic compounds are known to be excellent catalysts for the hydrosilation reaction and they have consequently attracted scientific interest [1]. However, cyclopentadienyl platinum complexes and in particular the cyclopentadienyl trialkylplatinum (named in the following $CpPt(CH_3)_3$) have been used much less extensively [2]. Indeed, the application of these complexes as effective photoinitiator for hydrosilation reactions involving vinyl/hydride silicone mixtures was demonstrated later on [3]-[4]. This complex was also used as hydrosilation catalyst in light-curable silicone elastomer casting compounds in applications such as dental imprints, adhesives as well as in the production of light emitting devices (LEDs) using silicon-based encapsulants [5].

The reactivity of this $CpPt(CH_3)_3$ complex was investigated both in the UV and visible regions and was compared to the reactivity of the catalyst used in the previous experiments.

8.1. Introduction on (Me-Cp)Pt(Me)$_3$complexes

The use of theses complexes for the hydrosilation reaction was discovered recently [3]. Indeed, these complexes were in a first time overlooked because previous studies indicated that they presented low quantum efficiency for photo-reaction (Φ = 0.0044 in methylcyclohexane at 350 nm) [6]. However, recent studies showed that they represent an alternative system to thermally based Pt complexes (and others catalysts) with high quantum efficiency (Φ = 0.34 in methylcyclohexane at 366 nm) [3]. Therefore, this molecule undergoes an extremely efficient photochemical reaction following UV-light excitation.

It's photolysis in the presence of silicon hydride $HSiEt_3$ leads to two different intermediates that is a methyl platinum complex $CpPtCH_3$and a dimethyl alkyl

platinum complex $CpPt(CH_3)_2R$. They are then partitioned under the reaction conditions between colloidal platinum and a $CpPt(CH_3)RH$ complex [3],[6]. The scheme of this reaction was reported in Figure 8.1.

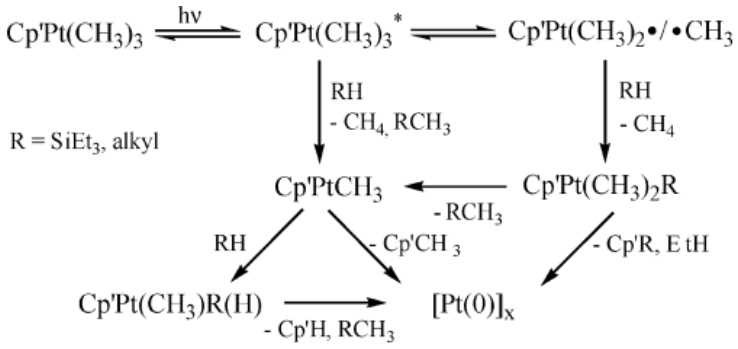

Figure 8.1: Scheme of the hydrosilation reaction using cyclopentadienyl trialkylplatinum as catalyst

The main disadvantage of these low-molecular platinum complexes such as $CpPt(Me)_3$ are their high volatility [7] which combined with their toxicity is problematic for the workplace safety. To avoid these drawbacks silyl substituents or alkyl groups can be introduced at the cyclopentadienyl ligand such as (R_3'Si - Cp)PtR_3 or (Me – Cp)PtR_3 [8].

The behavior of the trimethyl(methylcyclopentadienyl)-platinum(IV) complex was studied in our system containing equimolar amount of PDMS-V and MH-PDMS. In the following it will be named (Me-Cp)$Pt(Me)_3$. As reported in Figure 8.2 the absorption spectrum of the platinum complex in n-pentane is dominated by a band centered at 255 nm and lower energy shoulder at ~ 289 nm. The energy positions of these two features were observed not to be solvent dependent so they can be considered valid for our system.

These photoactivable catalysts are preferably used in applications such as dental imprints, adhesives as well as in the production of light emitting devices (LEDs) using silicon-based encapsulants [5] by using blue light activation.

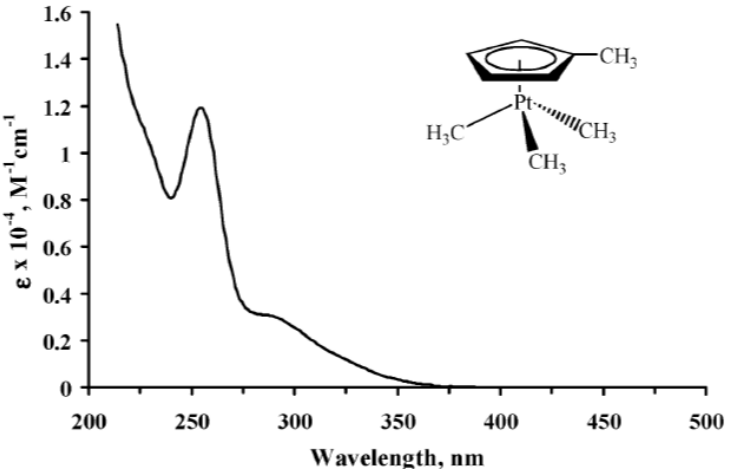

Figure 8.2: UV-Vis absorption spectrum of (Me-Cp)PtMe catalyst in n-pentane

Visible light radiation curing requires less energy than does either ultraviolet curing or thermal curing and provides greater safety than does the use of ultraviolet radiation. It results therefore an efficient way to induce the hydrosilation reaction [9].

Sensitizers can optionally be included in the formulation to both increase the overall rate of the curing process at a given wavelength of initiating radiation (as in the UV region for example) and/or shift the optimum effective wavelength of the initiating to longer values (in the visible region) [5]. Indeed, a sensitizer is capable of transferring energy to the platinum complex such that the hydrosilation reaction is initiated upon exposure to actinic radiation (light having a wavelength between 200 and 800 nm). This compound must have a triplet energy level of at least 31 kcal/mole and must not inhibit the hydrosilation reaction.

Most common sensitizers used are 2-chlorothioxanthen-9-one (CTX), 9,10-dimethylanthracene, 9,10-dichloroanthracene or camphorquinone. The main disadvantage of the last one in the air inhibition and so is not usually used for the hydrosilation reaction. It results from literature [9] that the CTX is the most effective sensitizer for this reaction where gel enhancement is 4 times faster. The amount should be otherwise at least 100 ppm and no greater than 5000 ppm [5],[10]. This sensitizer presents a high absorption band in the range between 350 and 400 nm as reported by UV-Vis absorption spectrum (Figure 8.3).

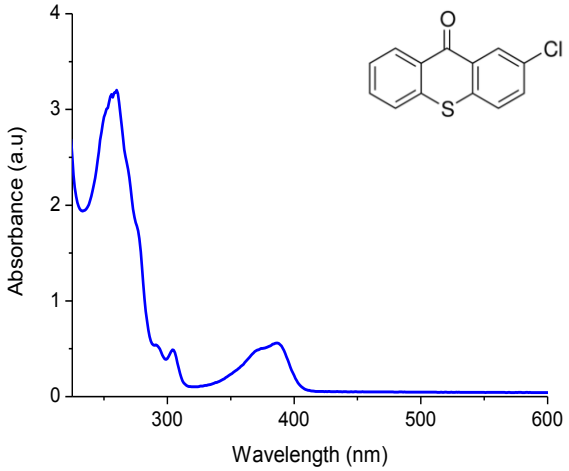

Figure 8.3: UV-Vis absorption spectrum of the CTX in 1,3-dioxolane

The trimethyl (methylcyclopentadienyl) platinum complex was used for the hydrosilation reaction of our system both by UV and blue light activation. The results were then compared to those obtained with the $Pt(acac)_2$ both in term of reactivity and final properties of the material.

8.2. Investigation of the $(Me\text{-}Cp)Pt(Me)_3$ in the UV region

8.2.1. Kinetics of polymerization

Formulations containing amount of $(Me\text{-}Cp)Pt(Me)_3$ranging from 250 to 2000ppm were prepared. The mixtures contained equimolar amount of PDMS-V and MH-PDMS. The platinum catalyst was first solved in 1,3-dioxolane (concentration 2,4%) and then added in the formulations.

The kinetic of polymerization was evaluated following the silane conversion as a function of the irradiation time. For comparison, formulation containing 500ppm of $Pt(acac)_2$was used as reference.

The results reported in Figure 8.4 showed that the $(Me\text{-}Cp)Pt(Me)_3$was more reactive than the $Pt(acac)_2$ even by using lower amount of catalyst. An increase of the amount of catalyst lead to a progressive increase of the conversion up to 85%

with 750ppm. A further addition of catalyst content did not induce a significant increase of the final conversion. It should be interesting to evaluate the behavior of this catalyst in thick unfilled and filled samples and in particular the eventual front propagation velocity.

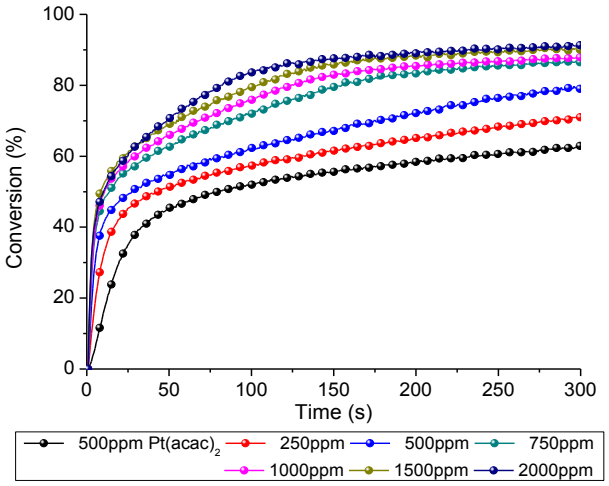

Figure 8.4: Silane conversion as a function of irradiation time for different amount of Me-Cp)Pt(Me)$_3$ catalyst

The properties of the cured materials were then studied by varying the amount of (Me-Cp)Pt(Me)$_3$ from 250 to 1000ppm in order to evaluate the suitable quantity of catalyst for the next investigations.

8.2.2. Properties of unfilled cured material

Thermal analyses were performed for samples containing amount of platinum ranging from 250 to 1000 ppm and were compared to the pristine system containing 500 ppm of Pt(acac)$_2$ catalyst. The results were reported in Figure 8.5. By using the (Me-Cp)Pt(Me)$_3$ catalyst lower thermal stability was achieved at low temperatures but all the samples present similar trend and final residues. The gel content was still higher than 95% indicating that a high crosslinking occured during the reaction (Table 8.1).

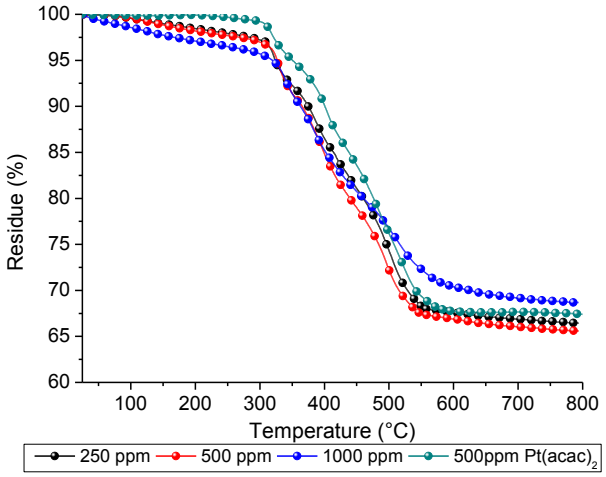

Figure 8.5: TGA analyses for samples cured with different amount of catalyst

Table 8.1: Gel content of cured samples with different amount of catalyst

	250ppm	**500ppm**	**1000ppm**	**500ppm Pt(acac)$_2$**
Gel content (%)	96	95	95	99

DMTA analyses (Figure 8.6) evidenced an increase of the Tg by using the (Me-Cp)Pt(Me)$_3$ catalyst. This increment was not dependent of catalyst amount but only of catalyst nature. The values for all the samples were reported in Table 8.2.

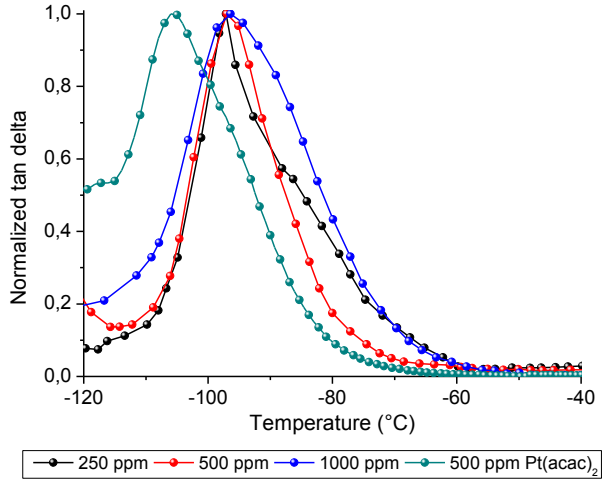

Figure 8.6: DMTA analyses for samples cured with different amount of catalyst

Table 8.2: Tg values of samples cured with different amount of catalyst

	250ppm	500ppm	1000ppm	500ppm $Pt(acac)_2$
Tg value (°C)	-97	-97	-96	-108

8.2.3. Frontal polymerization in the unfilled system

The study of frontal propagation was performed for formulations containing different amount of (Me-Cp)$Pt(Me)_3$ catalyst ranging from 250 to 1000ppm. First, the dark-curing on thin samples was evaluated by FT-IR analyses and the enthalpy of reaction by DSC measurements. Then the front propagation was evaluated by optical pyrometry. The results were then compared to the pristine system containing 500ppm of $Pt(acac)_2$.

8.2.3.1. Dark-curing

In order to evaluate the extent of the dark curing, silane conversion was followed by FT-IR analyses for mixtures containing equimolar amount of PDMS-V and MH-PDMS with 250 (Figure 8.7a) and 1000 ppm (Figure 8.7b) of (Me-Cp)$Pt(Me)_3$ catalyst. The mixtures were coated on a SiC substrate with a thickness of 50 µm and then irradiated for 10, 30 and 60s with UV light. The FT-IR spectra of the sample were collected before and after the irradiation at different times.

A high silane conversion was observed just after irradiation (t=0s) for both formulations, even when the samples were irradiated for only 10s. It was possible to conclude that the dark-curing was not the predominant phenomena with this catalyst. However, dark-curing was present. The final conversion after one hour of dark-curing was independent of the irradiation time. Nonetheless, increasing the amount of catalyst from 250 to 1000ppm lead to an increase of the final silane conversion from 70% to 80%.

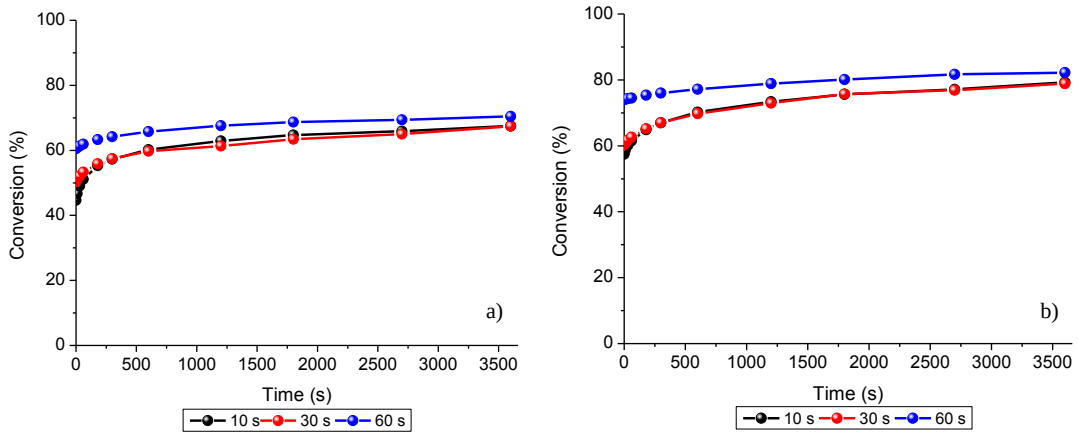

Figure 8.7: Evaluation of dark-curing after different time of UV-irradiation for a) 250ppm and b) 1000ppm of (Me-Cp)Pt(Me)$_3$ catalyst

For comparison, the dark-curing for the formulation containing 500 ppm of Pt(acac)$_2$ was reported in Figure 8.8. A significant increase of the SiH conversion in the dark was evidenced as a function of UV-irradiation length: the longer was the irradiation time the higher was the final conversion. Therefore, it could be concluded that the (Me-Cp)Pt(Me)$_3$ catalyst leads to higher silane conversion with lower irradiation times.

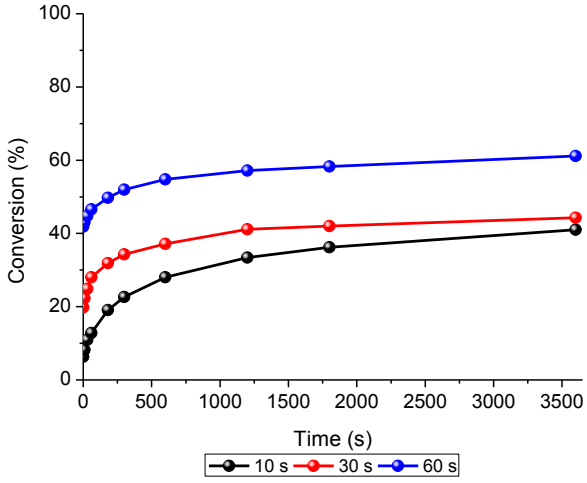

Figure 8.8: Evaluation of dark-curing after different time of UV-irradiation for 500ppm of Pt(acac)$_2$ catalyst

8.2.3.2. Enthalpy of reaction

Photo-DSC were performed in order to evaluate the enthalpy of reaction as a function of catalyst amount. The data were reported in Figure 8.9. The (Me-Cp)Pt(Me)$_3$ catalyst lead to higher enthalpies of reaction even with lower amount of catalyst with respect to the Pt(acac)$_2$. The reactivity was also increased as the peak of enthalpy was sharper. By increasing the amount of (Me-Cp)Pt(Me)$_3$ catalyst, an increase of the enthalpy and an higher reactivity was observed (peak of enthalpy at lower time of irradiation).

DSC performed at 10°C/min up to 140°C on the cured samples after 4 minutes of irradiation (Figure 8.10) evidenced a reduction of the residual enthalpy by increasing the amount of catalyst, indicating a better crosslinking. The values were reported in Table 8.3.

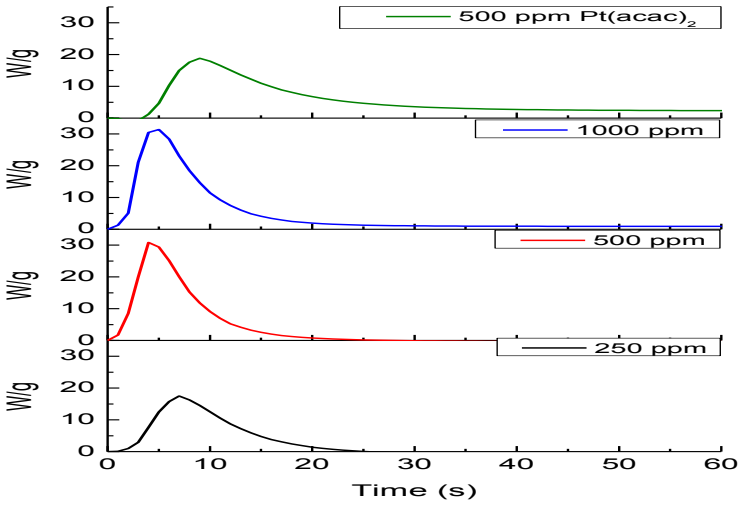

Figure 8.9: Photo-DSC for formulations containing different amount of catalyst

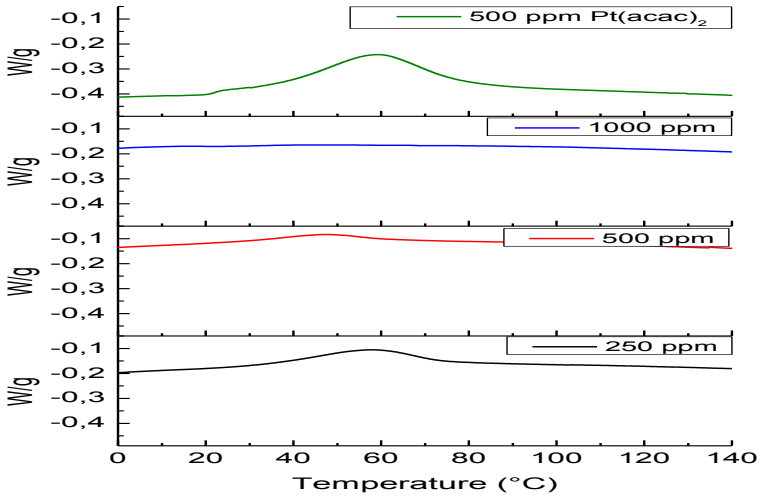

Figure 8.10: DSC performed after 4 minutes of UV-irradiation

Table 8.3: Enthalpies of reaction during and after UV-curing

	250ppm	**500ppm**	**1000ppm**	**500ppm $Pt(acac)_2$**
Enthalpy during UV-irradiation (J/g)	160	210	240	106
Enthalpy after UV-irradiation (J/g)	14	6	1	36

8.2.3.3. Frontal propagation

Mixtures were prepared by adding an equimolar amount of vinyl and silane reactive groups. The (Me-Cp)$Pt(Me)_3$catalyst was solubilized in 1,3-dioxolane and added to the formulation at different content up to 1000 ppm.The temperature profiles of the formulations were reported in Figure 8.11.The temperature profile obtained with 500 ppm of $Pt(acac)_2$was added for comparison.

A higher reactivity was observed by using the trimethyl (methylcyclopentadienyl) platinum complex as the maximum temperature was reached after a lower time (about 50s against 100s for $Pt(acac)_2$). This phenomena was already observed by FT-IR analyses (Figure 8.4) where the initial slope was higher by using the (Me-Cp)$Pt(Me)_3$. An increase of catalyst amount mainly lead to an increase of the maximum temperature reached but did not speed up the front velocity.

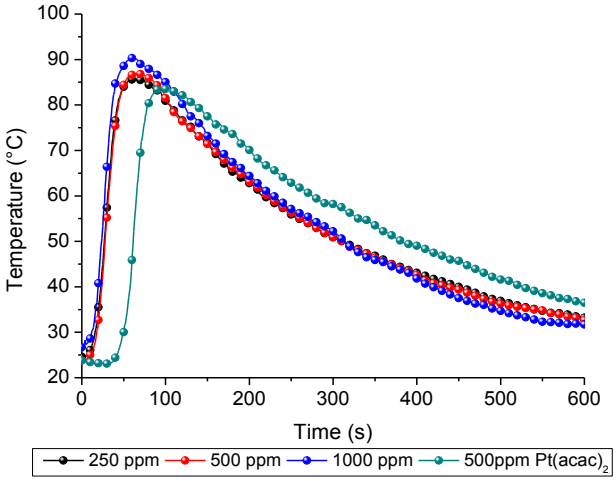

Figure 8.11: Temperature profiles at 1cm from the top for different catalyst amount

The amount of (Me-Cp)Pt(Me)$_3$was then fixed at 250 ppm and the temperature profiles of formulations up to 5 cm thick were recorded by optical pyrometry. The aim was toconfirm that a front propagation occurred also in the presence of the trimethyl(methylcyclopentadienyl) platinum complex. The results were reported in Figure 8.12. High temperatures were reached indicating an efficient propagation of heat inside the formulations. For a 5cm thick samples, the maximum temperature reached was about 65°C. By reporting the distance of the front as a function of the highest temperature reached in formulation, the front velocity was estimated [11]. Indeed, the polymerization front propagates at constant speed and linear behavior strongly supports the front propagation mechanism.

The results obtained in Figure 8.13 confirmed that a front propagation also occurs with the (Me-Cp)Pt(Me)$_3$catalyst and that thick samples could be obtained in low times of curing and dark-curing (if no dissipation heat occurs among the sample).

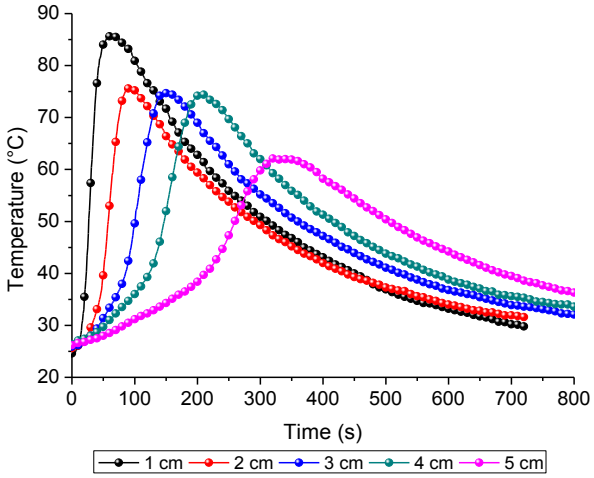

Figure 8.12: Temperature profiles at different distance from the top for 250ppm of (Me-Cp)Pt(Me)$_3$ catalyst

The front position as a function of time, for the formulation containing 500ppm of Pt(acac)$_2$ was used in order to compare the propagation speed of the two systems.On the basis of the experimental data it could be concluded that the (Me-Cp)Pt(Me)$_3$catalyst was much more reactive than the Pt(acac)$_2$ even with lower amount of catalyst. The estimated speeds were around 9cm.min^{-1} (0,15 mm.s^{-1}) for 250 ppm of the (Me-Cp)Pt(Me)$_3$ catalyst and 5cm.min^{-1} (0,08 mm.s^{-1}) for 500 ppm of the Pt(acac)$_2$ catalyst.

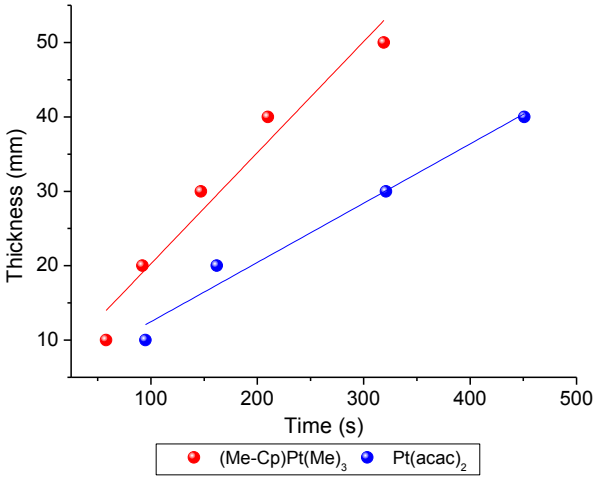

Figure 8.13: Front position as a function of time for 250ppm of (Me-Cp)Pt(Me)$_3$ and 500ppm of Pt(acac)$_2$ catalysts

The (Me-Cp)Pt(Me)$_3$ catalyst presented an higher reactivity in the UV region with respect to the Pt(acac)$_2$one. Higher silane conversion could be reached with lower amount of catalyst and the final properties of the material were comparable. The only difference concerned the increase of Tg value as this system presented higher reactivity and therefore higher crosslinking.

8.2.4. Investigation of the bottom-up approach with TEOS

It was observed in the pristine system containing 500ppm of Pt(acac)$_2$ that a front was able to propagate up to 3cm for formulations containing up to 25 phr of TEOS. Optical pyrometry measurements performed on formulations containing 250ppm of (Me-Cp)Pt(Me)$_3$catalyst evidenced that a higher front velocity was achieved for this catalyst with respect to the previous Pt(acac)$_2$. It resulted therefore interesting to investigate the front propagation of filled samples containing 250ppm of (Me-Cp)Pt(Me)$_3$ in order to evaluate if thicker samples could be obtained.

Silica particles were generated in the vinyl oligomer prior curing by putting the mixture of vinyl terminated PDMS and TEOS in a jar containing a solution of water and 2% wt of triethylamine. The solution was placed in an oven at 80°C, the reaction was allowed to proceed for 24h and then vacuum drying was achieved to constant weight. The silane (MH-PDMS) and 250 ppm of the (Me-Cp)Pt(Me)$_3$ catalyst were then added to the formulation.

The influence of silica precursor (TEOS) amount on the properties of the material were investigated and the front propagation was evaluated for different thickness of samples.

8.2.4.1. Characterization of systems with different amount of TEOS

The silane conversion was followed by FT-IR analyses for formulations containing amount of TEOS ranging from 10 to 75 phr (Figure 8.14). A slight

decrease of the kinetic was observed for formulations containing 50 and 75 phr of TEOS but the final silane conversion remained unchanged.

DMTA analyses (Figure 8.15) did not evidenced any significant increase of the Tg value with respect to the unfilled system (Table 8.4). However, these values were comparable to those obtained with the $Pt(acac)_2$ catalyst (Table 7.6).

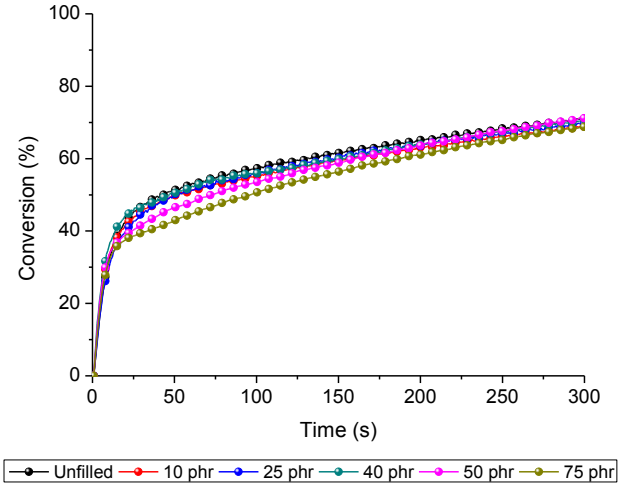

Figure 8.14: Silane conversion for samples with different amount of TEOS after 24h of sol-gel reaction time

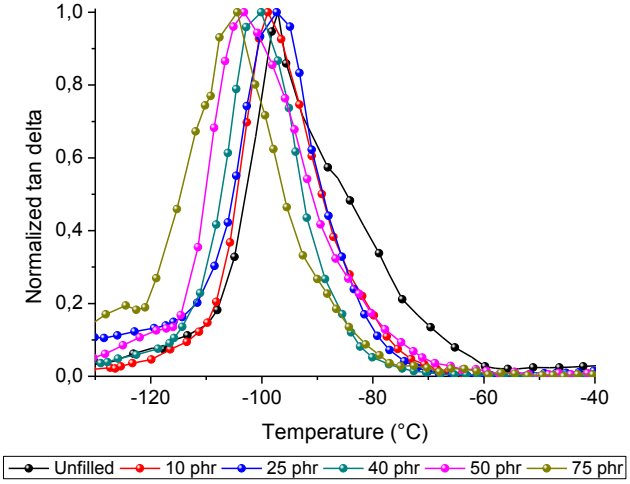

Figure 8.15: DMTA analyses for samples with different amount of TEOS after 24h of sol-gel reaction

Table 8.4: Tg values of cured samples with different amount of TEOS

	Reference	10 phr	25 phr	40 phr	50 phr	75 phr
Tg value (°C)	-97	-99	-97	-103	-104	-102

8.2.4.2. Front propagation in presence of generated silica particles

It was previously reported (7.3.2.3) that in the presence of 500 ppm of $Pt(acac)_2$ samples 2cm thick, containing in-situ generated silica particles, were obtained for amount of TEOS up to 25 phr. It was also reported that in the presence of 250 ppm of the $(Me\text{-}Cp)Pt(Me)_3$ catalyst the front propagation of unfilled formulation was twice higher than in the presence of 500 ppm of $Pt(acac)_2$. It resulted therefore interesting to investigate the possibility to reach thicker samples with higher amount of in-situ generated silica particles by using the $(Me\text{-}Cp)Pt(Me)_3$catalyst.

Formulations 3cm thick were prepared with amount of silica precursor up to 100 phr and the front propagation was followed with an optical pyrometer (Figure 8.16). Cured samples could be obtained with amount of TEOS up to 100 phr. This indicated that the amount of generated silica could be increased in the presence of the $(Me\text{-}Cp)Pt(Me)_3$ catalyst. Further addition of TEOS did not allow the front to propagate for such thickness.

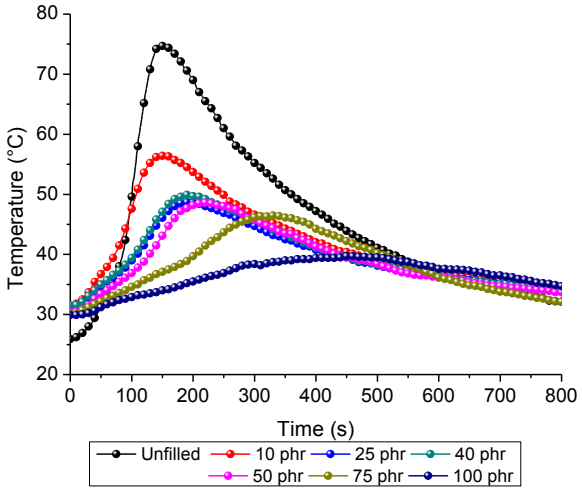

Figure 8.16: Temperature profiles for 3cm thick formulations containing different amount of TEOS

In order to increment the amount of in-situ generated silica,the amount of (Me-Cp)Pt(Me)$_3$ catalyst was increased from 250 to 1000ppm for samples containing 75phr of TEOS. The temperature profiles of 2cm thick formulations were reported in Figure 8.17. Neither an increase of the maximum temperature reached nor a speed up of the front propagation was achieved by increasing the catalyst content. On the contrary, a decrease of the maximum temperature was observed. It was also observed that the cured samples contained bubbles when increasing the catalyst content indicating a too high exothermicity in the formulation. This phenomena could be responsible for the slowing down of the maximum temperature reached. The amount of catalyst was therefore fixed at 250 ppm.

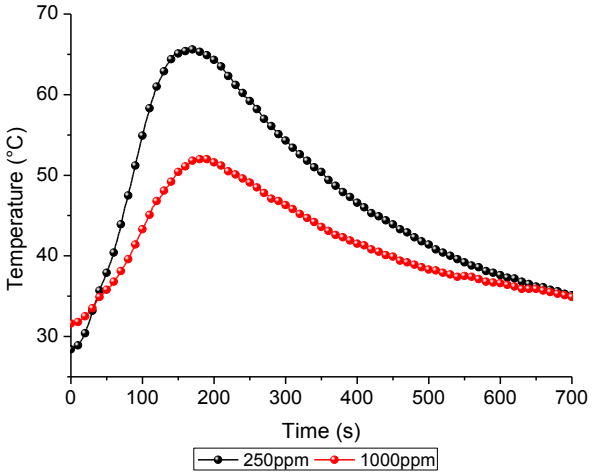

Figure 8.17: Temperature profiles for 2cm thick formulations containing 75phr of TEOS

It was then studied how the presence of the in-situ generated silica particles delay the front propagation. The velocity was calculated by following the temperature profiles of formulations containing 75phr of TEOS for thickness from 1 to 3cm (Figure 8.18). The maximum temperature reached were then reported as a function of sample thickness (Figure 8.19).

For the unfilled formulation (with 250 ppm of the (Me-Cp)Pt(Me)$_3$ catalyst) the estimated speed was around 9cm.min^{-1} (0,15 mm.s^{-1}) while for the formulation containing 75 phr of TEOS the velocity was reduced to 5cm.min^{-1} (0,08 mm.s^{-1}). The front speed of the filled system was comparable to the one obtained for the

unfilled system containing 500ppm of $Pt(acac)_2$ showing the higher reactivity of the $(Me\text{-}Cp)Pt(Me)_3$ catalyst.

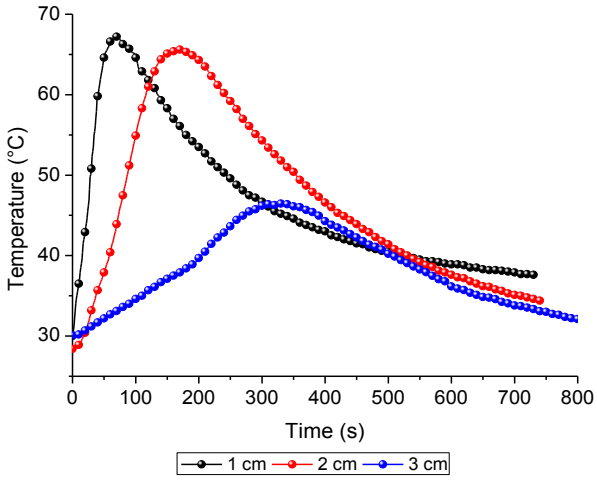

Figure 8.18: Temperature profiles for different thickness of formulation containing 75phr of TEOS

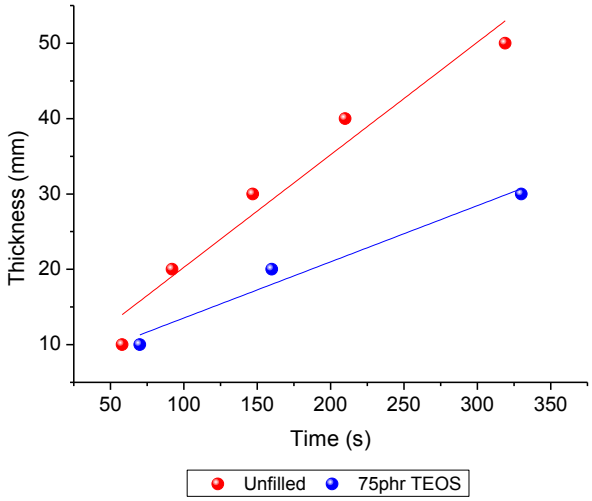

Figure 8.19: Front position as a function of time for the unfilled and 75phr of TEOS formulations

8.2.5. Investigation of the top-down approach with silica filler

It was previously observed that the presence of micrometric fillers in the formulation lead to an increase of the Dry Arc Resistance values. The main

drawback was the heat dissipation of the particles avoiding the front propagation among the sample thickness. It was therefore tried to increase the thickness curability by using the (Me-Cp)$Pt(Me)_3$catalyst.

The experiments were performed by using PVC tubes (13mm of diameter 10mm in length) closed on one side and filled with formulations containing different amounts of silica $2SiO_2$particles (properties reported in Table 6.1).The curing penetration depth was measured as a function of UV light exposure time (from 30s to 90s). The cured silicones were demolded 30 minutes after irradiation in order to let the dark curing proceed and the thicknesses were then measured. The results were reported in Table 8.5. No significant increase of curing depth was reached by using the (Me-Cp)$Pt(Me)_3$ catalyst with respect to $Pt(acac)_2$. Further addition of catalyst (up to 1000ppm) did not lead to any improvement. The heat dissipation was therefore avoiding the front propagation even by using the (Me-Cp)$Pt(Me)_3$ catalyst which presented higher reactivity.

Table 8.5: Curing depth for formulations containing different amount of silica filler $2SiO_2$ for the two platinum catalyst and for different irradiation time

Irradiation time (s)	**30s**	**60s**	**90s**
100phr of $2SiO_2$500ppm $Pt(acac)_2$	1.4 mm	1.8 mm	2.5 mm
100phr of $2SiO_2$ 250ppm (Me-Cp)$Pt(Me)_3$	1.6 mm	1.9 mm	2.3 mm
300phr of $2SiO_2$500ppm $Pt(acac)_2$	1.0 mm	1.5 mm	1.6 mm
100phr of $2SiO_2$ 250ppm (Me-Cp)$Pt(Me)_3$	1.3 mm	1.4 mm	1.6 mm
100phr of $2SiO_2$ 1000ppm (Me-Cp)$Pt(Me)_3$	1.2 mm	1.5 mm	1.6 mm

8.3. Reactivity of (Me-Cp)$Pt(Me)_3$ in the visible region

8.3.1. Influence of sensitizer

Visible light curing was investigated for formulations containing 1000 ppm of (Me-Cp)$Pt(Me)_3$ catalyst. A sensitizer was introduced in order to evaluate its influence on the curing rate. A blue light emitting diode with an intensity of

approximately 500 $mW.cm^{-2}$ and a wavelength range of 380-515 nm was used for the polymerization.

Amount of 2-chlorothioxanthen-9-one (CTX) photosensitizer ranging from 500 to 4000ppm were added to formulations containing an equimolar amount of PDMS-V and MH-PDMS and 1000ppm of $(Me\text{-}Cp)Pt(Me)_3$ catalyst. The kinetic of polymerization was evaluated following the silane conversion as a function of the irradiation time.

Data related to the formulation containing only 1000ppm $(Me\text{-}Cp)Pt(Me)_3$ catalyst (without any sensitizer) was not reported as no silane conversion was observed. On the contrary, a silane conversion of 40% could be reached in the presence of CTX sensitizer with amount up to 1000ppm (Figure 8.20). A further increase up to 4000ppm lead to a silane conversion of 55%.

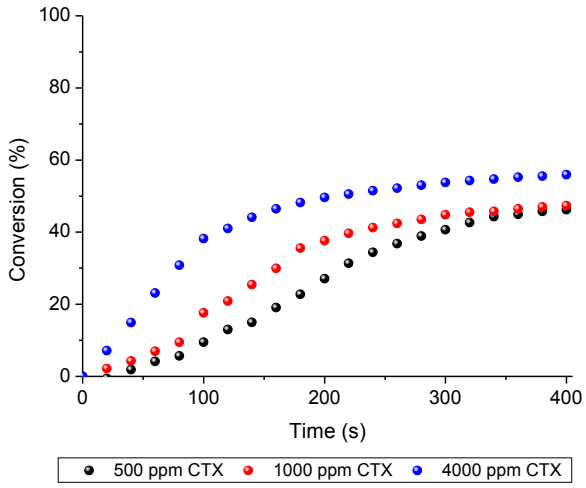

Figure 8.20: Silane conversion for different amount of CTX (1000ppm of $(Me\text{-}Cp)Pt(Me)_3$ catalyst)

The amount of CTX was then kept fixed at 4000ppm as it gave rise to higher silane conversion.

8.3.2. Characterization of cured unfilled material

The thermal properties of the unfilled system obtained by blue light curing were compared with the system prepared with the same amount (1000ppm) of (Me-Cp)Pt(Me)$_3$by UV light activation (Figure 8.21). The thermal stability obtained by blue light curing was comparable to what was obtained by UV curing and gel content values were equivalent (Table 8.6).

DMTA analyses (Figure 8.22) performed for the two unfilled systems evidenced that lower Tg was achieved in the case of blue light curing. The values were reported in Table 8.6. This could be explained by lower silane conversion reached by blue light curing with respect to the UV curing: the value was about 55% in blue light (Figure 8.20) and 85% in UV light (Figure 8.4).

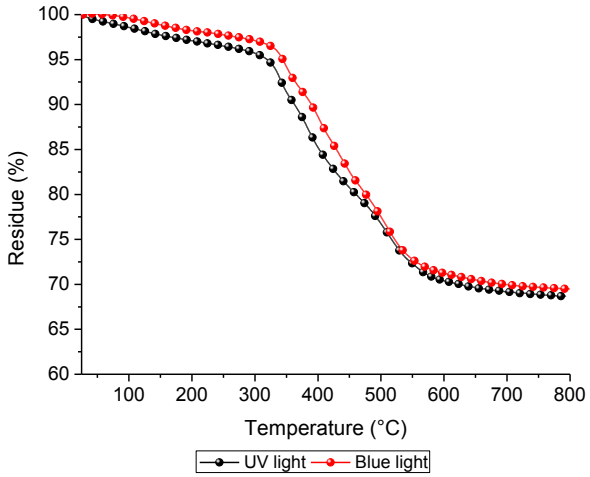

Figure 8.21: TGA analyses for the unfilled system cured with UV or blue light

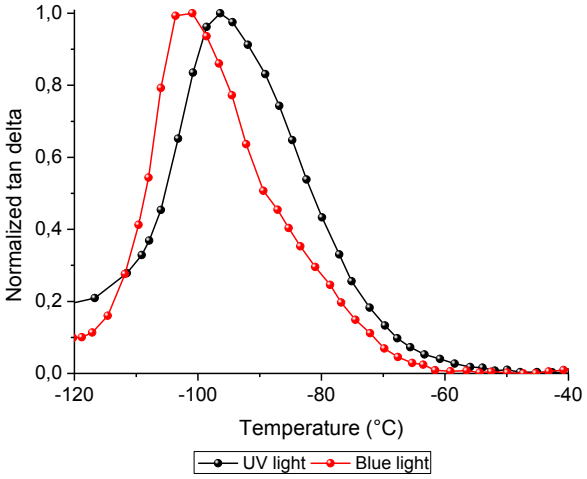

Figure 8.22: DMTA analyses for the unfilled system cured with UV or blue light

Table 8.6: Tg values of cured unfilled samples with UV or blue light

	UV light	**Blue light**
Tg value (°C)	-96	-102
Gel content (%)	95	97

8.3.3. Investigation of dark-curing

The proceeding of dark-curing by blue light activation was investigated for the formulation containing 1000ppm of (Me-Cp)Pt(Me)$_3$ and 4000ppm of CTX. The irradiation time was varied between 10 and 60s and the silane conversion was followed for one hour (Figure 8.23). It was possible to observe that even after 10s of irradiation there was a high extent of dark-curing with a silane conversion increasing from 5% (just after irradiation) to 30% (after one hour). Longer irradiation time lead to similar final conversion of about 60% both after 30 and 60s of irradiation. In the first case the dark-curing extent was more pronounced.

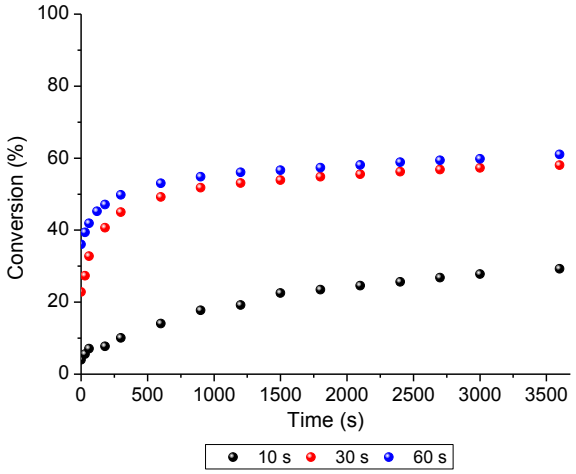

Figure 8.23: Evaluation of dark-curing after different irradiation times

8.3.4. Investigation of frontal propagation

The possibility to have a frontal propagation by using blue light activation was studied. Formulations 1cm thick containing 1000ppm of (Me-Cp)Pt(Me)$_3$ and 4000ppm of CTX were irradiated for different irradiation time ranging from 2 to 4 minutes. The results were reported in Figure 8.24. An increase of the maximum temperature reached was observed for longer irradiation times. However, the time of irradiation required for polymerization of 1cm thick formulation was higher with respect to the UV light. It was also noticed that the maximum temperature was still reached few seconds after the light turn off as if the front need to be sustained to propagate.

Formulations 1 and 2cm thick were then irradiated for 4 minutes and the temperature profiles were recorded (Figure 8.25). It was observed that the front was not able to propagate for 2cm of thickness and the resulting formulation was not cured.

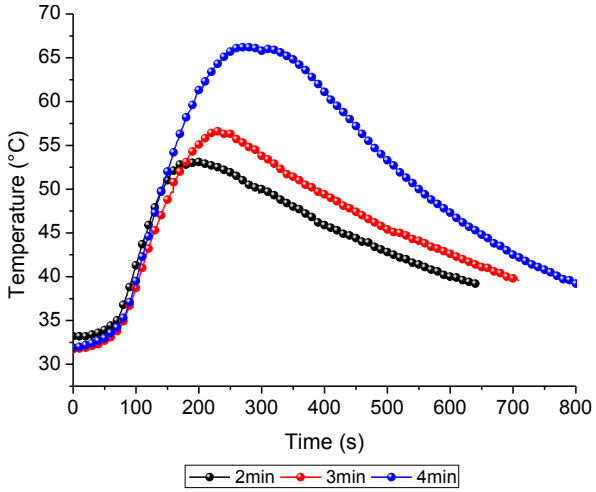

Figure 8.24: Temperature profiles for 1cm thick formulations after different irradiation time

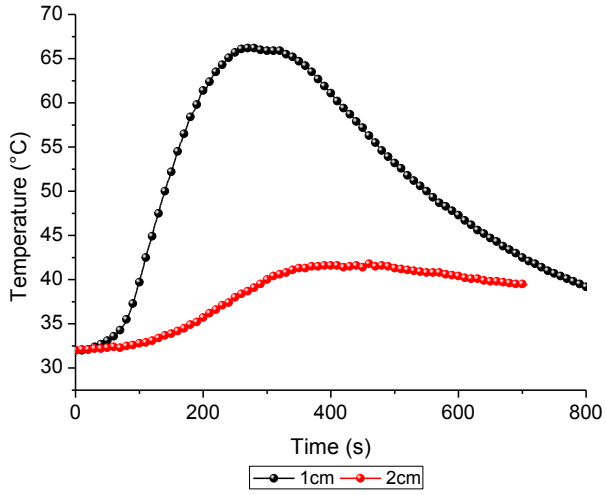

Figure 8.25: Temperature profiles for 4 minutes of irradiation for different thickness

Curing depth measurements were performed after 2 and 4 minutes of blue light irradiation. The resulting thicknesses were 0.9 and 1.5 cm as reported in Figure 8.26. Therefore it could be concluded that a front was able to propagate under blue light irradiation but its velocity was deeply reduced with respect to what was observed in the UV activation. This blue light activation resulted consequently not suitable for the preparation of filled materials.

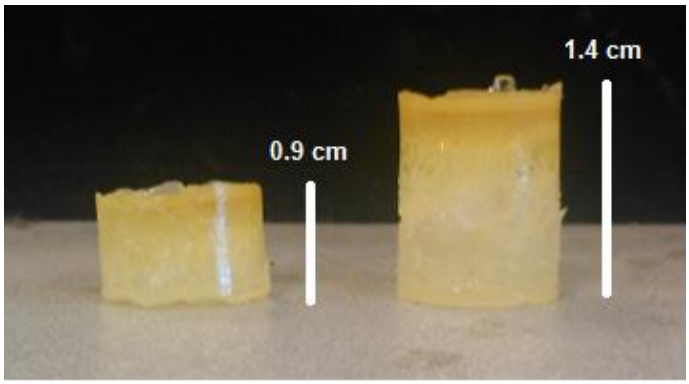

Figure 8.26: Unfilled cured materials after 2 and 4 minutes of blue light irradiation

8.4. Conclusions

The (Me-Cp)Pt(Me)$_3$ catalyst presented a higher reactivity in the UV region with respect to the Pt(acac)$_2$. Higher silane conversion could be obtained with lower amount of catalyst. The properties of the unfilled material cured using the (Me-Cp)Pt(Me)$_3$ catalyst were compared to the pristine system. A slight increase of the Tg value was observed (due to higher crosslinking) but the thermal properties remained unchanged. A dark-curing was also evidenced as previously reported for the Pt(acac)$_2$ catalyst. The thickness curability in the UV region was increased by using the (Me-Cp)Pt(Me)$_3$ catalyst. Indeed, 75phr of silica precursor added in the formulation lead to a front propagation comparable to what was obtained for the unfilled formulation cured in the presence of the Pt(acac)$_2$ catalyst. However, no increase was observed for addition of fillers by the top-down approach.

Blue light cured material was achieved by adding a photosensitizer in the formulation (4000ppm of CTX).The dark-curing was also present in the high wavelength activation. Thick samples could be obtained if the front propagation was sustained by the blue light irradiation.

References

[1]V. Jakubek, A.J. Lees. Inorg. Chem. 39 (**2000**) 5779.

[2]L.D. Boardman. Organometallics 11 (**1992**) 4194.

[3]V. Jakubek, A.J. Lees. Inorg. Chem. 43(**2004**) 6869.

[4]D. Troegel, J. Stohrer. Coordin. Chem. Rev. 255(**2011**) 1440.

[5]L.D. Boardman, D.S. Thompson, C.A. Leatherdale, A.J. Ouderkirk. Patent 3M Innovative Properties Co. EP1812973B1 **(2006)**.

[6]O. Hackelberg, A. Wojcicki. Inorg. Chim. Acta 44(**1980**) L63.

[7]Z. Xue, M.J. Strouse, D.K. Shuh, C.B. Knobler, H.D. Kaesz, R.F. Hicks, R.S. Williams. J. Am. Chem. Soc. 11(**1989**) 8779.

[8]S. Rist, S. Bosshammer, M. Putzer, T. Naumann, U. Irmer. Patent Momentive Performance Materials GmbH EP1817372(**2009**).

[9]L.D Boardman, J.D. Oxman. Visible radiation activated hydrosilation reaction. Patent Minnesota Mining and Mfg. Co.EP0358452 B1 (**1999**).

[10]J.D. Oxman, L.D. Boardman. Patent 3M Innovative Properties Co.US6376569 B1 (**2002**).

[11]E. Frulloni, M.M Salinas, L. Torre, A. Mariani, J.M. Kenny. J. of Appl. Pol. Sci. 96(**2005**)1756.

CONCLUSIONS

Insulators for high voltage transmission lines have been used for more than 150 years and can be made mainly from glass, porcelain or polymer composites. The main properties necessary for the electrical insulators are low losses during transmission and distribution of the current and low size of the components. Therefore, the insulators need good electrical and mechanical performances in order to withstand those requirements. Moreover, they also need resistance to weathering, chemical and physical degradation by water, UV and chemical attacks due to the wide range of operating conditions. Polymeric insulators are progressively replacing the traditional porcelain and glass insulators due to their many advantages such as lightweight, good electrical and mechanical properties. In particular, silicone rubbers, which present high hydrophobic surface, low density, low surface and bulk conductivity are the main materials used for polymeric outdoor insulators.

Silicone polymers can be cured by a hydrosilation reaction at high temperature by using a platinum catalyst. Usually, a catalyst is used to promote the addition of silane groups across a double bond. It was recently reported that this reaction can also be achieved by UV irradiation at room temperature leading to lower time of reaction and lower energy consumption. This mechanism was studied in this thesis in order to prepare silicone nanocomposites for outdoor insulators.

In a first part, the influence of the catalyst used and the molecular weight of the monomers were investigated. It resulted that the $Pt(acac)_2$ is the most active for the system chosen. A modulation of the final properties of the silicone material could be achieved by varying the vinyl oligomer molecular weight. A significant increase of the curing in the dark was also evidenced together with a high enthalpy of reaction. Therefore, a frontal polymerization among the system was achieved (only for the system with the lowest molecular weight) leading to the curing of thick samples in short times of irradiation.

Then micro-sized fillers were incorporated into the formulations in order to improve the electrical insulating properties. A progressive increase of the dry arc resistance was achieved with respect to the unfilled system independently of the nature of the filler. The main drawback was the decrease of the thickness curability attributed to heat dissipation by the ceramic fillers. This phenomena could be in part avoided by adding nano-sized particles. The low dimensions allowed the front propagation among thickness of 2cm with 30s of irradiation. Moreover, Tg values of the nanocomposites were comparable to those obtained with a high amount of micro-sized fillers. The low amount of nanosized particles in the formulations did not lead to any improvement of the electrical insulating properties: the dry arc resistance values were analogous to the unfilled system. Morphological analyses evidenced a good filler dispersion inside the silicone matrix for both nano and micro-sized particles.

Organic-inorganic hybrid materials were then prepared by in-situ generation of nanodomains by sol-gel reaction. The formation of the inorganic network comes from hydrolysis and condensation reactions from metal-alkoxysilanes in alcoholic solutions. This process was used to generate silica, titania and aluminum oxide. First, the swelling method of crosslinked PDMS was achieved for the formation of silica nanoclusters which presence was verified by both morphological and thermal analyses. Then, another method used was the generation of silica carried out in the vinyl oligomer prior curing. The silane and the platinum catalyst were then added to the formulation for the crosslinking. The suitable conditions for the reaction were studied by evaluating the effect of the sol-gel reaction time and the amount of inorganic precursor on the final properties of the composites. This process allowed the curing of 2cm thick samples including higher amount of silica nanoclusters with respect to the top-down approach. This is mainly due to a better dispersion of the filler in the matrix by in-situ generation with respect to direct mixing. Due to lower conductivity of aluminum oxide and titania with respect to silica, only samples thick several mm could be achieved. However, all these samples did not evidenced any improvement of the dry arc resistance values.

In the last part, the blue light activation of hydrosilation reaction was studied using a (Me-Cp)Pt(Me)$_3$ catalyst. Its reactivity was first investigated in the UV

region and compared to the $Pt(acac)_2$. Higher silane conversion could be achieved with lower amount of catalyst with respect to the pristine system and the properties of the unfilled materials were similar. A dark curing and a front propagation were also evidenced for this catalyst and the velocity was doubled. Therefore, samples up to 3cm thick and containing up to 75phr of inorganic precursor could be cured with a front velocity comparable to what was obtained for the unfilled system cured with the $Pt(acac)_2$ catalyst. However, no increase of thickness curability was achieved by the direct addition of fillers in the formulation (by top-down approach). The blue light curing was performed by adding 4000ppm of a photosensitizer capable of absorbing the actinic radiation at these wavelengths. A dark curing was also present for this system and a front propagation could be reached by a sustained blue light irradiation.

It could be interesting to investigate deeper the visible radiation activated hydrosilation reaction. This could be a way to consume less energy than does thermal curing and provide greater safety than is possible with the ultraviolet radiations. Moreover, this reaction could be used to make light emitting device using silicon-containing encapsulants. In fact, conventional LEDS are encapsulated in epoxy resins but tend to yellow over time reducing the brightness and changing the colour rendering index of the light emitted.

LIST OFPUBLICATIONS

- **S. Marchi**, M. Sangermano, P. Meier, X. Kornmann.

"Preparation and Characterization of PDMS Composites by UV-hydrosilation for Outdoor Polymeric Insulators".

Polymer Composites. **2013**. DOI 10.1002/pc.22775

- **S. Marchi**, S. Pagliolico, G. Sassi.

"Characterization of panels containing micro-encapsulated Phase Change Materials".

Energy Conversion and Management. **2013**, 74, 261-268.

- R. Bongiovanni, **S. Marchi**, E. Zeno, A. Pollicino, R.R. Thomas.

"Water resistance improvement of filter paper by UV-grafting modification with a fluoromonomer".

Colloids and Surfaces A. **2013**, 418, 52-59.

- M. Sangermano, **S. Marchi**, D. Ligorio, P. Meier, X. Kornmann.

"UV-induced frontal polymerization of a Pt-catalyzed hydrosilation reaction"

Macromolecular Chemistry and Physics. **2013**, 214, 943-947.

- M. Sangermano, **S. Marchi**, P. Meier, X. Kornmann.

"UV-activated hydrosilation reaction for silicone polymer crosslinking"

Journal of Applied Polymer Science. **2013**, 128, 1521-1526.

- Y. Yagci, O. Sahin, T. Ozturk, **S. Marchi**, S. Grassini, M. Sangermano.

"Synthesis of silver/epoxy nanocomposites by visible light sensitization using highly conjugated thiophene derivatives"

Reactive and Functional Polymers. **2011**, 71, 857-562.

- M. Sangermano, **S. Marchi**, L. Valentini, S. Bittolo Bon.

"Transparent and conductive grapheme oxide/poly(ethylene glycol) diacrylate coatings obtained by photopolymerization"
Macromolecular Materials and Engineering. **2011**, 296, 401-407.

PROCEEDINGS

- **S. Marchi**

"Transparent and conductive grapheme oxide/poly(ethylene glycol) diacrylate coatings obtained by photopolymerization"
Smart and Functional Coatings Conference, 26-27 September 2013, Turin, Italy.

- **S. Marchi**

"UV-induced hydrosilation for preparation of silicone polymers and nanocomposite silicone materials"
European Polymer Federation (EPF), 16-21 June 2013, Pisa, Italy.

- M. Sangermano, **S. Marchi**, P. Meier, X. Kornmann.

"UV-activated hydrosilation reaction for silicone polymer crosslinking"
European Symposium of Photopolymer Science (ESPS), 4-7 September 2012, Turin, Italy.

- M. Sangermano, **S. Marchi**, P. Meier, X. Kornmann.

"UV-induced hydrosilation for preparation of silicone polymers and nanocomposites silicone materials"
European Centre for Nanostructured Polymers (ECNP), 24-27 April 2012, Praga, Czech Republic.

- Y. Yagci, O. Sahin, T. Ozturk, **S. Marchi**, S. Grassini, M. Sangermano.

"Synthesis of silver/epoxy nanocomposites by visible light sensitization using highly conjugated thiophene derivatives"

4th European Center for Nanostructured Polymers (ECNP) Young ResearcherConference, 7-10 November 2011, Lyon, France.